UNIVERSITÉ DE MONTRÉAL

HIGH-DENSITY 3D PYRAMID-SHAPED MICROELECTRODE ARRAYS FOR BRAIN-MACHINE INTERFACE APPLICATIONS

BAHAREH GHANE MOTLAGH

INSTITUT DE GÉNIE BIOMÉDICAL

ÉCOLE POLYTECHNIQUE DE MONTRÉAL

THÈSE PRÉSENTÉE EN VUE DE L'OBTENTION

DU DIPLÔME DE PHILOSOPHIAE DOCTOR

(GÉNIE BIOMÉDICAL)

NOVEMBRE 2015

UNIVERSITÉ DE MONTRÉAL

ÉCOLE POLYTECHNIQUE DE MONTRÉAL

Cette thèse intitulée :

HIGH-DENSITY 3D PYRAMID-SHAPED MICROELECTRODE ARRAYS FOR BRAIN-MACHINE INTERFACE APPLICATIONS

présentée par : GHANE MOTLAGH Bahareh

en vue de l'obtention du diplôme de : Philosophiae Doctor

a été dûment acceptée par le jury d'examen constitué de :

M. SAVARD Pierre, Ph. D., président

M. SAWAN Mohamad, Ph. D., membre et directeur de recherche

M. SAVADOGO Oumarou, D. d'état, membre

M. WÜTHRICH Rolf, Ph. D., membre externe

DEDICATION

To Kianoush & My parents…

For their never-ending love and support

ACKNOWLEDGEMENTS

The completion of this dissertation has been an amazing journey filled with many experience from the labs to the real life!

I had the opportunity to work under the supervision of truly astonishing individual Prof. Mohamad Sawan. Thank you for accepting me into your scientific group and providing me your guidance and support. There have been several occasions where I remember feeling discouraged and skeptical about the path that I am taking but a meeting with you has refreshed my enthusiasm and raised my courage infinitely. Your dedicated support and guidance have been outstanding over the past five years and it has been a privilege to work under your supervision.

I would like to express my gratitude to Prof. Richard Martel and Prof. Kevin J. Wilkinson for their precious advice and contribution to this research and thesis. Thank you for kindly granting your time and answering many of my questions.

I gratefully appreciate the time of my dissertation committee members, Prof. Pierre Savard, Prof. Oumarou Savadogo, and Prof. Rolf Wüthrich to read this thesis and to help me move this forward. Their questions and comments certainly helped to improve my thesis.

I would like to thank my research mates and collaborators, May Choueib, Alireza H. Mesgar, Taraneh Javanbakht, Amal Kassab, Md Hasanuzzaman, and Ehsan Kamrani for offering their expertise and advice along this project.

I would like to gratefully acknowledge the help of Christophe Clément and Laurent Mouden for technical support in cleanroom, LASEM, and Biostim. The work has not been completed without the technical team that keeps everything working. Thank you for so generously providing me with your assistance and time. My sincere thanks to Marie-Hélèn Bernier and Richard Vernhes for providing their expertise in micro/nanofabrication and characterizing my sample.

The past several years have not been an easy ride and I realized the importance of family and friends to completion of a project of this magnitude. I am extremely fortunate to have a support group of my friends to encourage me and make a strong interest in my continued development and growth.

Last but not least, I am grateful to my parents for their unconditional love and continued support. I would not have made it this far without them. Special thanks to my beloved Kianoush, without whose endless love and moral support, this task could have never been completed.

RÉSUMÉ

Les dispositifs médicaux dédiés aux enregistrements des activités neuronales et à la stimulation de tissus nerveux sont appelés interfaces cerveau-machines. Ils offrent un potentiel important pour restaurer diverses fonctions neurologiques perdues. Un élément clé dans la mise en œuvre des dispositifs est le réseau de microélectrodes (MEAs pour MicroElectrode Arrays en anglais) servant d'interface avec les tissus nerveux. Les MEA jouent un rôle important dans les implants lors d'expérimentations chroniques, ils doivent être fiables, stables et efficaces pour l'enregistrement et la stimulation à long terme. Les propriétés électrochimiques et la compatibilité biologique des microélectrodes sont des facteurs essentiels qui doivent être prises en compte lors de leur conception et fabrication.

La présente thèse traite de la conception et la fabrication de MEA en silicium micro-usiné à haute densité et en forme de pyramides qui sont destinés à l'enregistrement et la stimulation intracorticals 3D. Nous nous concentrons principalement sur les techniques de microfabrication des électrodes et le développement de procédure du revêtement de matériaux nécessaires pour la biocompatibilité et protection des dispositifs implantables. Nous élaborons des microélectrodes à hauteur variable pour enregistrer des signaux neuronaux, sans perdre la capacité de microstimulation et tout en maintenant des impédances de faibles valeurs. Cette caractéristique est obtenue en modifiant la géométrie et la composition de matériaux utilisés, ce qui facilite l'injection de charge et la résolution spatiale élevée.

Nous présentons une nouvelle technique de micro-usinage 3D à nombre réduit de masques comparé aux techniques existantes. Nous décrivons la mise en œuvre d'un MEA à haute densité (25 électrodes / 1,96 mm^2) et à différentes longueurs d'électrodes. En outre, une nouvelle technique de masquage à base de film sec a été développée pour obtenir de très petites surfaces actives pour les microélectrodes qui sont à hauteur variable. Nous avons réduit les étapes du procédé de masquage de 14 à 6 par rapport à la méthode classique de masquage utilisé dans la littérature. Nous avons ensuite effectué, pour la première fois, une croissance directe sélective de nanotubes de carbone sur les têtes de microélectrodes de longueurs variables en utilisant la technique du dépôt chimique en phase vapeur assisté par plasma (Plasma-Enhanced Chemical Vapor Deposition - PECVD). Ce recouvrement a amélioré les propriétés électriques des

électrodes de façon significative. En effet, ce revêtement par des nanotubes de carbone a impliqué une diminution d’un facteur 5 de l'impédance et une augmentation de 600 fois le transfert de charges par rapport à une électrode de Platine. Enfin, nous avons mis en évidence par des tests de cellules de culture *in vitro*, l'importance de revêtement des MEA avec des molécules bioactives (Poly-D-lysine) et de polyéthylène glycol hydrogels pour minimiser la réponse immunitaire du tissu neuronal aux MEA implantés.

ABSTRACT

Neuroprosthetic devices that can record neural activities and stimulate the central nervous system (CNS), called brain-machine interfaces (BMI), offer significant potential to restore various lost neurologic functions. A key element in functions restoration is Microelectrode arrays (MEAs) implanted in neural tissues. MEAs, which act as an interface between bioelectronic devices and neural tissues, play an important role in chronic implants and must be reliable, stable, and efficient for long-term recording and stimulation. Electrochemical properties and biological compatibility of chronic microelectrodes are essential factors that must be taken into account in their design and fabrication.

The present thesis deals with the design and fabrication of silicon micromachined, high-density, pyramid-shaped neural MEAs for intracortical 3D recording and stimulation. The focused is mainly on the MEAs fabrication techniques and development of coating materials process required with implantable devices with an ultimate purpose: elaborate variable-height microelectrodes to obtain consistent recording signals from small groups of neurons without losing microstimulation capabilities, while maintaining low-impedance pathways for charge injection, high charge transfer, and high-spatial resolution by altering the geometries and material compositions of the array.

In the first part of the thesis, we present a new 3D micromachining technique with a single masking step in a time and cost effective manner. A high density 25 electrodes/ 1.96 mm^2 MEA with varying lengths electrodes to access neurons that are located in different depths of cortical tissue was designed and fabricated. Furthermore, a novel dry-film based masking technique for procuring extremely small active area for variable-height electrodes has been developed. With this technology, we have reduced the masking process steps from 14 to 6 compared to the conventional masking method. We have then reported for the first time a selective direct growth of carbon nanotubes (CNTs) on the tips of 3D MEAs using Plasma Enhanced Chemical Vapor Deposition (PECVD) that could enhance electrical properties of the electrodes significantly. The CNT coating led to a 5-fold decrease in impedance and a 600-fold increase in charge transfer compared with Pt electrode. Finally, we have highlighted the importance of the coating MEAs with bioactive molecules (Poly-D-lysine) and polyethylene glycol (PEG) hydrogels to minimize the immune response of the neural tissue to implanted MEAs by *in vitro* cell-culture tests.

TABLE OF CONTENTS

DEDICATION iii
ACKNOWLEDGEMENTS iv
RÉSUMÉ vi
ABSTRACT viii
LIST OF TABLES xii
LIST OF FIGURES xiii
LIST OF ABBREVIATIONS xix
CHAPTER 1 INTRODUCTION 1
1.1 Scope of the thesis 1
1.2 The advent of penetrating Microelectrode arrays (MEA) 1
1.3 Current challenges 2
1.4 Microelectrode arrays: a key element in neuroprosthetic devices 4
1.5 Objectives of the present work 5
1.6 Specifications of projected MEAs 6
1.7 Summary of contributions 7
1.8 Organization of the thesis 8
1.9 Publications 9
CHAPTER 2 OVERVIEW OF IMPLANTABLE MICROELECTRODE ARRAYS 11
2.1 Introduction to neural MEAs 11
2.2 Properties of MEAs 13
2.3 Application of penetrating MEAs 14
2.4 Fabrication technologies of penetrating MEAs 15
2.4.1 Traditional Microelectrode arrays 16
2.4.2 Microwires 18
2.4.3 Micromachined MEAs 20
2.4.4 Other approaches to MEAs fabrication 26
2.5 Comparison of penetrating microelectrodes technologies 30
2.6 Planar microelectrode arrays (pMEA) 33
2.7 Improve biocompatibility of microelectrodes 37

2.7.1 Material science strategies 37
2.7.2 Bioactive molecule strategies 38
2.8 Electrical circuit model of MEAs 40
2.9 Perspective of the work in this thesis 42
CHAPTER 3 EXPERIMENTAL PROCEDURES OF MEAs' PREPARATION 44
3.1 Design and fabrication of neural 3D MEAs using micromachining techniques 44
3.1.1 MEAs backside fabrication process 44
3.1.2 MEAs frontside fabrication process 46
3.1.3 Shank insulation 50
3.1.4 Masking process to de-insulate active sites of the electrodes 51
3.1.5 Electrodes tip-coating 52
3.1.6 Tip-metallization and lift-off 53
3.1.7 CNTs tip-coating 54
3.2 Characterization of the neural MEAs 56
3.2.1 Scanning electron microscopy (SEM) imaging 57
3.2.2 Energy-dispersive X-ray spectroscopy (EDX) analysis 57
3.2.3 Electrochemical characterization; Electrochemical impedance spectroscopy (EIS), Cyclic voltammetry (CV), and Charge injection capacity (Q_{inj}) 58
3.3 Results and discussion 59
3.3.1 Fabrication of 3D MEAs 59
3.3.2 Masking process 61
3.3.3 Tip-metal deposition 61
3.3.4 Tip-CNTs Growth 62
3.3.5 Tip-CNTs deposition (Coffee stains technique) 64
3.3.6 MEAs Electrical Properties 65
3.3.7 Equivalent circuit model 68
3.4 Discussions 72
3.5 Conclusion 74
CHAPTER 4 BIOCOMPATIBILITY OF MEAs 75
4.1 Bioactive molecule deposition 75
4.1.1 MEAs preparation 76
4.1.2 Coating of the MEAs with polyethylene glycol (PEG) 78

4.1.3 Conjugation of peptide (poly-D-lysine) to the MEAs 78
4.1.4 Fourier transform infrared spectroscopy (FTIR) analysis 79
4.2 Cell cultures and *in vitro* cell test 79
4.2.1 Culture neuroblast cell line (CCL-131) 79
4.2.2 Cell-counting 79
4.2.3 Cell incubation with the electrodes before and after PDL coating 80
4.2.4 Statistical analysis 80
4.3 Results 80
4.3.1 Conjugation of PDL and PEG to the MEAs 80
4.3.2 Conjugation of peptides to MEAs 81
4.3.3 FTIR analysis 82
4.3.4 Effect of polymer coating on the cell size, morphology, and proliferation 85
4.3.5 Cell proliferation on the peptide-conjugated MEAs 86
4.4 Discussion 90
4.5 Conclusion 91
CHAPTER 5 CONCLUSION, GENERAL DISCUSSION, AND PERSPECTIVES 93
5.1 Summary of the results and contributions 93
5.2 Perspectives for future work 96
BIBLIOGRAPHY 99

LIST OF TABLES

Table 2.1. Advantages and drawbacks of MEAs fabrication methods [1-4]…….……31
Table 2.2. Characterization of MEAs technologies [5, 6]…….32
Table 2.3. Comparison of microelectrodes structure [7-10]…….…….32
Table 2.4. Impedance of the poly-silicon electrode before and after CNTs deposition [11]…..…35
Table 2.5. Measured impedance of electrodes with diameter of 40 µm as a function of gold nanopillar height [12]……..36
Table 3. 1. Comparison of conventional and proposed masking processes…….…...53
Table 3. 2. Sputtered deposition parameters for the electrodes' tip-metallization…….…..…54
Table 3.3. Average impedance of different electrode-tip coatings…….……67
Table 3. 4. Fitting results from the EIS model…….…....69
Table 3. 5. Comparison of neural Microelectrode arrays……..……..71
Table 4. 1. Sputtered deposition parameters for the electrodes' tip-metallization…….……..…77
Table 4. 2. The number of cells per electrode site for each tip coating before and after PDL coating……88

LIST OF FIGURES

Figure 1.1. Schematic view of a silicon micromachined neural MEA with variable heights of 1.45, 1.55, and 1.65 mm. The shank was covered with parylene-C (and PEG) and the active sites of each array were coated with Pt, sputtered iridium oxide (SIRO), or CNTs. The thickness of the electrodes was 200 μm at the base and about 2 μm at the tip with 100 μm spacing……...…….……...…7

Figure 2.1. Implanted microelectrode in the cortex. Neural stimulation occurs via current passes through the tip to the surrounding neurons. Reprinted with permission from Ref. [13]……...……...…...15

Figure 2.2. Scanning electron microscopy (SEM) images of Glass insulation and the metal part (Pt) of the metal-wire electrode. Reprinted with permission from Ref. [14]…….16

Figure 2.3. SEM (top) and Optical microscopy images of pre-processed and conventionally processed glass pipettes. Reprinted with permission from Ref. [15]…….17

Figure 2.4. Microwires: (a) Wire microelectrodes embedded in ceramic substrate. The anchors ensure that the array stay in the brain, (b) Ceramic well-structure connected to parylene-C insulated gold wires. Electrodes are inserted perpendicular into the substrate, (c) SEM image of microwire insulated with 3 μm parylene-C except at the tip. Reprinted with permission from Ref. [16]…….18

Figure 2.5. SEM images of metal microelectrodes coated with CNTs: (a) CNTs covalently attached to the tungsten electrode, (b) CNTs were electrochemically deposited at the recording sites of the electrode. Reprinted with permission from Ref. [17]……..19

Figure 2.6. Michigan MEA: (a) Basic structure of a multisite microprobe presenting the substrate, insulation layers, and recording sites, (b) SEM image of the tip of neural microelectrode. Reprinted with permission from Ref. [18]……...21

Figure 2.7. Typical Michigan array: (a) A prototype of the array, consisting of 64 sites on 200 μm centers with 1640 μm width and 4 mm long shanks. The interface is shown with the 1 mm × 1 mm × 0.5 mm base resting on a penny, (b) General schematic of the four-shank electrodes forming 16-channels probe. Reprinted with permission from Ref. [19]…….21

Figure 2.8. Flexible multi-channel MEAs: (a) 3D flexible MEAs after folding, (b) Each probe with 3 recording sites. Reprinted with permission from Ref. [20]……...…….……..23

Figure 2.9. Flexible MEA: (a) A magnified photo of the 4×4 electrode array, (b) SEM image of the grown CNTs, (c) High-resolution transmission electron microscopy (HRTEM) image of the grown CNTs. Reprinted with permission from Ref. [21]……...23

Figure 2.10. SOI-based probe: (a) Schematic of the probe structure, (b) SEM image of a probe tip. The thickness of the interconnect lines is 1 μm, (c) SEM image of the 1 μm × 1 μm iridium recording site. Reprinted with permission from Ref. [22]……..24

Figure 2.11. Utah silicon-based MEAs: (a) 2D flat electrode array; (b) Slanted electrode array. Reprinted with permission from Ref. [23]……..25

Figure 2.12. Metal-based MEAs using EDM technique: (a) SEM image of a parylene-coated assembly, consisting of Pt-coated electrode tips, (b) Stainless steel electrode arrays after electrochemical polishing. Reprinted with permission from Ref. [24, 25]……26

Figure 2.13. Patch clamp recording form the neuron cell. In the cell-attached configuration, the patch electrode is sealed to the surface of the intact cell allowing channel activity in the patch of membrane under the electrode tip. Reprinted with permission from Ref. [26]…….27

Figure 2.14. The silicon-wire probe on Si (111) with W wiring circuit: (a) SEM image of silicon-wire probe combined with wring process for on-chip circuits on same a silicon wafer, (b) Silicon probe in 30 μm in length and 2 μm in diameter at a growth temperature of 600 ºC for 30 min, (c) 2 × 2 array of selective silicon-wire probes with 160 μm in length and 3.5 μm diameter at tips. The VLS growth was performed at 700 ºC for 2 h. Reprinted with permission from Ref. [27]…….28

Figure 2.15. Combination of ion-channel on a transistor: (a) HEK293 cells with a hSlo potassium channel on a silicon chip with a linear array of transistors. The cells appear in the color of the florescence of GFP, (b) Nerve cells from the leech on the open gate oxide of a field-effect transistor. The n-type silicon chip are shown in dark, the p-doped sources and drains are bright. The gates with the length of 1.8 μm and the width of 20 μm show no contract. The cell was injected using a glass capillary. Reprinted with permission from Ref. [28]……...……...29

Figure 2.16. Neuronal network on silicon chip: (a) SEM image of a two-way contact with the pins of polyimide. St (stimulator wings) and transistor (S: source, D: drain, G: gate), (b) SEM

image of immobilized neurons form the pond snail after three days in culture, (c) SEM of a neuronal network with the cell bodies on a double circle of two-ways contacts after two days in culture. Reprinted with permission from Ref. [28]……...…….……30

Figure 2.17. SEM images of planar microelectrode array with 60 individual CNT electrodes. Circuit paths are insulated with 100 nm silicon dioxide layer: (a) Top view of the planar microelectrode array showing the 60 individual electrodes, (b-d) Different magnification of vertical CNT electrode network and a single CNT electrode. Reprinted with permission from Ref. [11]…….33

Figure 2.18. Process flow of microelectrodes fabrication with vertically aligned CNT networks: (a) Deposition of poly-silicon on silicon dioxide by photolithography and dry reactive ion etching, (b) Insulation electrodes and circuit path with a thermal oxide layer using dry thermal oxidation, (c) Resist spin coating and photolithography, (d) Hydrofluoric etching to open the electrode sites, (e) Aluminum and iron deposition that works as catalysts, (f) Remove the resist, (g) Direct CVD growth of vertically aligned CNTs. Reprinted with permission from Ref. [11]……...……..34

Figure 2.19. SEM images of planar microelectrodes with gold nanopillars onto the recording sites: (a-c) Top-view of planar microelectrodes with different magnification. Gold nanopillars appear dark, (d) nanostructure of goldpillars with a diameter of 200 nm and the height of 22.5 µm. Reprinted with permission from Ref. [12]…….36

Figure 2.20. Microelectrodes with different size, shape and cross-section that produced the same foreign body response and glial scar. SEM images of electrode prepared by (a) KOH etching, (b) RIE, (c) Center for Neural Communication Technology (CNCT) device. Reprinted with permission from Ref. [29]……..37

Figure 2.21. Possible mechanisms of biological responses to an implant: (a) Early reactive response in 1-3 weeks, (b) Prolonged reactive response in 6-8 weeks post implantation. Neurons are pink, astrocytes are red, microglial are blue, and vasculatures are purple. Reprinted with permission from Ref. [29]……..38

Figure 2.22. Equivalent circuit models of electrode-electrolyte interface: (a) Warburg model, (b) Fricke model, (c) Randles model, (d) Robinson model for metal electrode, (e) Kovacs model.

Reprinted with permission from Ref. [30], © 2007, IEEE EMBS Conference on Neural Engineering and Ref. [31]……..41

Figure 2.23. A flow diagram for electrode-electrolyte interface measurement and characterization. Reprinted with permission from Ref. [32]…….42

Figure 3.1. Main silicon-based MEAs micromachining steps: (a) Backside dicing, (b) Backside glassing and polishing, (c) Backside metallization, (d) Frontside dicing, (e) Frontside wet-etching……45

Figure 3.2. Schematic top-view of backside dicing including 9 collections of 5×5 matrix……...45

Figure 3.3. Isoetch contours and surface topography of etched silicon for the HF-HNO_3-acetic acid diluents [33]. Numbers in parentheses shows etch rates of silicon in μm/min……...48

Figure 3.4. Experimental setup for dynamic etching process to round the side-walls of the square columns of the electrodes……...……....49

Figure 3.5. Experimental setup for static etch process: (a,b) Photographs of the static etching process. In this step of etching, the tips are sharpened by applying the N_2 gas from the bottom; (preferential etching)…….…..49

Figure 3.6. Process flow of electrodes tips-coating: (a) Parylene-C deposition, (b) Cover with dry-film photoresist, (c) Reactive Ion Etching, (d) Tip-metallization, (e) Lift-off in acetone….……..50

Figure 3.7. Structural phases during self-assembly of SWNT coffee stains: (a) SEM images of continuous, holey, striped, and spotty phases, (b) Schematic structural diagram as a function of SWNT and SDS concentrations. Reprinted with permission from Ref. [34]……57

Figure 3.8. A schematic of electrochemical measurement setup. Ag/AgCl act as a reference electrode, large area Pt wire as a counter, and electrodes of the array as a working electrode…...59

Figure 3.9. SEM images of electrodes backside: (a) Backside dicing, (b) Cross-section of the backside kerfs which have been filled with the glass paste, (c) 3D pyramid-shaped electrode array with three different heights. The outer row of electrodes is for etching process uniformity and will remove after etching step……..……..…….59

Figure 3.10. SEM images of the electrode etching process: (a) Frontside cutting, (b) Rounding corners by stirring the etching solution, (c-e) Polishing and sharpening the tips of electrodes by applying N2 gas from the bottom of the solution, (f) One 3D 7×7 MEA…….60

Figure 3.11. SEM images of masking process: (a) Electrode array covered with dry-film photoresist after RIE process. Dry-film photoresist follows the 3D structure of the electrodes, (b) Uniform tip-exposure of variable height electrodes after RIE and oxygen plasma etching process, (c) Electrode-tip after removing the mask……..……..……..61

Figure 3.12. SEM images of microelectrodes after tip-metallization with Pt (a,b, c) and SIRO (d, e, f) at different magnification. The SIRO surface is rougher than Pt. SIRO has dendritic structure while Pt has granular morphology……..62

Figure 3.13. SEM images of microelectrodes after tip-coating with CNTs: (a-b) At different magnification. The geometry of CNTs increased the accessible surface area, (c) Pt particles at the end of CNTs……...63

Figure 3.14. SEM images of microelectrodes after tip-coating with CNTs using coffee stains technique: (a-d) At different magnification. Small white particles are SDS that were evaporated after heating the electrodes…….64

Figure 3.15. Impedance spectroscopy of Pt- and CNTs-coated electrodes: (a) Magnitude of impedance as a function of frequency, (b) Phase of the impedance as a function of frequency, (c) & (d) CV curves for CNTs- and Pt-coated electrodes of the MEA under similar condition, respectively…….66

Figure 3.16. Electrode tip dimensions; the height (h) and radius (r) of the tip…….……..67

Figure 3.17. Electrochemical measurement setup: Equivalent circuit of the electrode-electrolyte interface……..69

Figure 3.18. Simulation and experimental results of equivalent electrode-electrolyte interface: (a) Pt-tips, (b) SIRO tip, (c) CNT-tip……...71

Figure 4.1. Schematic view of a silicon micromachined neural MEA with variable heights of 1.45, 1.55, and 1.65 mm. The shank was covered with parylene-C (or PEG) and the recording sites of each array were coated with Pt, Mo, Au, SIRO, or CNTs. The thickness of the electrodes was 200 μm at the base and less than 2 μm at the tip with 100 μm spacing……..……...78

Figure 4.2. A schematic view of hemocytometer as seen from the microscope. The cells marked as a circle in sections 1, 2, 3, and 4 was counted……...80

Figure 4.3. SEM images of microelectrodes: (a) Silicon-based microelectrode before coating with parylene-C and PEG, (b) Microelectrode coated with parylene-C, (c) Microelectrode covered with PDL, (d) Microelectrode covered with PEG…….……81

Figure 4.4. SEM images of the MEA surfaces coated with: (a) and (b) Pt, (c) and (d) Au, (e) and (f) SIRO before and after coating with the PDL, respectively…….....……..82

Figure 4.5. FTIR spectrum of silicon MEA insulated with parylene-C and tip coated with PDL: (a) and (b) Mo tip-coating before and after coating with the PDL, respectively. (c) and (d) Pt tip-coating before and after coating with the PDL, respectively…….83

Figure 4.6. FTIR spectrum of silicon MEA insulated with parylene-C and tip coated with PDL: (a) and (b) Au tip-coating before and after coating with the PDL, respectively. (c) and (d) SIRO tip-coating before and after coating with the PDL, respectively. (e) and (f) CNTs tip-coating

before and after coating with the PDL, respectively. These measurements have been done using Perkin Elmer spectrum with a 65 FTIR spectrometer……...84

Figure 4.7. Optical microscopy of the electrode tips incubated with neuroblast cells: (a) Before coating with polymers, (b) Following coating with parylene-C, (c) Following coating with PEG hydrogel…….85

Figure 4.8. Total cell number before and after parylene-C and PEG deposition, (N=6)……..86

Figure 4.9. Optical microscopy of the MEAs incubated with neuroblast cells: (a) and (b) Pt, (c) and (d) Au, (e) and (f) SIRO, (g) and (h) Mo, (i) and (j) CNTs tips before and after PDL coating, respectively. Significantly more cells were attached to the PDL-coated electrodes than the uncoated ones (Table 4.2)……..88

Figure 4.10. Cell proliferation before and after PDL coating: (a) Total cell number of each tip-coating before and after peptide deposition. (b) Cell proliferation per electrode site for each tip-coating before and after peptide deposition (N = 9). The cell proliferation has increased in the presence of the electrodes conjugated with PDL……...89

Figure 4.11. Growth curve for neuroblast cells via manual count using hemocytometer after 6, 12, 24, and 48 h. The lines present a mean value of four points obtained in three separate experiments. Standard deviations have been indicated……...…….……..90

LIST OF ABBREVIATIONS

CNS	Central Nervous System
BMI	Brain-Machine Interface
MEA	Microelectrode Array
CNTs	Carbon Nanotubes
PECVD	Plasma Enhanced Chemical Vapor Deposition
PEG	Polyethylene Glycol
PDL	Poly-D-Lysine
FTIR	Fourier Transform Infrared
SEM	Scanning Electron Microscopy
ETC	Electrode-Tissue Contact
EIS	Electrochemical Impedance Spectroscopy
CV	Cyclic Voltammetry
SIRO	Sputtered Iridium Oxide
MEMS	Micro-Electro-Mechanical Systems
SNR	Signal-to-Noise Ratio
Ppy	Polypyrrole
PEDOT	Poly (3, or 4- ethylenedioxythiophene)
CMOS	Complementary Metal–Oxide–Semiconductor
HRTEM	High-resolution transmission electron microscopy
DRIE	Deep Reactive Ion Etching
SOI	Silicon-On-Insulator
PDMS	Polydimethylsiloxane
EDM	Electrical Discharge Machining
VLS	Vapor-Liquid-Solid

CPE	Constant Phase Element
CoV	Covalent
MWCNTs	Multi-Walled Carbon Nanotubes
PSS	Polystyrene Sulfonate
TDT	Tucker Davis Technologies
HF	Hydrofluoric acid
pMEA	Planar Microelectrode Array
CVD	Chemical Vapor Deposition
RIE	Reactive-Ion Etching
SWNTs	Single-Wall Carbon Nanotubes
SDS	Sodium-Dodecyl-Sulfate
EDX	Energy-Dispersive X-ray
LSA	Lateral Surface Area
EMEM	Eagle's Minimal Essential Medium
FBS	Fetal Bovine Serum
ROS	Reactive Oxygen Species
H_2O_2	Hydrogen Peroxide
$OH^{\cdot}$	Hydroxyl Radical
$HO_2\cdot$	Hydroperoxyl Radical
O_2^{-}	Superoxide Onion
PEG-PL	Polyethylene Glycol-Lipid
HFCVD	Hot Filament Chemical Vapor Deposition
LPCVD	Low Pressure Chemical Vapor Deposition

CHAPTER 1 INTRODUCTION

1.1 Scope of the thesis

Neural microelectrode arrays (MEAs), which act as an interface between neural tissues and bioelectronic devices, play an important role in chronic implants and must be reliable, stable, and efficient for long-term recording and stimulation. Electrochemical properties and biological compatibility of chronic microelectrodes are essential factors that must be taken into account in their design and fabrication. This thesis brings aspects of these two factors together, exploiting the unique properties of new MEA to address challenges currently faced by neural implants.

In this thesis, a new 3D micromachining technique along with organic coatings is proposed for the fabrication of high performance MEAs. All the process steps starting from substrate preparation, to coating procedures using metallic thin-films and organic materials, along with electrochemical characterization and biocompatibility tests are presented in details. The role of geometry and materials on MEAs performance is particularly discussed and clarified.

In this chapter, we first summarize the current performance, limitations, and challenges of implantable microelectrodes. We then highlight the specification of new fabricated MEAs and explain how these can improve microelectrodes performance.

1.2 The advent of penetrating Microelectrode arrays (MEA)

Intracortical implants as a part of neuroprosthetic devices are in direct contact with the cerebral cortex of the brain. During the past four decades, the concept of interfacing with the brain cortex for both recording and stimulation the nervous system has rapidly evolved [35, 36]. Intracortical prosthesis that penetrates into the brain can stimulate an immediate area of the brain by directly interfacing the cortex depending on their design and placement [37, 38]. Besides, required electrical currents to stimulate neurons through penetrating electrodes are much smaller than those used to excite neurons through surface stimulation.

Penetrating MEAs have been developed for vision, auditory, and cognitive implants. Visual implants can partially restore vision by directly stimulating the visual cortex and is still the only hope of providing vision for patients with pathologies when the optic nerve is disconnected from

retina to the vision center of the brain. The first attempt to restore vision through cortical stimulation began in 1970 with Brindley and Dobelle [39-41]. Dobelle's 64 channel surface electrode array was placed on the top of visual cortex which allowed blind patients to recognize shapes in slightly close distances. The challenges were a lack of control of the number of phosphenes, pain induced by the large current stimulation of large electrodes, and more importantly no access to inner neurons that is necessary to stimulate. Intracortical stimulation was introduced to overcome those problems. Penetrating MEAs provide high fidelity images with a lower energy leading to less damage to neural tissues. Moreover, these MEAs could produce a more localized stimulus with less current. Schmidt et al. [42] showed that phosphenes could be evoked with lower currents than surface stimulation current and simple patterned perceptions could be evoked by small groups of penetrating MEAs. Penetrating microelectrodes provide capability for simultaneous cortical and thalamic recording from auditory cortex [43]. They have also shown great promise for restoring neurological lost functions, stroke, or injury [23]. However, considerable obstacles have to be overcome for these cortical implants go from the lab-bench on to the commercial reality.

1.3 Current challenges

Perhaps the most significant obstacles to the MEAs technologies are low impedance pathway for higher charge transfer, high-spatial resolution, and biological compatibility of the microelectrodes. For electrical stimulation and recording, electrodes with multi-dimensional geometry, high selectivity and sensitivity are needed. The selectivity is defined as an ability to activate individual neurons without activating identical neighbors. In order to obtain high selectivity, electrodes must be in close contact with tissues and this can be achieved using a 3D high-density MEA with small surface area of active sites [44, 45]. 3D penetrating MEA where the active sites of the electrodes are not in a same plane offers the best spatial selectivity. However, when the area of electrode decreases, the electrode impedance increases, which affects the stimulating/ recording characteristics (sensitivity) [46]. Electrode performance is a compromise between high selectivity that can be obtained by using smaller electrodes and the resulting increase in impedance and lower sensitivity. An approach to lower the impedance of the electrodes is modifying the interface material, for example by using organic nanomaterials with large surface area [47, 48].

Another significant limitation of the MEAs technologies is biocompatibility of the electrodes which is an important issue that must also be addressed. For clinical applications, MEAs must be reliable, stable, and efficient for long-term recording and stimulation [49]. When the MEA are inserted into brain tissue, numerous foreign body responses can occur, often resulting in a lack of biocompatibility of the implants. For example, if the electrodes are implanted for long periods of time, the formation of glial scar tissue can occur, which can encapsulate and isolate the electrodes from the neurons, resulting in a loss of electrical connectivity and increased impedance [50]. To avoid this problem, it is important to improve the biocompatibility of the electrodes. One of the strategies that can be used to minimize immune response to implanted electrodes is by coating them with bioactive molecules such as cell adhesion peptides or proteins. These peptides not only improve cell adhesion but also increase the cell proliferation [51].

Brain implant surgical operations are extremely high-risk for patients, so electrodes safety and efficiency must be well examined and verified before implant. Neuroprostethic devices are susceptible to the tissue response that causes failure in implanted electrodes. Therefore, the impact of implant presence *in vivo* over extended periods of time must be monitored.

Despite all the limitations and challenges, intracortical implants are the only way that have shown promise for restoring neurological functions lost to patients who have, for example in vision domain, a complex damaged retina, optic nerve, or lateral geniculate body [37].

It is widely understood that the challenges faced by the MEAs technology is largely finding appropriate geometry and materials that enhance consistent long-term recording/stimulation of large neuronal populations and improve electrodes biocompatibility. In recent years, nanotechnology has increased enormously to provide novel fabrication methods and materials. Conducting polymers and carbon nanotubes (CNTs) have attracted much interest as suitable materials for coating the electrodes. CNTs possess the exceptional chemical stability, electrical transport and mechanical properties to ameliorate both recording and electrical stimulation from/of neurons [17]. Strength and stiffness of CNTs prevents the tips of the electrodes from being fractured. The molecular/cellular biology approach attempts to minimize the immune response to implanted electrodes by using bioactive molecules. Such an approach is focused on

coating electrodes with peptides or proteins [51]. Still the implant microelectrodes technology needs to truly improve the technology to the level of clinical implementation.

1.4 Microelectrode arrays: a key element in neuroprosthetic devices

The major goal of the emerging field of neurotechnology is restoration of nervous system disorders. Neuroprosthetic devices that can record neural activities and stimulate the central nervous system (CNS), called brain-machine interfaces (BMI), enable direct communication with still-functioning parts of the neural pathways and offer significant potential to restore various lost neurologic functions of patients with vision impairment, epilepsy, Parkinson's or depression [52]. A key element in functions restoration is MEA dedicated to interface neural tissues [53]. The ultimate role of the MEA is to provide precise measurement and provide safe electrical stimulation of neural activities when chronically implanted in the cortex.

Remarkable progress has been reported at most bioelectronic levels of implantable BMI, but the electrode-tissue contacts (ETCs) remain one of the major obstacles. Contacts achieved using MEAs do not comply with the remaining parts of these BMIs due to the biological response to chronic implantation and to the electronic properties of MEAs. The success of these BMIs relies on electrodes which are in contact with the neural tissue. However, design and fabrication of an ideal interface with selectivity, good electric characteristics, sensitivity, biocompatibility, and long-term chemical and recording stability remain a tough challenge.

To date, implantable MEAs have been fabricated by three common techniques: microwire, micro-machined, and flexible arrays [1]. Microwires (made from tungsten or stainless steel) are used to focus on the individual neuron [54].One particular advantage of microwires is that they can be applied to access deep brain structures but the accurate location of the electrode tips relative to each other is not controllable because of the wire bending during implantation. Micro-machined electrode arrays can be silicon- or metal-based. This technique provides a higher density of electrode-tissue interface which reduces tissue displacement compared to microwires and contains active electronics integrated into the arrays [3, 25, 55]. These electrodes are designed to be implanted in the cerebral cortex or peripheral nerves. Flexible multi-electrode array is another type of electrode that provide an advantage over the rigid electrode arrays because of the closer mechanical match with brain tissue; however, the flexible nature of these electrodes involves some difficulties during insertion [56].

In recent years, MEAs techniques have been developed to have a long-term and stable interface with the tissues with the brain. Several research groups try to obtain consistent recording signals from small groups of neurons without losing microstimulation capabilities while maintaining low-impedance pathways for higher charge injection and high-spatial resolution by altering the material compositions and geometries of the arrays [57]. So far, none of these attempts have lead to a major breakthrough.

Our goal this thesis is to elaborate a biocompatible 3D MEA with high selectivity and sensitivity, good electrical conductivity, and high density of microelectrodes.

1.5 Objectives of the present work

The objectives we set out to accomplish at the beginning of this doctoral thesis project was design and fabrication of 3D, high-density, penetrating MEA for intracortical neural recording and stimulation. In particular, we wanted to improve the effectiveness of MEAs by a 3D structure when the needles have variable lengths such that the tips are no longer in the same plane, increase the density of the electrodes, decrease the impedance, and increase charge transfer. We also wanted to improve biocompatibility and durability of the electrodes for long term operation of the device implanted in neural tissue. The MEAs should cause minimum tissue response, i.e. encapsulation and inflammation. In addition, the ease of fabrication was important because when arrays become 3D, smaller, and higher in density, fabrication techniques are challenged to meet the dimensional and processing tolerances.

The thesis project can be summarized by the following objectives:

- Implement a novel micromachining technique to fabricate variable-height, penetrating, high-density neural MEAs that enable intracortical 3D recording and stimulation from/ of neural tissues
- Novel dry-film based masking technology that enhances uniform tip-exposure for electrodes with variable-heights and improve the conventional process which is costly and time-consuming
- Optimize the electrical properties of electrodes in order to achieve both the low impedance and high charge transfer by selective direct growth of CNTs on the tips of 3D MEAs

- Study the electrochemical behavior of MEAs as a function of frequency; electrochemical impedance spectroscopy (EIS), cyclic voltammetry (CV), and electrodes modeling
- Evaluate the impact of parylene-C, polyethylene glycol (PEG) hydrogel, and poly-D-lysine (PDL) on the biocompatibility of the MEAs while ensuring compatibility of the microelectrodes with neuroblast cells; cell culture and *in vitro* tests

1.6 Specifications of projected MEAs

The 3D MEAs, shown in Figure 1.1, provide a multichannel interfaces to the cerebral cortex. Micromachined electrode array is a 5×5 matrix of 1.65, 1.55, and 1.45 mm long electrodes in two perpendicular directions in order to create a pyramid-shaped array. The thickness of the electrodes is 200 μm at the base and about 2 μm at the tip with 100 μm spacing. Electrodes project out form a single block of a thin (2150±25 μm) p-type silicon (100) with a resistivity of 0.0153-0.0158 Ωcm while electrically isolated one from each other with glass paste from the backside. To make electrical connection to each electrode, the backside of each pin is metalized. The entire upper surface of the MEA (i.e. excluding the tips) is insulated with parylene-C. The tips of the electrodes are sputter-coated with Pt and iridium oxide using a novel masking method that enhances uniform tip-exposure for variable-heights electrodes. The tips of other group of arrays are coated by selective direct growth of CNTs while the shanks are insulated with native SiO_2. The variable-height penetrating MEAs presents a large surface area to the cortex and has the strong advantage that it floats in the cortical tissues. As the cortex moves the array moves with it, as a result producing little or no relative motion between the active sites and the neurons around it.

In order to improve biocompatibility of the MEAs, the surface of the electrodes is coated with PEG hydrogel which is a biocompatible polymer. To improve neural-cell adhesion and proliferation and also prevent electrodes encapsulation when they are implanted *in vivo*, electrodes are coated with bioactive molecules (PDL). The novel architecture of this MEA makes it unique among the currently available micromachined electrode arrays, as it provides higher density contacts between the electrodes and targeted neural tissue facilitating stimulation or recording from different depths of the brain.

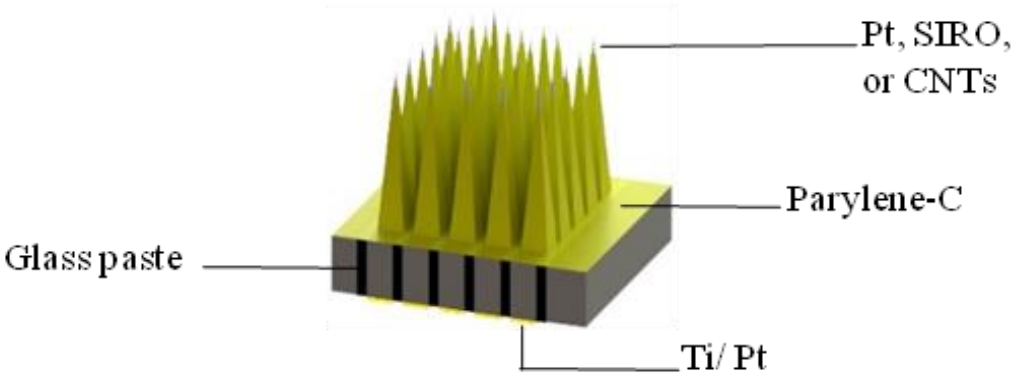

Figure 1.1. Schematic view of a silicon micromachined neural MEA with variable heights of 1.45, 1.55, and 1.65 mm. The shank was covered with parylene-C (and PEG) and the active sites of each array were coated with Pt, sputtered iridium oxide (SIRO), or CNTs. The thickness of the electrodes was 200 μm at the base and about 2 μm at the tip with 100 μm spacing.

1.7 Summary of contributions

In this thesis, we have achieved 4 main contributions with respect to the improvement of the neural MEAs performance implanted in neural tissues.

- Implement a novel pyramid-shaped, high-density, penetrating MEA: a micromachining technique was developed for building penetrating 3D MEA with a high electrode-density when the tips are no longer in the same plane in 2 perpendicular directions. The issue with current available array is that it is 2D and provides recording data from a plane of the brain. Even the slanted one is quasi-3D instead of 3D [23]. Such 3D high electrode-density array (25 electrodes/1.96 mm^2) is expected to record from different depths of the brain and provide more contacts between the electrodes and targeted neural tissue (greater access to neurons). The importance of such pyramid-shaped MEA has not been quantified but may have significance during injection electrodes inside the tissue. Variable-height electrodes may help to investigate more about neurons causal interactions ("effective connectivity").
- Introduce a novel masking technology: to coat the 3D pyramid-shaped MEA, a novel masking method was developed that resulted uniform tip-exposure for variable-height

electrodes and improved process time and cost significantly. The new method needs single masking step and reduced the conventional masking process steps from 14 to 6. The new procedure has several advantages including simpler and easier fabrication process, reduced production time and cost, and more uniform tip-exposure. More importantly, the conventional masking methods may not be practical for 3D MEAs since they cannot follow 3D structures.

- Optimize the electrical properties of MEAs: the impedance is one of the most important electrical properties for microelectrodes. In order to achieve both the low impedance and high charge transfer, the electrodes were coated with CNTs by selective direct growth on the tips of 3D MEAs for the first time using Plasma Enhanced Chemical Vapor Deposition (PECVD). The CNTs coating led to a 5-fold decrease in impedance and a 600-fold increase in charge transfer compared with Pt electrode.
- Improve biocompatibility of the MEAs: electrodes were coated with PEG hydrogel (well-known biocompatible polymer) to improve biological compatibility of the electrodes. In the next step, electrodes were coated with bioactive molecule; PDL. An *in vitro* study was performed to test the capacity of PDL to improve neural-cell adhesion and proliferation. Increased proliferation of the neuroblast cells on the microelectrodes was observed in the presence of the PDL. The PDL coating increased cell adhesion by more than 50%. It is noteworthy that the arrays with CNT active sites had greater cell numbers than the electrodes with metallic tips, both before and after PDL deposition. These results show that the CNTs increased biocompatibility and enhanced cellular responsiveness by attracting more neural cells.

1.8 Organization of the thesis

This thesis is presented in 5 chapters. In chapter 2, we review and compare different MEAs technologies and their characteristics. A technical overview of recent advances in the field of microelectrodes fabrication, characterization, and modeling is given. Moreover, the effect of different coatings to improve electrical properties and biocompatibility of the electrodes is presented.

The main body of the thesis is presented in chapter 3 and 4. In chapter 3, the experimental procedures of MEAs fabrication are described in detail. This chapter provides in depth explanation to the experimental techniques and characterization tools that were used during the course of this work. Next, the experimental results of MEAs microfabrication process, novel masking technology, direct growth of CNTs at the tips of the 3D MEAs, and the influence of CNTs on the electrical properties of the electrodes are presented. Besides, electrical circuit model of microelectrodes is presented in this chapter. In chapter 4, two different techniques to improve MEAs biocompatibility are presented. The role of biocompatible polymers and bioactive molecules to promote and stabilize cell attachment on the surface of the microelectrodes will evaluate by *in vitro* cell-culture tests.

Finally, Chapter 5 provides a general discussion of the results that are presented in the thesis. We will discuss what implications our work will have in the future of intracortical MEAs. The document will end with general conclusions and possible future work on fabricated MEA.

1.9 Publications

This thesis research has generated several results which were published in the form of scientific journal articles, poster, and oral presentations.

PUBLICATIONS:

- B. Ghane-Motlagh, M. Choueib, A. H. Mesgar, Md Hasanuzzaman, and M. Sawan, "Direct growth of carbon nanotubes on new high-density 3D pyramid-shaped Microelectrode Arrays for Brain-Machine Interfaces," Submitted to the *Journal of Biomedical Microdevices*.
- B. Ghane-Motlagh, T. Javanbakht, F. Shoghi, K. J. Wilkinson, R. Martel, and M. Sawan, "Physicochemical properties of peptide-conjugated microelectrode arrays and their in vitro effects on Neuroblast cells," Submitted to the *Journal of Materials Science and Engineering.*
- B. Ghane-Motlagh, Mohamad Sawan, "High-Density Implantable Microelectrode Arrays for Brain-Machine Interface Applications, " *Advances in Science and Technology*, 2014, 96, 95-101 .
- B. Ghane-Motlagh, M. Sawan, "Design and Implementation Challenges of Microelectrode Arrays: A Review," *Materials Sciences and Applications*, 2013, 4, 483-495.

POSTER AND PRESENTATIONS:

- B. Ghane-Motlagh, T. Javanbakht, F. Shoghi, K. J. Wilkinson, R. Martel, and M. Sawan, "High-Density 3D Microelectrode Arrays for Brain-Machine Interfaces," *37th Annual International Conference of the IEEE Engineering in Medicine and Biology Society (EMBC15)*, Milan, Italy, 2015.
- B. Ghane-Motlagh, M. Sawan, "High-Density 3D Pyramid-Shaped Microelectrode Arrays for Brain-Machine Interface Applications," *10th BioCAS Conference of the IEEE*, Lausanne, Switzerland, October 2014.
- B. Ghane-Motlagh, M. Sawan, "High-Density 3D Silicon-Based Microelectrode Arrays for Brain-Machine Interface Applications," *36th Annual International Conference of the IEEE Engineering in Medicine and Biology Society (EMBC14)*, Chicago, USA, 2014.
- B. Ghane-Motlagh, M. Sawan, "A Review of Microelectrode Array Technologies: Design and Implementation Challenges," *Second International Conference on Advances in Biomedical Engineering (ICABME13)*, Tripoli, Lebanon, 2013.
- B. Ghane-Motlagh, M. Sawan, "High-Density Microelctrode arrays," *6th International Research Network on Nano and Micro Systems (NAMIS) Autumn School*, Tokyo, Japan, 2012.

CHAPTER 2 OVERVIEW OF IMPLANTABLE MICROELECTRODE ARRAYS

This chapter will be devoted to a review of the microelectrode arrays (MEAs) which are using for stimulation and recording of/ from neural tissue. Both stimulation and recording microelectrodes use the same type of fabrication technologies. Next, the electrical and mechanical properties of the MEAs will be presented. Moreover, MEAs applications and variety of technologies that have been used to fabricate MEAs will be described and discussed. In addition, different methods to improve biocompatibility of the electrodes will be reviewed. Finally, an overview of recent advances in the field of implantable MEAs, equivalent circuit model, and perspective of this work will be given.

2.1 Introduction to neural MEAs

Neural MEAs are spatial arrangement of microelectrodes which serve as the first critical interface to the neural tissue for either signal recording or for tissue stimulation. Neural microelectrodes can be either penetrating or surface electrodes. The penetrating MEAs can measure small signals and require less power to stimulate neurons due to their high selectivity and sensitivity. Therefore, they are preferred for stimulate single units and fast recordings. The surface electrodes have low selectivity and sensitivity; however, they cause less tissue damage because they do not penetrate in neural tissue. In this thesis, our scope is penetrating MEAs.

The first type of microelectrodes in neural investigations were metal wire electrodes to monitor the extracellular electrical activity in 1950s [31]. The rapid development in microfabrication technology accelerated the advent of silicon-based MEAs. In 1970s, Wise et al. reported the first micromachined silicon-based MEAs to interface neural tissues [58]. Since this pioneer work, silicon-based microfabrication techniques are among the dominant tools in fabrication of neural microelectrodes. Silicon MEMS (micro-electro-mechanical systems) technology including micromachining techniques, photolithography, and thin-film deposition provided well-defined size and spacing of recording sites, high accuracy, the repeatability, and low cost fabrication scheme [59]. Besides, silicon micromachining facilitate the direct integration of electronic circuitry on the backend of active microelectrodes [60-62]. Silicon-based MEAs have been shown promising results in terms of biocompatibility for chronic implant *in vivo*; however, to improve the signal quality and long-term reliability the issues including implantation method,

physical and chemical properties of coating materials have to be considered [63-66]. The progress in microfabrication techniques enhanced the combination of functional silicon and polymer parts to reduce the mechanical mismatch between the neural tissue and the implant [67, 68]. Furthermore, 3D structure of the arrays has shown the potential for high-density recording and stimulation [69]. All the above results present the versatility of silicon MEAs technology for specific neural applications. The recent breakthroughs can conclude that there is still a lot of room to combine the state-of-the-art technology with that of silicon microtechnology for new possibilities to increase the resolution of stimulation and recording techniques [70].

Different types of MEAs are functionally similar in terms of recording or stimulation requirements, but the devices are different in depth including spatial arrangements and size of active sites, fabrication techniques, materials, and extensibility of advanced and organic materials. Critical parameters which affect the performance and effectiveness of the MEAs are:

- The density of the electrodes which is the ability of an array for higher or lower spatial resolution during recording and stimulation.
- The architecture of the MEAs as it can enhance the access to different depth of the brain and also to individual neurons.
- The impedance of the electrodes that should be low to reduce the stimulation voltage and the power. The high electrode impedance limits the ability to resolve the relatively weak neural signals.
- The mechanical compatibility of the electrodes (coating electrodes with polymers) with neural tissue that may minimize trauma to tissue during insertion.
- The durability and reliability of the MEAs is important for long-term operation of the electrodes.
- The biocompatibility of the electrodes must be taken into account to minimize the tissue response.
- Ease of fabrication should be considered as MEAs become smaller and challenges will be increased.

2.2 Properties of MEAs

The mechanical, electrical, and biological properties affecting the performance of the MEAs are discussed and reviewed in this section.

Mechanical properties: the shape, architecture, and materials are some of the important factors that can affect the mechanical properties of the electrodes [71]. The MEAs should be architecturally compatible with the geometry of the targeted tissue. A fit match between the array and the neural tissue avoid gap between them resulting less fibrotic tissue developed between the array and the target area. The 3D structure of the array with high electrode density may excite more population of neurons. Furthermore, the array geometry plays an important role in the tissue damage during the insertion e.g. design very sharp electrodes can help to reduce tissue damage. The brain tissue to compare with the electrode materials is relatively soft. The Young's module of the brain is between 15.9 Pa and 42.6 Pa [72]. To reduce reactive response, we have to choose the materials with Young's modulus close to the brain tissue.

Electrical properties: one of the most important electrical properties of the electrodes is impedance which is characterized as the magnitude of the impedance at 1 kHz; frequency that is used for neural electrodes since the center of energy of action potentials is about 1 kHz [73]. The impedance of the electrodes depends on the surface area ($R = \rho l/S$) of the active site (tip exposure). To reduce tissue damage and increase the selectivity, smaller electrodes are desired and the result will be high impedance and less sensitivity. Using materials with intrinsically larger surface area not only decreases the impedance but also increases the charge transfer through electrodes to the targeted tissue. In order to have identical electrical properties of each electrode in an array and interpret recorded signals during physiological experiments reliably, tip exposures should be uniform.

Biocompatibility: the implanted MEAs should not damage cells, tissue or enzymes, should not evoke a toxic, and should be stable in a long term without encapsulation. The most dominant reasons for short-term immune response are geometry (shape and size) [29], mechanical impact (design and implantation parameters) [74, 75], and surface properties [76]. Aforementioned parameters can efficiently contribute to delay or control immune response of the surrounding tissue in chronic implants. When the MEA are inserted into brain tissue, numerous foreign body

responses can occur. For example, if the electrodes are implanted for long periods of time, the formation of glial scar tissue can occur, which can encapsulate and isolate the electrodes from the neurons, resulting in a loss of electrical connectivity and increased impedance [50].

2.3 Application of penetrating MEAs

Neural interfaces, which allow direct and selective stimulation and recording of/ from neural tissues, offer significant potential to understand neurophysiological processes of human functions and behavior. They have also represented great promise restoring various neurological functions lost to disease, stroke or injury, control of assistive instrumentation for the patient with motor dysfunction, and neural prostheses to restore vision and auditory perception. In patients with neurological disorders, the communication between central or peripheral nervous system is damaged or disconnected that can cause full or partial paralysis of motor or sensory skills. The field of neuroprosthetic devices has been focused for many decades to improve the quality of life of paralyzed patients [77-80]. A part of goal of developing neural interfaces is to record neural signals. The firing pattern of neural signals, coming from the motor cortex, during a certain operation are recorded by implanted high-density MEAs then decoded and combined with behavioral changes to correlate the signals with certain "movement interactions". Thereby, a neural interface can potentially allow a patient to control her prosthetic limbs using intuitive movement intentions.

The design of neural interface devices depends on the application. Neural interface devices have been developed for application in the brain cortex, eye, ear, or around peripheral nerves [39, 81]. Over the past few years, an increasing number of studies have focused on MEAs that will interface to neurons of the visual cortex [12, 42] or to neurons of the retina [37, 82]. Neural interface devices are implanted chronically onto the visual cortex of a blind patient to electrical stimulation to restore the vision. Cochlear implant is the most successful biomimetic device which is already in commercial use [83]. The relative complexity of visual system and intracortical implant presents challenges to researchers attempting visual prostheses.

Develop a chronically stable interface for exchange of information between implanted device and biological environment is essential for any neural prosthesis. The current neural interface

application is based on using metal-, silicon-, or polymer-based microelectrodes placed in proximity of the target neurons (Figure 2.1).

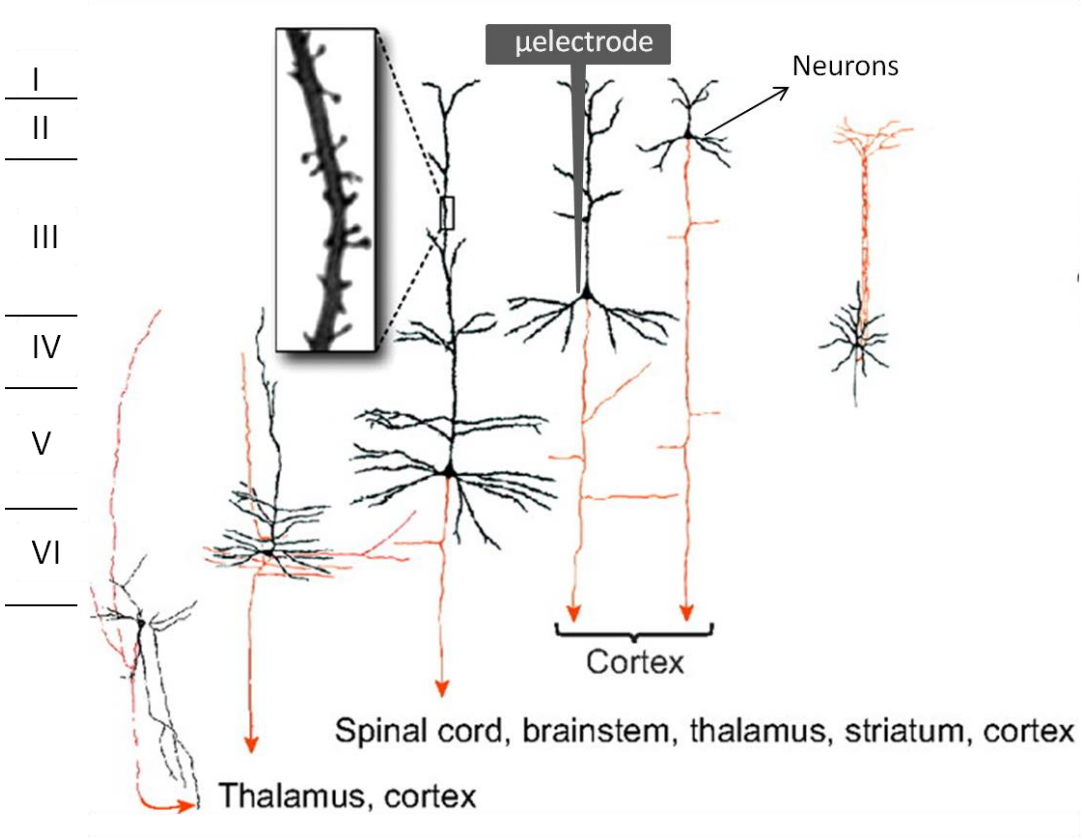

Figure 2.1**.** Implanted microelectrode in the cortex. Neural stimulation occurs via current passes through the tip to the surrounding neurons. Reprinted with permission from Ref. [13].

2.4 Fabrication technologies of penetrating MEAs

To this date, penetrating MEAs have been fabricated by a number of different techniques: microwires, micromachining, and flexible electrode approach. Since the fabrication technique affects the functionality of the microelectrodes some essentials should be taken into account in their design and fabrication such as 1) ease of fabrication to allow mass production, 2) ability to develop high-density sharp electrodes with various 3D architecture suitable for insertion into the cortex, and 3) compatible with IC manufacturing techniques. In terms of substrate material for the MEAs, silicon is still preferred material for fabrication and has been shown promising results; especially its chronic *in vivo* performance is quite remarkable also it can be shaped with

precision greater than perhaps any other material. Moreover, integrated electronic connect directly to the MEAs with using different packaging techniques.

In this section, we will review and discuss aforementioned techniques and their advantages and drawbacks.

2.4.1 Traditional Microelectrode arrays

Metal-wire electrodes

One of the traditional neural probes is single metal-wire electrode consist of a metal needle covered by insulation except at the tip. The tip of the wire is etched to form a sharp needle-shaped electrode. The entire surface of the metal-wire (excluding the tips) is insulated with quarts glass, Teflon (trafluoroethylene- TFE), or polymer films such as parylene and polyimide. Different types of metals like stainless steel, tungsten, platinum, iridium, and titanium nitride are used as a wire (Figure 2.2). Although the metal-wire electrode has a very sharp tip it is difficult to control the position and size of the opening of the electrodes.

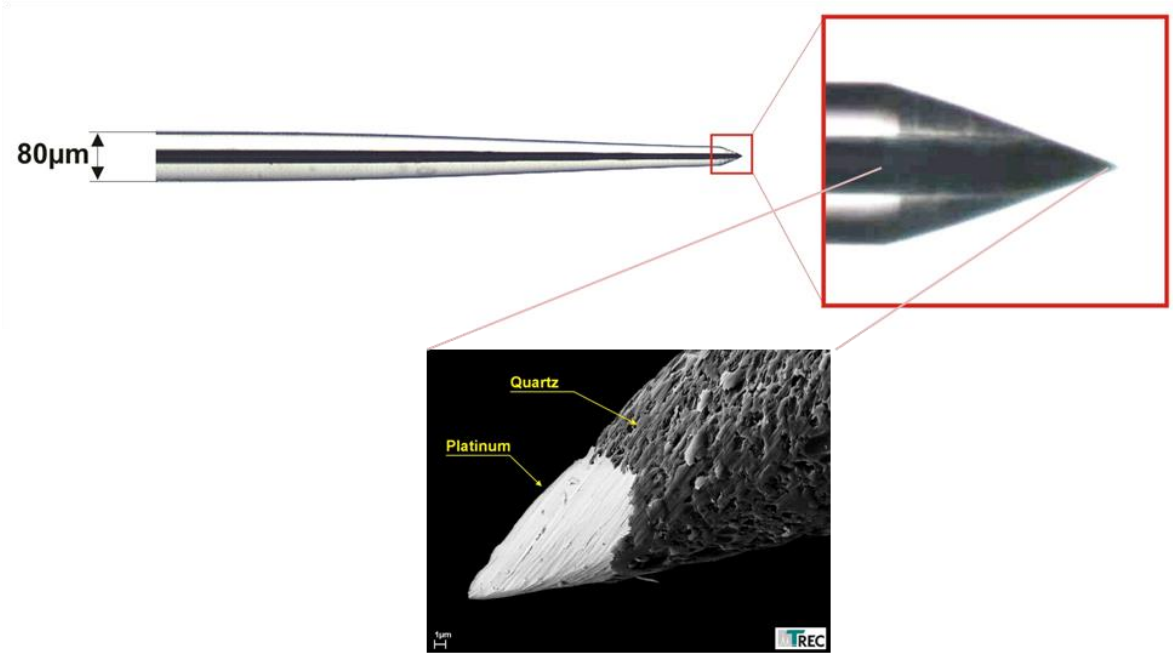

Figure 2.2. Scanning electron microscopy (SEM) images of Glass insulation and the metal part (Pt) of the metal-wire electrode. Reprinted with permission from Ref. [14].

Glass electrodes

Another type of neural electrodes are micropipettes that penetrate to the cell membrane and are generally used for intracellular studies. The common technique in the fabrication of such micropipette electrodes involves a two-stage pulling process. Briefly, a thin walled glass capillary tube which is 1 to 2 mm in diameter is heated electrically along the two extremities. When some extension occurs at the softened glass then larger tension is applied to make sharp tips at the breaking point. The diameter of the tip and the shank can be controlled by changing the pulling force and the temperature. To form the conductive path to the tissue, the micropipette is filled with an electrolyte like KCl. Such micropipettes have a very thin cone at the tips which is very fragile and hard to fill with electrolyte. They have also very high electrical resistivity. These types of neural probes are limited by high impedance and making an array of electrodes [84]. Figure 2.3 shows scanning electron microscopy (SEM) images of pre-processed pipettes (top) and optical microscopy images of conventionally processed pipettes.

Figure 2.3. SEM (top) and Optical microscopy images of pre-processed and conventionally processed glass pipettes. Reprinted with permission from Ref. [15].

2.4.2 Microwires

Microwires, made from tungsten or stainless steel, were the first implantable electrode arrays to record chronically from the brain. Their narrow structures let them be placed very close to single neurons *in vivo*. One advantage of microwires is that they can be applied to access deep brain structures [54]. Microwires typically consist of metal needles insulated with polymer film (parylene or polyimide) except at the tips. The tips of the metal wires are electrochemically etched to form a sharp tip. The diameter of the wires is normally less than 100 µm. Electrodes are then micro-welded and glued to a laser-drilled ceramic substrate to make a multiple-electrode array (Figure 2.4) [85, 86].

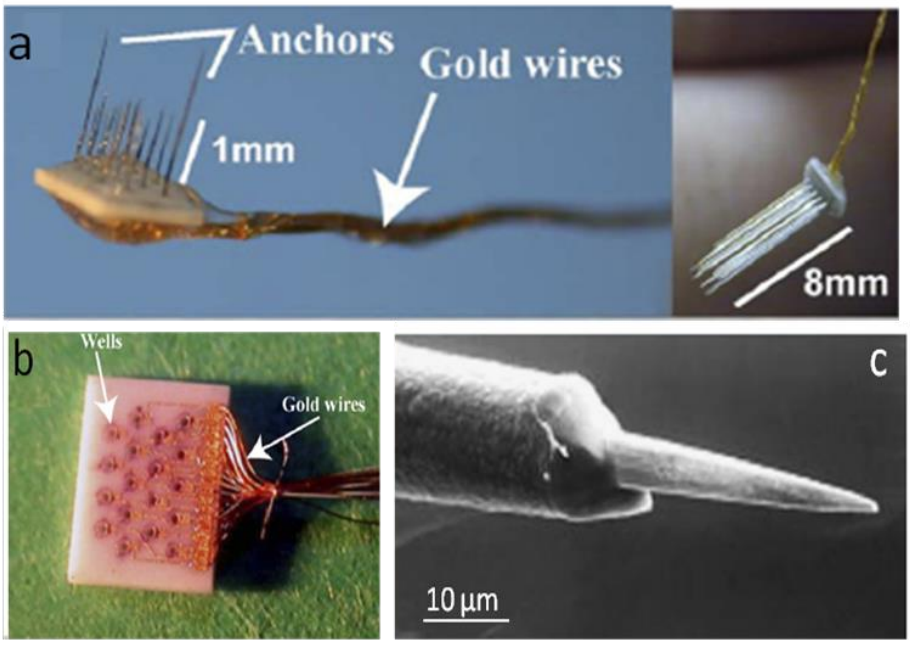

Figure 2.4. Microwires: (a) Wire microelectrodes embedded in ceramic substrate. The anchors ensure that the array stay in the brain, (b) Ceramic well-structure connected to parylene-C insulated gold wires. Electrodes are inserted perpendicular into the substrate, (c) SEM image of microwire insulated with 3 µm parylene-C except at the tip. Reprinted with permission from Ref. [16].

Metal microelectrodes are fabricated from different types of materials such as stainless steel, tungsten, platinum, iridium, or gold. Since stainless steel is fragile near the tips, tungsten was replaced due to the stiffness and rugged structure, and to provide very stable recordings;

however, tungsten is very noisy at low frequencies [87]. A platinum electrode plated with platinum black gives stable recordings, high signal-to-noise ratio (SNR), and creates a porous low-impedance structure, but it is mechanically fragile [88]. Iridium metal wire is extremely stiff, highly resistance to corrosion, and its surface is electrochemically activated, which causes it to increase the maximum charge density [89]. Microwires remain in use today and fabrication methods have not changed basically. They give long-lasting individual neurons recording, sometimes more than one year, so they allow neuroscientists to focus on individual neurons [86]. In all the above-cited cases, the final contact between electrodes and brain tissue is a metal.

Recently, carbon nanotubes (CNTs) have been used to coat the tips of the metal wire electrodes. In 2008, a group of researchers in Texas coated the tips of conventional tungsten and stainless steel wire electrodes with CNTs using electrochemical deposition method (Figure 2.5). CNT-coated electrodes not only provided an appropriate substrate for neural growth but also improved both the recording and stimulating characteristics of neural electrodes [17].

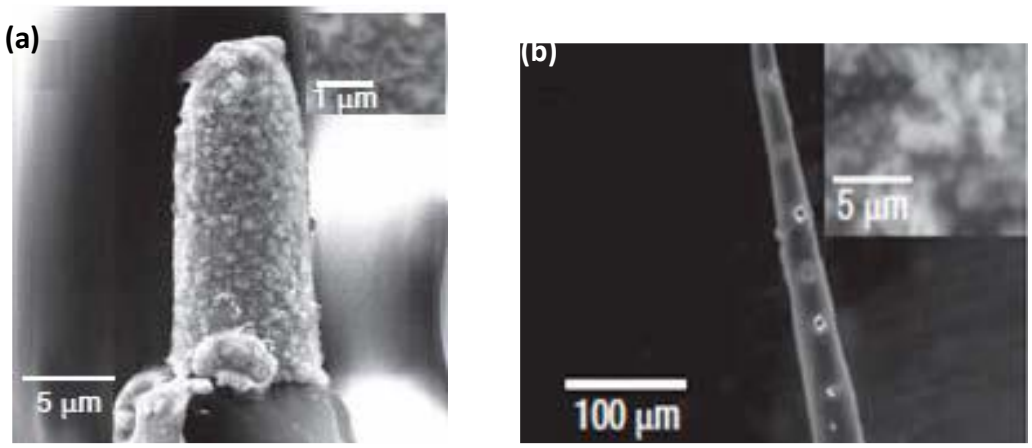

Figure 2.5. SEM images of metal microelectrodes coated with CNTs: (a) CNTs covalently attached to the tungsten electrode, (b) CNTs were electrochemically deposited at the recording sites of the electrode. Reprinted with permission from Ref. [17].

One particular disadvantage of microwires is bending of the wires during implantation, so the accurate location of the electrode tips relative to each other is not controllable. The micro wire electrode arrays are also limited in their geometry and reproducibility, causing considerable insertion tissue damage, and they are not always compatible with silicon-based integrated circuits.

2.4.3 Micromachined MEAs

Arrays of microelectrodes to record signals for a population of neurons or stimulate a network of neurons are necessary. Micromachined MEAs/ MEMS-based microelectrodes have advantages over other types of technologies including reproducibility, various architectures, high precision, and Complementary metal–oxide–semiconductor (CMOS)-technology compatible [44]. Silicon photolithography and micromachining techniques allow for exceptional control over electrode size, shape, spacing, and multiple active sites along the shank. Such a high level control on the structure of the MEAs enhances recording and/or stimulation from/of different depth of the brain. Furthermore, this technology provides the possibility to suit the geometry of the MEAs to the neural system under study. Finally, MEMS technology adds more possibilities, such as microfluidics for drug delivery and integrated micro actuators [90, 91]. The fabrication of micromachined electrodes mostly relies on two basic approaches; In-plane and out-of-plane penetrating MEAs. These types of microelectrodes will review and discussed in details in the following sections.

2.4.3.1 In-plane microelectrodes

Michigan Array

One of the first architecture was developed at the University of Michigan and Stanford University. In these MEAs, microelectrode contacts are patterned along the shanks. University of Michigan has designed a variety of penetrating microelectrodes including single-shaft, multi-shaft, and 3D structure of the shafts [58, 92-94]. Microelectrodes were fabricated using thin-film technology and micromachining techniques. Boron diffusion on silicon followed by wet etching defines the substrate shape of the electrode probes. The recording sites were located on the silicon substrate consisted of gold, Pt, or iridium. The conductors are insulated above and below by multilayers of dielectric materials such as silicon dioxide (SiO_2) and silicon nitride (Si_3N_4) (Figure 2.6).

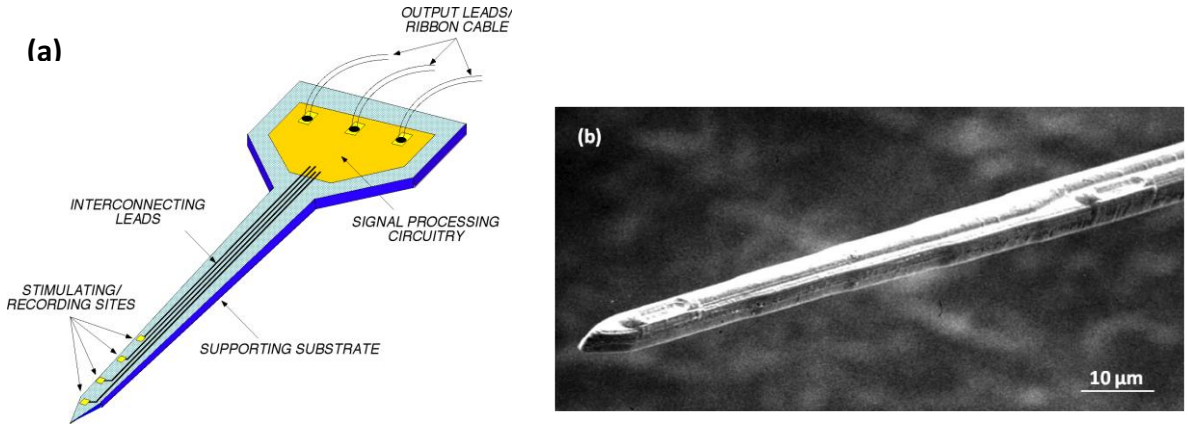

Figure 2.6. Michigan MEA: (a) Basic structure of a multisite microprobe presenting the substrate, insulation layers, and recording sites, (b) SEM image of the tip of neural microelectrode. Reprinted with permission from Ref. [18].

The silicon substrate shank is 15 µm thick, 3 mm long and 90 µm wide at the base, narrowing to 20 µm at the tip. The surface area of the recording sites is between 100 to 400 μm^2 (Figure 2.7).

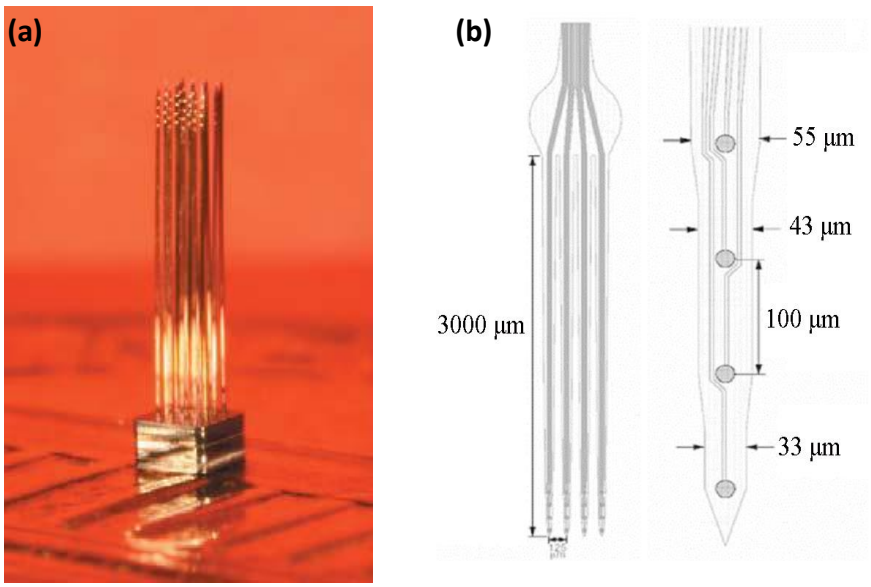

Figure 2.7. Typical Michigan array: (a) A prototype of the array, consisting of 64 sites on 200 µm centers with 1640 µm width and 4 mm long shanks. The interface is shown with the 1 mm × 1 mm × 0.5 mm base resting on a penny, (b) General schematic of the four-shank electrodes forming 16-channels probe. Reprinted with permission from Ref. [19].

The recording sites are typically made of iridium or gold. In order to improve long-term performance and electrical properties of the electrodes, recording sites were coated with conductive polymers such as polypyrrole (Ppy), poly (3, or 4- ethylenedioxythiophene-PEDOT), or CNTs. The results showed that CNTs incorporation by increasing the effective surface area could decrease site-tissue impedance [6, 95].

This kind of electrodes can easily merge with on-chip circuitry, signal processing, and wireless interfaces. Although these electrodes have been successfully used for a lot of application, there are few limitations of this technology. There is a minimum thickness limit for Michigan probes as wet etching process has been used for making sharp tips. The insertion of the probes need special guide. Thus, the shanks cause large tissue displacement and may damage significant number of neurons during insertion. These probes are fabricated through a process using several photolithography steps that is expensive and time consuming [96]. Thin silicon-film cable is easy to break and is not robust enough.

Flexible array

A variety of MEAs has been developed for recording and stimulation neural activities; however, most MEAs are based on a rigid substrate and cause neural damage and inflammation at the implant site for intracortical implant. Flexible arrays provide high mechanical flexibility, good biocompatibility, and high resistance to solvents [10]. Different polymers such as polyimide and parylene are used as a structural substrate. Polyimide-based intracortical MEAs are fabricated with standard planar photolithography CMOS compatible technique on silicon. In this technique, the electrode metal layer is sandwiched between two polyimide layers without using silicon structure. The 3D structure of the flexible probes are formed by bending the shanks out of the 2D plane (Figure 2.8) [20]. Polyimide also provides an ideal surface for the selective attachment of bioactive molecules onto the device which improve long-term reactions at the electrode-tissue interface [97].

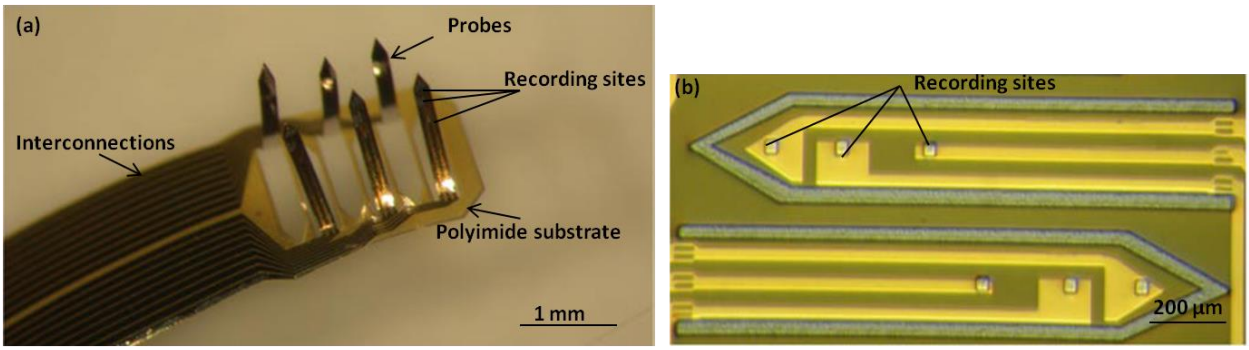

Figure 2.8. Flexible multi-channel MEAs: (a) 3D flexible MEAs after folding, (b) Each probe with 3 recording sites. Reprinted with permission from Ref. [20].

Growth CNTs on the recording sites of polyimide substrate could improve both the electrode impedance and the charge-transfer capacity (Figure 2.9) [21].

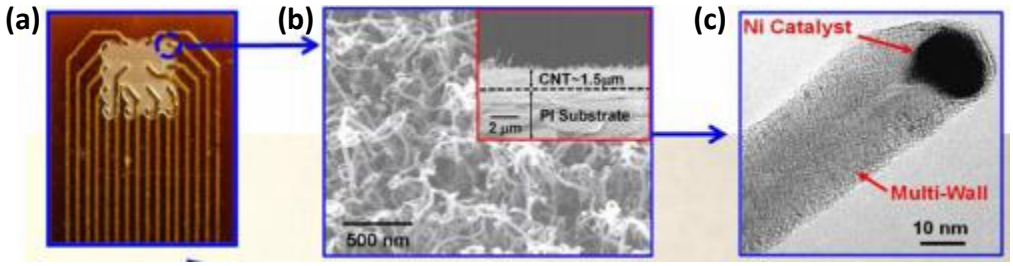

Figure 2.9. Flexible MEA: (a) A magnified photo of the 4×4 electrode array, (b) SEM image of the grown CNTs, (c) High-resolution transmission electron microscopy (HRTEM) image of the grown CNTs. Reprinted with permission from Ref. [21].

A new parylene-based multi-sided MEA with electrode sites at the top-side, back-side, and edge has been presented for neural recording and passive drug delivery. This feature creates the smallest footprint (85 μm^2) to date of a functional recording electrode [98].

The flexibility of polyimide may improve the mechanical mismatch between rigid electrodes and neural tissue but a major drawback to this technique is the microelectrodes are not enough stiff to insert into the brain on their own, so a stiff supporter is needed for the insertion. Moreover, polyimide-based MEAs are inclined to failure because of possible moisture absorption by

polyimide. Polymers interconnect cables that are used for the interconnections, required different bonding methods to compare with silicon neural probes.

Silicon on insulator (SOI) probes

A new silicon-on-insulator (SOI)-based MEAs was developed in Caltech and Stanford using a plasma and wet etching process to define the probe outline and make sharp tips [99]. The method was improved using only deep reactive ion etching (DRIE) process on SOI substrate with SiO_2 layer acting as an etch stop. The array of iridium and gold electrodes were patterned on top of the shaft by E-beam evaporation (Figure 2.10) [22]. In some fabrication methods polydimethylsiloxane (PDMS) was used as an adhesion layer between electrodes and neural tissue. In this technology, the thickness of the probe is determined by the thickness of the SOI wafer as a result only one thickness of probe can be fabricated from the same wafer. Since the SOI wafers are expensive the fabrication process will be costly.

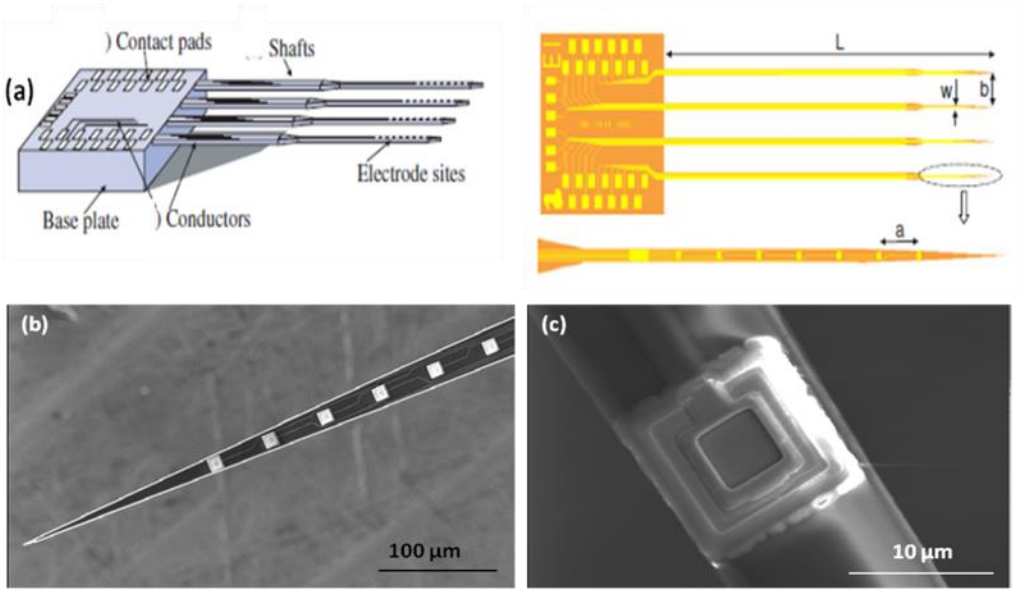

Figure 2.10. SOI-based probe: (a) Schematic of the probe structure, (b) SEM image of a probe tip. The thickness of the interconnect lines is 1 µm, (c) SEM image of the 1 µm × 1 µm iridium recording site. Reprinted with permission from Ref. [22].

2.4.3.2 Out-of-plane microelectrodes

Utah electrode array

Utah electrode array was invented by R. A. Normann at the University of Utah. Utah and Utah Slanted electrode arrays include sharpened silicon needles electrically isolated from each other. Electrodes are silicon-based and electrically separated from the backside using diamond saw and glass paste. Electrode columns are separated from the other side of the wafer by again sawing. Wet-etching process is used to transfer electrode columns to the needles. Parylene-C is used to insulate the body of the electrodes excluding the tips. The tip of the electrodes is coated with platinum or iridium oxide (Figure 2.11) [100]. The architecture of these electrodes enables single-unit recording with high-spatial resolution, and excites the neurons by electrical stimulation. This type of electrodes is fabricated out-of-plane. Thus, the maximum length of the electrodes depends on the silicon wafers thickness. The longest Utah electrode is 1.5 mm and only one recording site can be made in each pin as a result the MEAs provides more selective stimulation/ recording of/from the neural tissue to compared with in-plane MEAs. Connectors are wire-bonded to the electrodes.

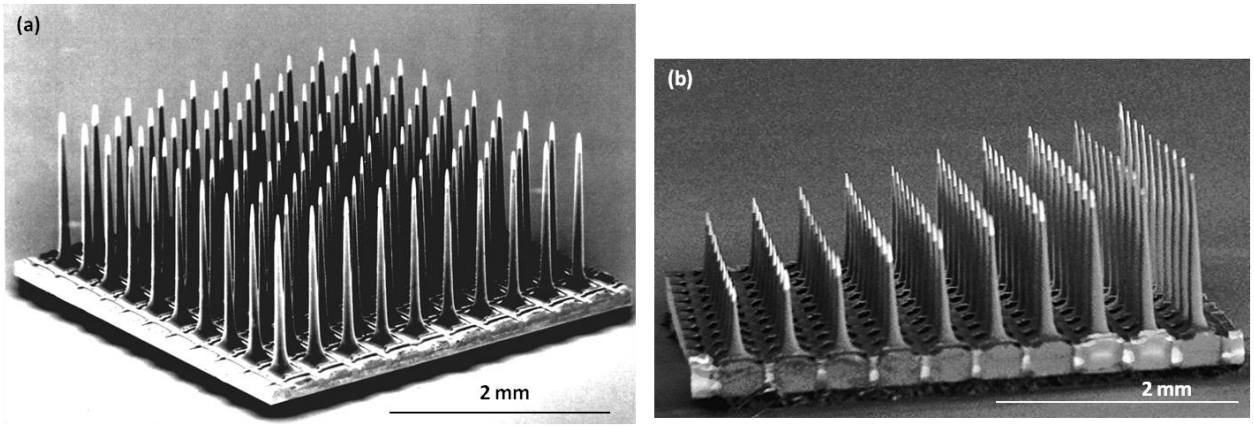

Figure 2.11. Utah silicon-based MEAs: (a) 2D flat electrode array; (b) Slanted electrode array. Reprinted with permission from Ref. [23].

The drawback of this MEA architecture is that it is 2D which provides recording data only from a plane area of the brain. Even the Slanted Utah array is quasi-3D instead of 3D [101]. The vast

wire-bonding is used to connect the array to electronic circuitry which limits the productivity. Moreover, the stiffness of the wire bundle makes some limitation during implantation.

Electrical discharge machining (EDM)

The ultra-high aspect ratio metal-based MEAs were fabricated using Electrical discharge machining **(**EDM) technique associated with electrochemical steps [25]. Fabricate variable architectures are possible with this technique. The electrodes were made from stainless steel or titanium. Electrodes were insulated from each other by epoxy. After chemical etching to smooth the electrodes surface, electrodes are insulated with parylene-C excluding the tips. Pt is electro-deposited at the tips to facilitate charge transfer from electrodes to the neural tissue (Figure 2.12). This MEA was developed to be assembled with integrated circuits on a thin substrate [24].

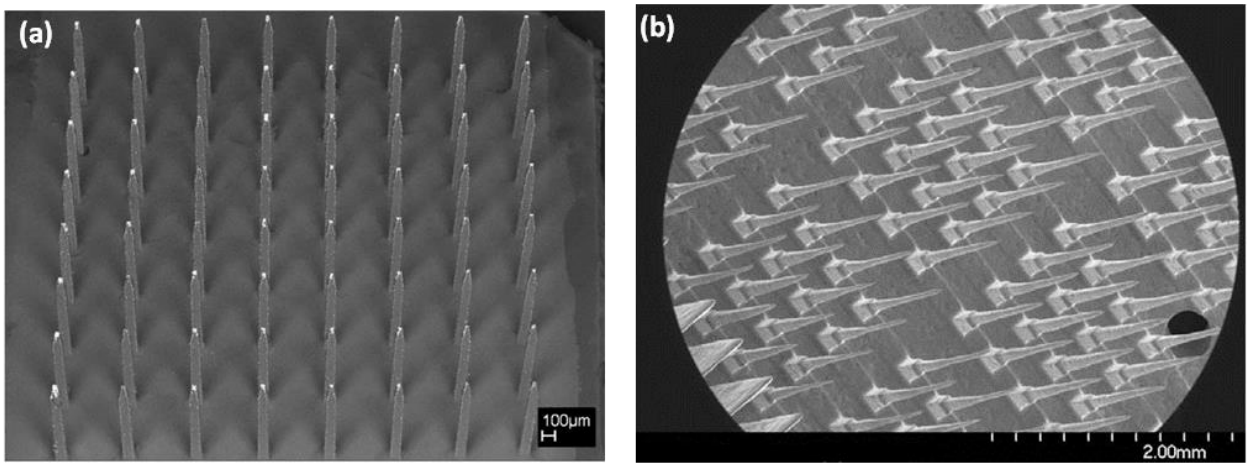

Figure 2.12. Metal-based MEAs using EDM technique: (a) SEM image of a parylene-coated assembly, consisting of Pt-coated electrode tips, (b) Stainless steel electrode arrays after electrochemical polishing. Reprinted with permission from Ref. [24, 25].

2.4.4 Other approaches to MEAs fabrication

Patch clamp

The patch clamp technique is used in the study of excitable cells such as neurons cardiomyocytes, muscle fibers, and pancreatic beta cells. This technique was developed in 1970s to record the current of single ion channel molecules for the first time, which improved

understanding of the role of channels in the fundamental cell processes such as action potential and nerve activity [71].

The patch-clamp consists of an electrode inside a glass pipette. Depending on the experiment the pipette can be filled with a solution matching the ionic composition of the cell. The pipette is brought in contact with a very small area or patch of neural membrane. By applying gentle suction to the pipette a giga-seal is formed between the pipette and the cell membrane. An electrical seal (high resistance) between the cell membrane and the pipette results in electrical isolation. Applying suction breaks the patch of the cell membrane in contact with the pipette and the inside of the cell is accessible (Figure 2.13). The currents passing through the ion channels of the cell can measure with electrode while keeping the membrane voltage constant. The issue with patch clamp is that maintaining contact with the cell for a long time is difficult and may result in destruction of the cells. Another problem is we cannot have an array of patch clamp electrodes for recording.

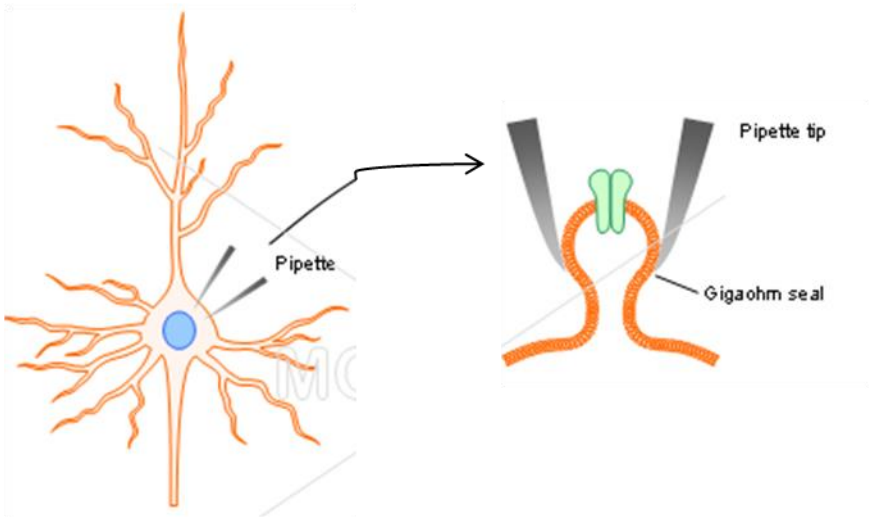

Figure 2.13. Patch clamp recording form the neuron cell. In the cell-attached configuration, the patch electrode is sealed to the surface of the intact cell allowing channel activity in the patch of membrane under the electrode tip. Reprinted with permission from Ref. [26].

Silicon-wire array

A micro silicon-wire penetrating MEA with on-chip circuits has been developed for neuroelectronic interface systems. The high-density and low-invasive silicon (Si) probe with a few microns in diameter was fabricated using selective vapor-liquid-solid (VLS) growth method

on Si (111) wafer in predetermined positions and probe sizes [27]. The diameter of the Si probes is controlled using patterned gold dots deposition while the probe length is controlled applying the growth rate of 0.5 µm/min. Silicon probes with the length of 160 µm and 3.5 µm diameter at tip, were obtained after 2 h growth at 700 ºC and the Si_2H_6 gas pressure of 3×10^{-3} Pa. Wring process for on-chip circuits on silicon wafer was performed prior to VLS growth. Si probes were grown perpendicular to the wafer surface. The greatest advantage of this fabrication technology is that the microelectrode array can be integrated with IC signal processors on the same substrate (Figure 2.14). Although the authors presented a novel fabrication method including of integration a probe with the IC; however, the performance of the IC in the *in vivo* has not been demonstrated yet.

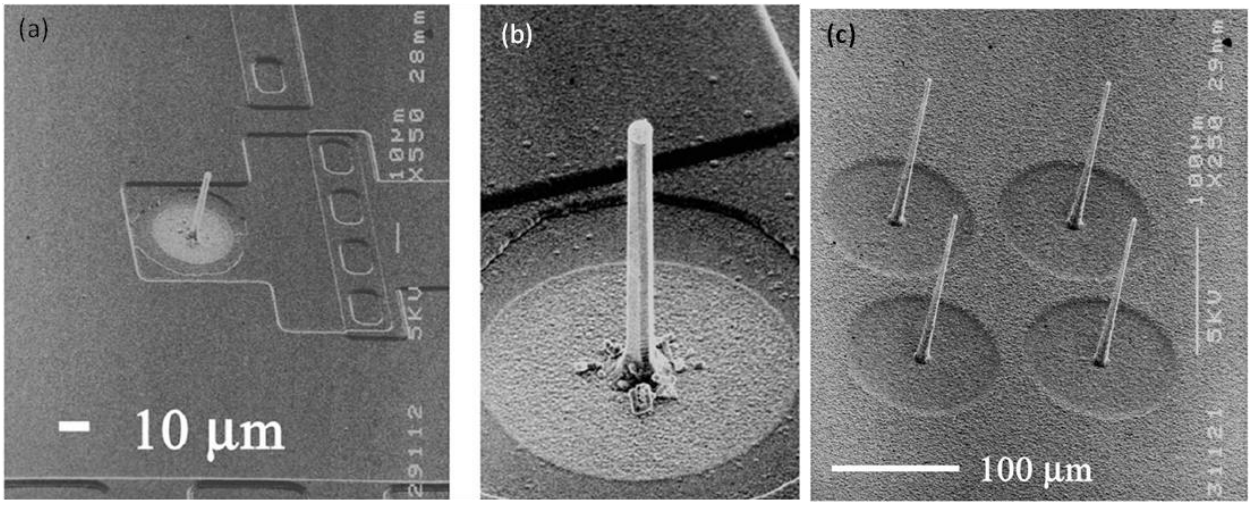

Figure 2.14. The silicon-wire probe on Si (111) with W wiring circuit: (a) SEM image of silicon-wire probe combined with wring process for on-chip circuits on same a silicon wafer, (b) Silicon probe in 30 µm in length and 2 µm in diameter at a growth temperature of 600 ºC for 30 min, (c) 2 × 2 array of selective silicon-wire probes with 160 µm in length and 3.5 µm diameter at tips. The VLS growth was performed at 700 ºC for 2 h. Reprinted with permission from Ref. [27].

Interfacing neurons and semiconductor chip

Another approach is direct non-invasive interfacing of neurons and transistors. In this method, a semiconductor chip joins to the nerve cells. Fromherz has worked on electrical interfacing of individual neurons and silicon microstructures, as well as the assembly of hybrid systems made of neuronal networks and semiconductor microelectronics. Transistors are coupled to neurons for

recording without electrochemical processes. To couple electron-conducting semiconductor and the ion-conducting neurons, a close contact of cell membrane and oxidized silicon with a high resistance of the junction is required. Neuron excitations (action potentials) can be recorded by capacitive contacts and by transistors. This integrated system can be achieved by the outgrowth of neuronal networks on the surface of silicon chip and implementing electrical circuits on the chip [28]. Figure 2.15 is shown the combination of ion channels on a transistor when the cells were injected on the device using a glass capillary.

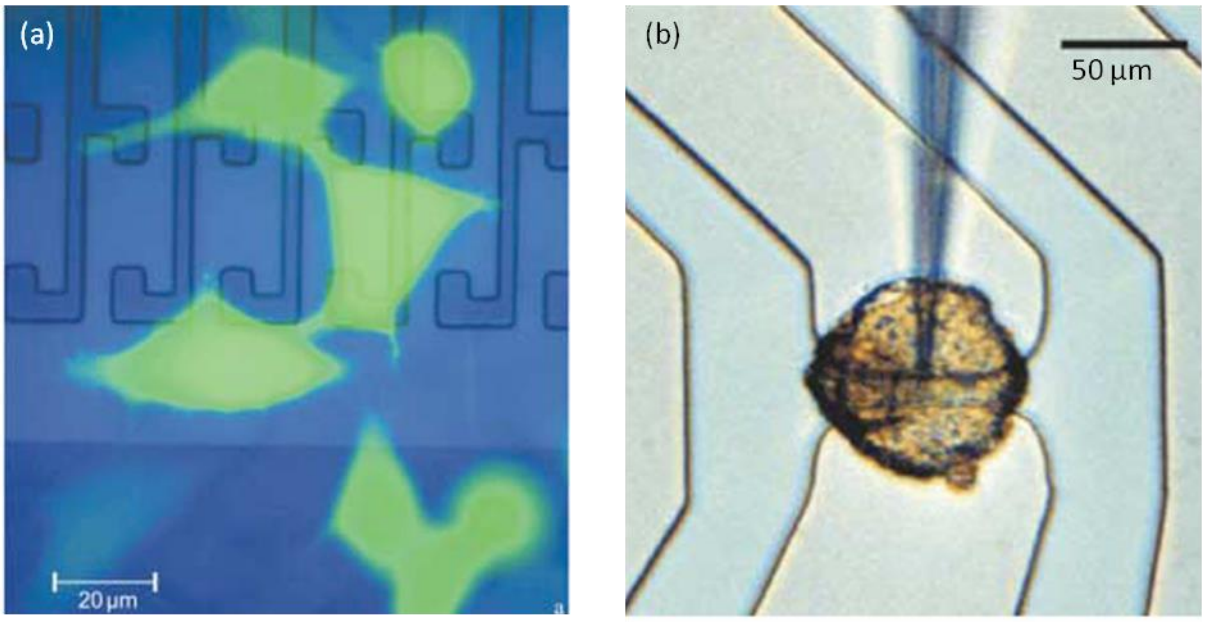

Figure 2.15. Combination of ion-channel on a transistor: (a) HEK293 cells with a hSlo potassium channel on a silicon chip with a linear array of transistors. The cells appear in the color of the florescence of GFP, (b) Nerve cells from the leech on the open gate oxide of a field-effect transistor. The n-type silicon chip are shown in dark, the p-doped sources and drains are bright. The gates with the length of 1.8 µm and the width of 20 µm show no contract. The cell was injected using a glass capillary. Reprinted with permission from Ref. [28].

In order to stimulate the neurons and inject sufficient current into the junction, a high capacitance per unit area of the chip under the cells is required due to solid-electrolyte interface without Faradic current. Stimulation spots were fabricated efficiently by high local doping of silicon and insulation with a thin layer of silicon dioxide.

To interface a neuronal network with a semiconductor chip, a circular array of two-way contacts made of a capacitive stimulation spot and a transistor was fabricated. Individual neurons from the pond snail were placed on the chip and let the neurons join by random outgrowth in the central area. Around each two-way contact, pins of polyimide were fabricated using photolithography to immobilize the neurons. Figure 2.16 demonstrates neuronal network on silicon chip. Voltage pulses were applied to stimulate neurons and elicit an action potential in neurons. The signal was recorded by an adjacent transistor.

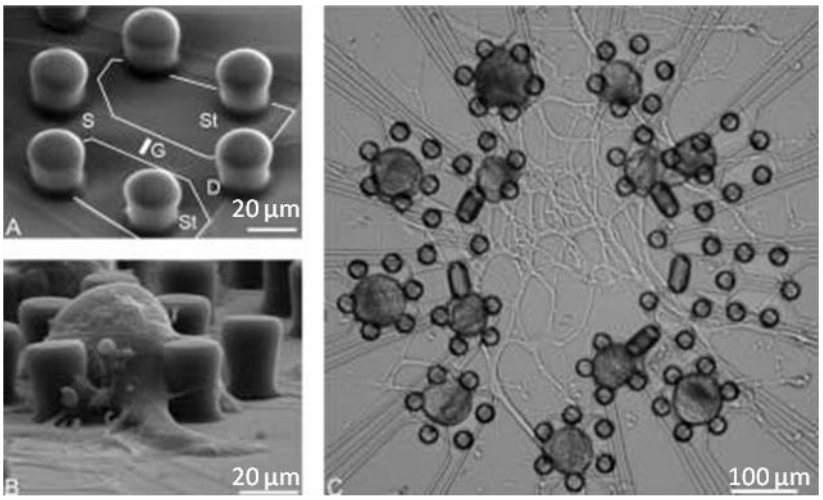

Figure 2.16. Neuronal network on silicon chip: (a) SEM image of a two-way contact with the pins of polyimide. St (stimulator wings) and transistor (S: source, D: drain, G: gate), (b) SEM image of immobilized neurons form the pond snail after three days in culture, (c) SEM of a neuronal network with the cell bodies on a double circle of two-ways contacts after two days in culture. Reprinted with permission from Ref. [28].

2.5 Comparison of penetrating microelectrodes technologies

Findings to date demonstrate different methods for recording and stimulating neuron activities; however, all these methods have some drawbacks. The following tables (Tables 2.1, 2.2, and 2.3) show a brief comparison of various techniques to fabricate penetrating MEAs.

Table 2.1. Advantages and drawbacks of MEAs fabrication methods [1-4]

Method		Advantages	Drawbacks
Microwires		-Long-lasting and single-neuron recording -Access to deep brain structures -Multi-neuronal recordings for simultaneous recording at the level of neural populations	-Electrode tips location cannot be controlled (to bend during implantation) -No embedded microfluidic channel -Incompatible with electronic integrated circuits which are silicon based -Limited in their geometry and reproducibility
Micromachined arrays	In-plane	-Spatial relation between the electrode sites remains fixed -Reproducible with high spatial resolution (thin-film technology) -Facilitates current source density analysis because of linear arrangement of recording sites along a single shank	-More tissue displacement because of the shank -Dura mater should be removed for inserting the electrodes -More damages in the brain tissue due to large electronic structure -Rigid and may fracture -Several photolithography steps (expensive and time consuming)
	Out-of-plane	-High degree of selectivity in stimulation and recording -Ease of implantation -Compatible with IC manufacturing technique (silicon-based MEAs)	-Rigid and may fracture -Lack of 3D structure - The vast wire-bonding limits the productivity
Flexible arrays		-Good electrical insulation and adhesion properties -Conformal coverage with the brain tissue surfaces -Reduces the chronic tissue inflammation response	-Flexibility nature implies difficulty in insertion -Possible moisture absorption by polymers

Table 2.2. Characterization of MEAs technologies [5, 6]

MEAs			Recording sites	Mean charge density (mC/cm^2)	Mean Z_{1kHz} ($k\Omega$)
Silicon-based	Utah array	SIROF	96	2	6.1 ± 0.2
		Pt	96	0.3	125 ± 0.25
	Michigan array	Ppy[1]	64	19.5 ± 2.1	184 ± 5.3
		PEDOT[2]	64	2.5 ± 1.4	392 ± 6.2
TDT[3] Microwires			48	5.10 ± 0.40	19.9 ± 0.82

[1]Ppy: Polypyrrole
[2]PEDOT: Poly (3, or 4- ethylenedioxythiophene
[3]TDT: Tucker Davis Technologies.

Table 2.3. Comparison of microelectrodes structure [7-10]

MEAs		Probe/ Site geometry	Substrate material	Recording site material
Microwires		Diameter: 50 µm Spacing: 400 µm Tip angle: 45°	Tungsten, Stainless steel, Pt, Titanium Polyimide/ Parylene-C insulation	Tungsten, Stainless steel, Pt, Titanium
Silicon-based arrays	Utah array	Shank length: 1.5 mm Base: 1.6 mm^2 Spacing: 400 µm	Boron doped Silicon Parylene-C insulation	Pt, SIROF[1], CNTs
	Michigan array	Shank length: 3mm Probe thickness: 15 µm Probe width: 33-55 µm Spacing: 100 µm	Silicon Silicon dioxide/ Silicon nitride/ Parylene-C insulation	Gold, Iridium oxide, PEDOT, CNTs
Flexible arrays		Shank thickness: 15 µm	Polyimide/ Parylene/ Benzocyclobutene	Gold, Ppy, PEDOT

[1]SIROF: Sputtered iridium oxide film

2.6 Planar microelectrode arrays (pMEA)

Planar microelectrode arrays (pMEA) represent a unique device to monitor the activity of neuronal networks. The first pMEA recording obtained from cultures of neurons (ganglia form neonatal rats) by Pine in 1980 [102]. These devices are fabricated by standard photolithography techniques and are like a petri dish with electrodes embedded into the culture substrate and connected to the recording/ stimulation system. Highly sensitive sensors require a low limit of signal detection and a high signal-to-noise ratio. This can be achieved by increasing the electrochemical active surface area without increasing the overall geometric dimensions. Nanostructures such as gold nanowires, platinum nanowires, silicon nanowires, and CNTs are promising structures when they are integrated onto sensing microelectrodes due to their high surface-to-volume ratio. CNT offers very large surface area comparing with other nanostructures. CNTs can be synthesized in-situ, synthesized on a growth substrate then transfer to the main substrate, or grow directly on substrate by a chemical vapor deposition (CVD) technique. SEM images of planar microelectrode array combined with vertically aligned CNTs onto recording sites has been shown in Figure 2.17.

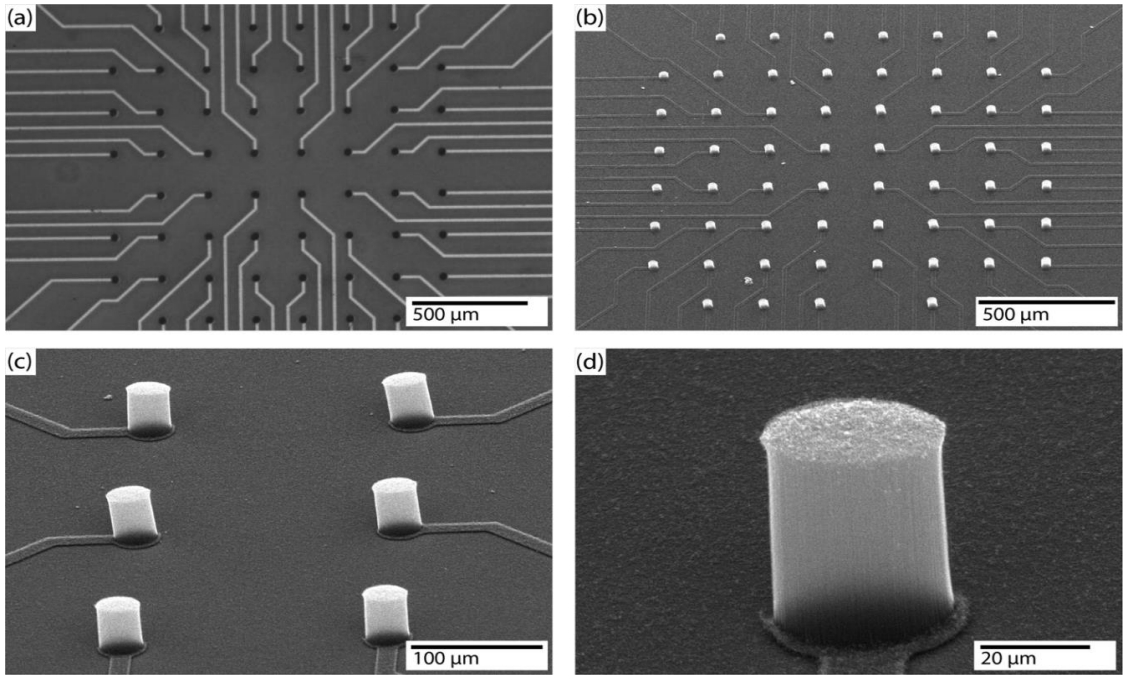

Figure 2.17. SEM images of planar microelectrode array with 60 individual CNT electrodes. Circuit paths are insulated with 100 nm silicon dioxide layer: (a) Top view of the planar microelectrode array showing the 60 individual electrodes, (b-d) Different magnification of

vertical CNT electrode network and a single CNT electrode. Reprinted with permission from Ref. [11].

To fabricate microelectrodes with vertically aligned nanotube networks, highly doped poly-silicon is deposited onto a silicon dioxide substrate then structured by photolithography and dry-etched by reactive ion etching. The resulting electrodes and circuit paths are insulated by an oxide layer. In the next step, resist is spin coated and structured by photolithography. Recording sites will be opened using hydrofluoric etching. The catalysts (Aluminum/ Iron) will deposit onto recording

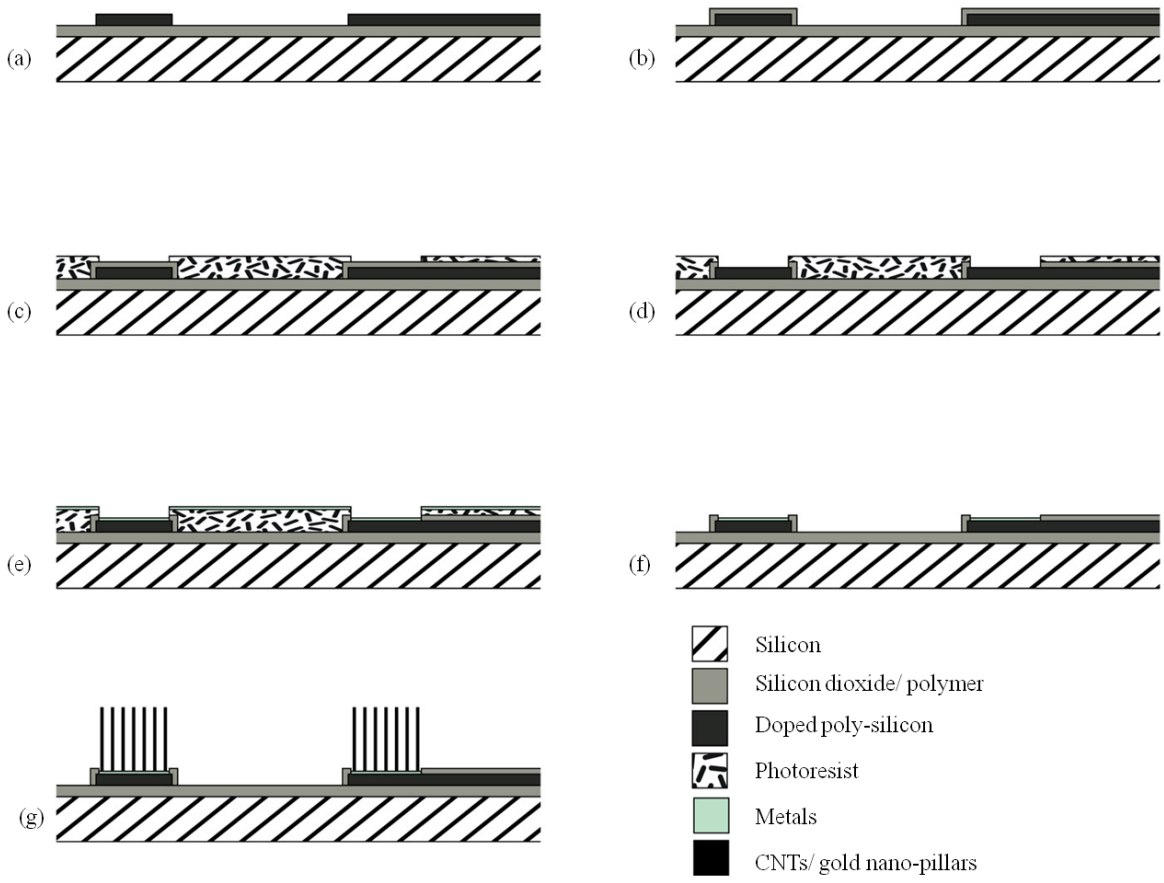

Figure 2.18. Process flow of microelectrodes fabrication with vertically aligned CNT networks: (a) Deposition of poly-silicon on silicon dioxide by photolithography and dry reactive ion etching, (b) Insulation electrodes and circuit path with a thermal oxide layer using dry thermal oxidation, (c) Resist spin coating and photolithography, (d) Hydrofluoric etching to open the electrode sites, (e) Aluminum and iron deposition that works as catalysts, (f) Remove the resist, (g) Direct CVD growth of vertically aligned CNTs. Reprinted with permission from Ref. [11].

sites prior to CNTs deposition. In the last step, vertical CNTs are grown using CVD technique (Figure 2.18) [11].

For electrochemical characterization, microelectrodes were studied by electrochemical impedance spectroscopy and cyclic voltammetry. Phosphate-buffered saline was used as an electrolyte and Ag/AgCl electrode as a reference electrode. Results for a planar poly-silicon electrode (before CNTs deposition) and electrodes with short vertically aligned CNTs grown on poly-silicon electrodes with a height of 2 μm are shown in Table 2.4.

Table 2.4. Impedance of the poly-silicon electrode before and after CNTs deposition [11]

CNTs height (μm)	Impedance at 1 kHz in kΩ
0	1687 ± 243
2	29.7 ± 7.5

To deposit gold nanopillars instead of vertical CNT networks onto active sites of the microelectrodes, the track-etched polycarbonate nanopore membrane is used as template which is commercially available and provides the fabrication of one dimensional metallic nanomaterials on substrates. The height of the metallic structure is several micrometers. The process is integrated into the fabrication process and no transfer of nanostructures is required.

The performance of nanopillar electrodes was investigated at 1 kHz frequency which is suited best to compare the performance of microelectrodes since the range of biological signals is 800-3000 Hz. Results of impedance measurements has been shown in Table 2.5 for different naopillars height [12]. SEM images of processed microelectrode arrays are shown in Figure 2.19. In first two microscopic pictures (Figure 2.19 (a) & (b)), nanopillars are appear in dark spots. The nanostructure of the gold nanopillars are shown in Figure 2.19 (c) & (d). The diameter of the nanopillars is 200 nm and the height is varies between 4 to 22.5 μm.

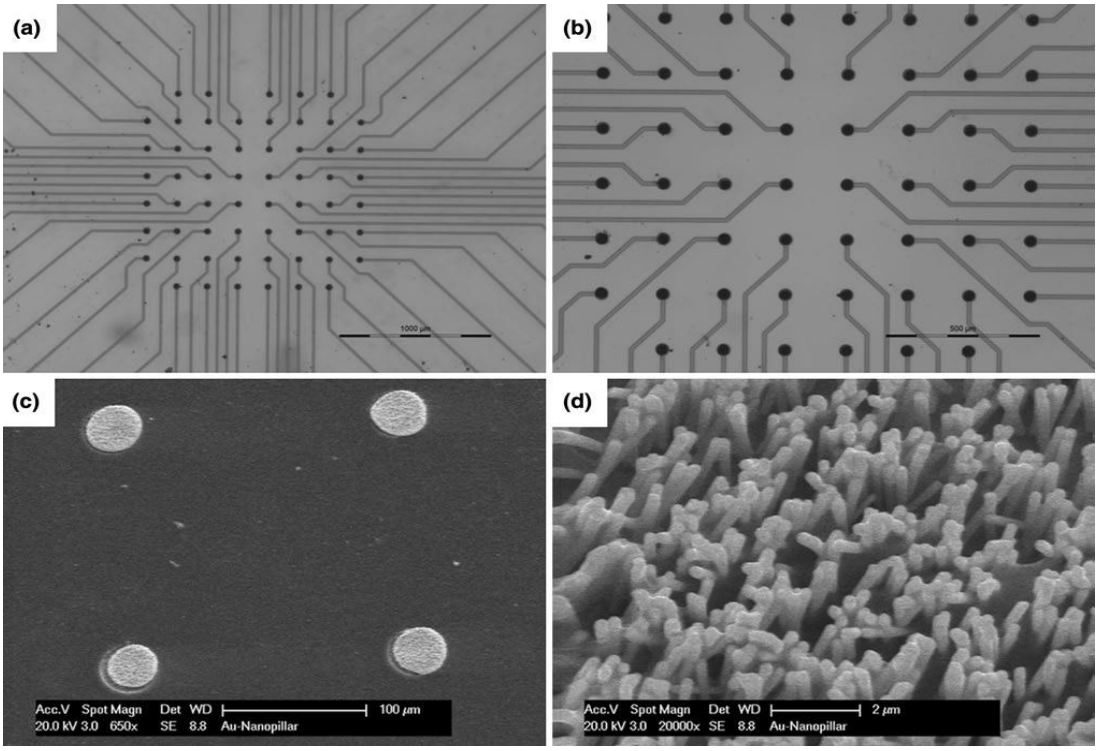

Figure 2.19. SEM images of planar microelectrodes with gold nanopillars onto the recording sites: (a-c) Top-view of planar microelectrodes with different magnification. Gold nanopillars appear dark, (d) nanostructure of goldpillars with a diameter of 200 nm and the height of 22.5 µm. Reprinted with permission from Ref. [12].

Table 2.5. Measured impedance of electrodes with diameter of 40 µm as a function of gold nanopillar height [12]

Gold nanopillar height (µm)	Impedance at 1 kHz in kΩ
0	1172.3 ± 241.6
4.8	362.3 ± 42.7
8.5	196.2 ± 43.2
12	103.62 ± 36.7
16	55.3 ± 8.7
19	26.1 ± 10.4
22.5	± 2.7

2.7 Improve biocompatibility of microelectrodes

Chronically implanted electrodes have the potential to ameliorate the quality of life of patients suffering from neurological diseases. These arrays are implanted for a long-term into the patient's cortical tissue to record extracellular potentials from neurons or stimulate nearby neurons. Intracortical microelectrodes often lose their functionality in chronic implants. A major failure mode of MEAs is tissue reaction against these implants (biocompatibility of the implants). In this section, we will present two different methods to improve the biocompatibility of the electrodes.

2.7.1 Material science strategies

Physical and mechanical properties of the electrodes such as electrodes size, shape, and cross-sectional area should be considered to elicit the smallest possible tissue response [71, 97, 103]. Although some reports show the importance of the implant texture and shape on tissue response the other studies downplay the importance of electrode shape, size, texture, and tip geometry. The study that has been done with Szarowski et al. compared the immune response to silicon electrode implants of different size, shape, and surface characterization [29]. The study concluded that while different geometries of the electrodes may affect the initial wound healing response, glial

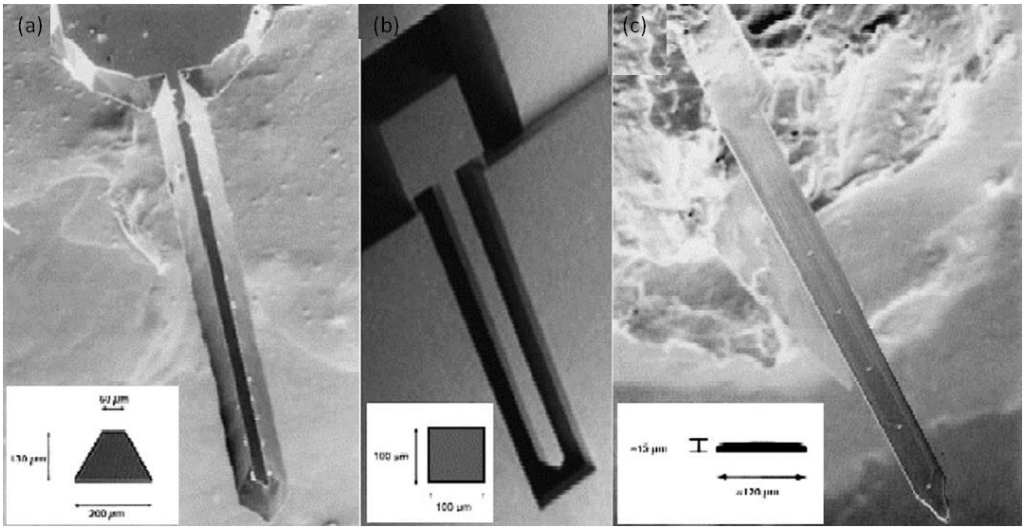

Figure 2.20. Microelectrodes with different size, shape and cross-section that produced the same foreign body response and glial scar. SEM images of electrode prepared by (a) KOH etching, (b)

RIE, (c) Center for Neural Communication Technology (CNCT) device. Reprinted with permission from Ref. [29].

encapsulation was not affected. Such studies support the idea that may shift to the strategies with focus on the cellular biology of the immune response can improve the effectiveness of the microelectrodes. Figure 2.20 shows the comparison of the immune response to silicon implants of different sizes, surface characteristics, and insertion techniques.

2.7.2 Bioactive molecule strategies

A large amount of data on intracortical implant biocompatibility can be considered for designing optimum microelectrodes. The complex biological reaction against the implanted electrodes can be classified in two responses; early reactive response and prolonged reactive response. Microglia play a dominant role in response to the insertion trauma in 1-3 weeks after implant. The astrocytic response starts at the time of insertion and is completed developing an encapsulation glial scar by 6-8 weeks post-implantation. These two biological responses declined the viability of the neurons following device insertion. Figure 2.21 shows possible mechanisms of cellular responses to an implant.

Neurons remain electrically active in the presence of foreign body and inflammation. Astrocutic scar separate neurons from the electrode and may increase the impedance of the electrodes which cause inconsistence performance of recording electrodes.

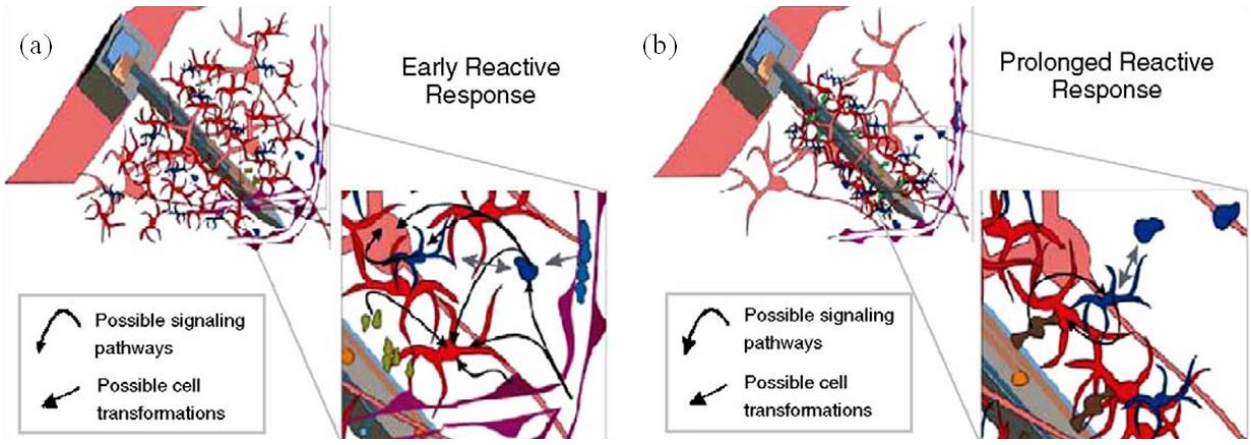

Figure 2.21. Possible mechanisms of biological responses to an implant: (a) Early reactive response in 1-3 weeks, (b) Prolonged reactive response in 6-8 weeks post implantation. Neurons

are pink, astrocytes are red, microglial are blue, and vasculatures are purple. Reprinted with permission from Ref. [29].

Better understanding of fundamental biological processes will help to obtain several strategies to decrease the immune response. Some studies have been shown that it is possible to attract neuronal processes to the electrode site and maintaining the signal before astrocytic scar develops and encapsulate the electrode. To do so, conductive polymers and biomolecules were grown on the recording sites of the electrodes [104].

One of the strategies that can be used to minimize immune response to implanted electrodes is by coating them with bioactive molecules such as cell adhesion peptides or proteins. These peptides not only improve cell adhesion but also increase the cell proliferation [51]. For example, peptides including Arg-Gly-Asp (RGD), Ile-Lys-Val-Ala-Val (IKVAV), lysine-histidine-isoleucine-phenyla-lanine-serine-aspartate-aspartate-serine-serine-glutamate (KHIFS-DDSSE), Tyr-Ile-Gly-Ser-Arg (YIGSR), Cys-Asp-Pro-Gly -YIGSR (CDPG-YIGSR), and poly-D-lysine (PDL) have been employed [105-109]. It is important to find biomolecules that facilitate neural adhesion onto the electrode devices, minimize astrogliosis and suppress chronic microglial activation. In that light, YIGSR and IKVAV polypeptide fragments [105, 106] and PDL [110] are promising candidates that are likely to modify neural cell behavior.

In order to facilitate cell adhesion, proteins and peptides have been attached to solid substrates such as glass, silicon, and metals using various surface modification methods including electrochemical polymerization, covalent bonding, self-assembling monolayers, electron spinning, and peptide-polymer conjugation [111-116]. In a recent study, Sam et al. showed that GlyHisGlyHis could be attached to a silicon surface by electrochemical methods [117]. Conducting polymers such as Ppy and poly(3, 4-ethylenedioxythiophene) can be added to electrode surfaces, where they can easily incorporate bioactive molecules. For example, Cui et al. were able to combine YIGSR peptide fragments from laminin onto Ppy coated recording sites using electrochemical polymerization [118].

Among the penetrating cortical electrode arrays, silicon micromachined electrodes have an excellent capacity to minimize reactions with foreign bodies due to their small size and high surficial density, allowing them to record/stimulate larger volumes of neural tissue.

2.8 Electrical circuit model of MEAs

MEAs are widely used for measuring electrochemical reactions in solutions and cells/tissue stimulation. The impedance characteristics for the electrode-electrolyte interface play an important role for implantable devices. A low electrode-electrolyte impedance interface is critical in electrode design. During stimulation specific current density is required to excite the cells. High impedance would result in a high applied electrode voltage causing undesirable electrochemical reactions that might be harmful for the cells and tissue. On the recording applications, if the impedance of the electrodes is not low enough the neuron signals which are weak will be lost in the noisy ion-based electrolyte media. Therefore, if the interface impedance is understood well and specified correctly, then it helps to design optimum MEAs.

Several equivalent circuit models have studied for the electrode-electrolyte interface [119-121]. In 1879 Helmholtz proposed a model of a double layer of charges at the interface. Warburg then proposed a circuit model for an infinity low current density in 1899. In Warburg model capacitance (C_w) was varied inversely with the square root of frequency and the phase angle was constant (Figure 2.22 (a)). Frick renewed the model of Warburg by changing the amount of phase (Figure 2.22 (b)). In 1947, Randles proposed a model consist of a double-layer polarization capacitance (C_p) in parallel with the series resistance (R) and capacitance (C) (Figure 2.22 (c)).

A well-known circuit model of metal electrode proposed by Robinson in 1968 and it is made up of passive elements in the circuit (Figure 2.22 (d)). The most important parameter in circuit is C_e, the double layer capacitance in the electrolyte-electrode interface. C_e is a capacitance at the metal-electrolyte solution interface and is measured at frequency of 1 kHz. R_e is the leakage resistance when charge carriers are crossing the double-layer. R_s and R_m are the resistance of the electrolyte solution and the resistance of the metallic portion of the microelectrode, respectively [31]. In 1994 Kovacs proposed a currently used equivalent circuit model, (Figure 2.22 (e)). In this model C_{dl}, R_{ct}, Z_w, and R_s are double layer capacitance, charge-transfer resistance, Warburg impedance, and solution resistance, respectively [30]. Warburg impedance is given by the following equation:

$$Z_\omega = (1 - j)/[k.\omega^{0.5}] \quad (2.1)$$

Currently, the constant phase element (CPE) has been replaced instead of C_{dl} in Figure 2.11 (e), because in electrochemical impedance spectroscopy (EIS) a capacitor does not behave ideally and act like a CPE [121]:

$$Z_{CPE} = 1/[A.(j\omega)^{\alpha} \quad (2.2)$$

When α = 1, above equation describes a capacitor and for the CPE α is smaller than 1.

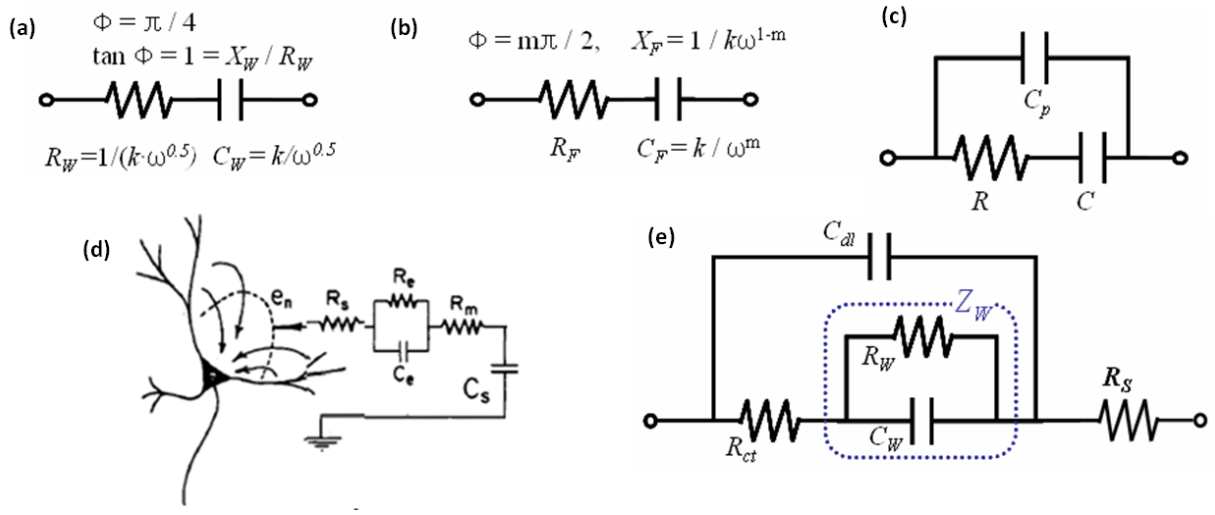

Figure 2.22. Equivalent circuit models of electrode-electrolyte interface: (a) Warburg model, (b) Fricke model, (c) Randles model, (d) Robinson model for metal electrode, (e) Kovacs model. Reprinted with permission from Ref. [30], © 2007, IEEE EMBS Conference on Neural Engineering and Ref. [31].

A following flow diagram shows a general measurement and characterization procedure of electrode-electrolyte interface (Figure 2.23) [32].

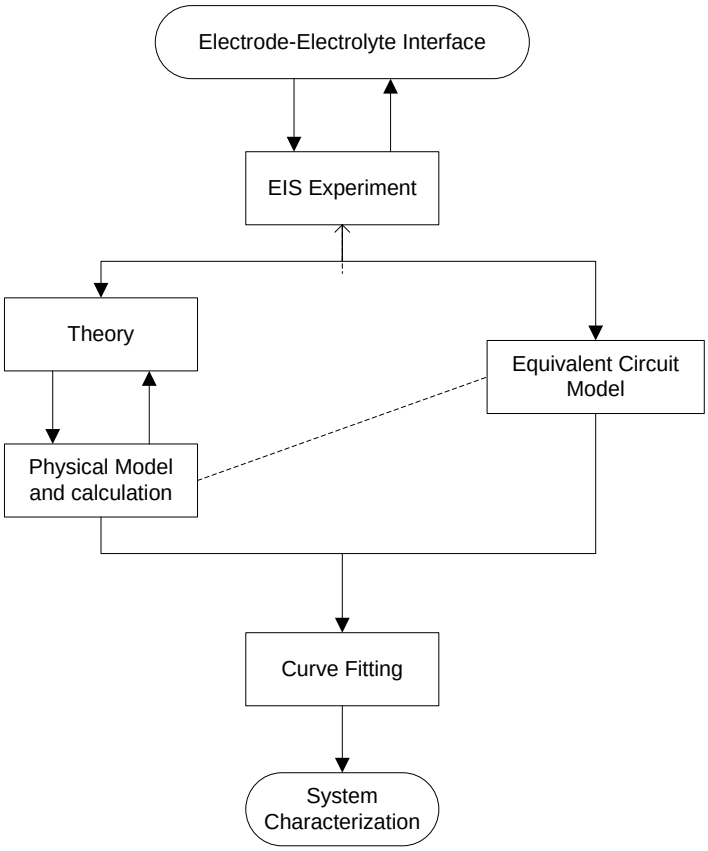

Figure 2.23. A flow diagram for electrode-electrolyte interface measurement and characterization. Reprinted with permission from Ref. [32].

2.9 Perspective of the work in this thesis

In recent years, MEAs emerging technologies have been developed to have a long-term and stable interface with the brain. Different research projects are conducted to obtain consistent recording signals from small groups of neurons without losing microstimulation capabilities, while maintaining low-impedance pathways for charge injection, high charge transfer, and high-spatial resolution by altering the geometries and material compositions of the arrays. So far, none of these attempts have lead to a major breakthrough. The lack of such 3D high-density low impedance MEAs motivated us to design and fabricate a new MEA in order to increase the functionality and effectiveness of the microelectrodes. First and foremost, we developed a 3D fabrication technique in a time and cost effective manner would be suitable to industrial manufacturing standards. We tackled this strategically by using 3D micromachining techniques

and a new masking technology to coat variable-height electrodes that had remained as a big challenge to obtain identical tip-exposures.

Later on, we developed a new selective direct growth of CNTs on the tips of 3D MEAs using Pt as a catalyst material that could enhance electrical properties of the electrodes significantly. To improve biocompatibility of the electrodes, they were coated with bioactive molecules. The results of these studies are detailed in chapters 3 and 4.

CHAPTER 3 EXPERIMENTAL PROCEDURES OF MEAs' PREPARATION

The achievements with implantable neural interfaces motivated us to develop a novel architecture of microelectrode arrays (MEAs) and improve the device performance. As discussed in previous chapters, a number of different techniques have been developed in order to fabricate an optimum MEAs; however, there are still some challenges to fulfill it. Although some of the MEAs have been commercialized and been used in research, the current process used to fabricate impose limitations in the electrode array geometry and uniformity. Moreover, existing fabrication costs have revealed the need to develop less costly but high precision fabrication process. In this chapter, a detailed description of the fabrication and characterization techniques that were used during the course of this research will be presented. All experimental procedures relating to MEAs device fabrication and testing will be presented, from the fabrication of microelectrodes structure to the coating process of electrodes.

3.1 Design and fabrication of neural 3D MEAs using micromachining techniques

The fabrication process of the proposed MEAs consists of two parts: The first one demonstrates the design and microfabrication of multi-electrode arrays; the second part covers various electrode coating techniques where several materials such as polymers, metals, and carbon nanotubes (CNTs) are investigated. Figure 3.1 presents the main steps of the process flow applied to construct a pyramid-shaped MEA.

3.1.1 MEAs backside fabrication process

The employed substrate representing the base for the probes is a 2150±25 μm thick p-type (100) 100 mm-diameter single-side polished silicon wafer with a resistivity of 0.0153-0.0158 Ωcm. The silicon wafer was cut into 12 pieces of 2 × 2 cm^2. To electrically isolate the electrodes one from each other, the polished side of the wafer was cut with an ADT 7100 dicing saw.

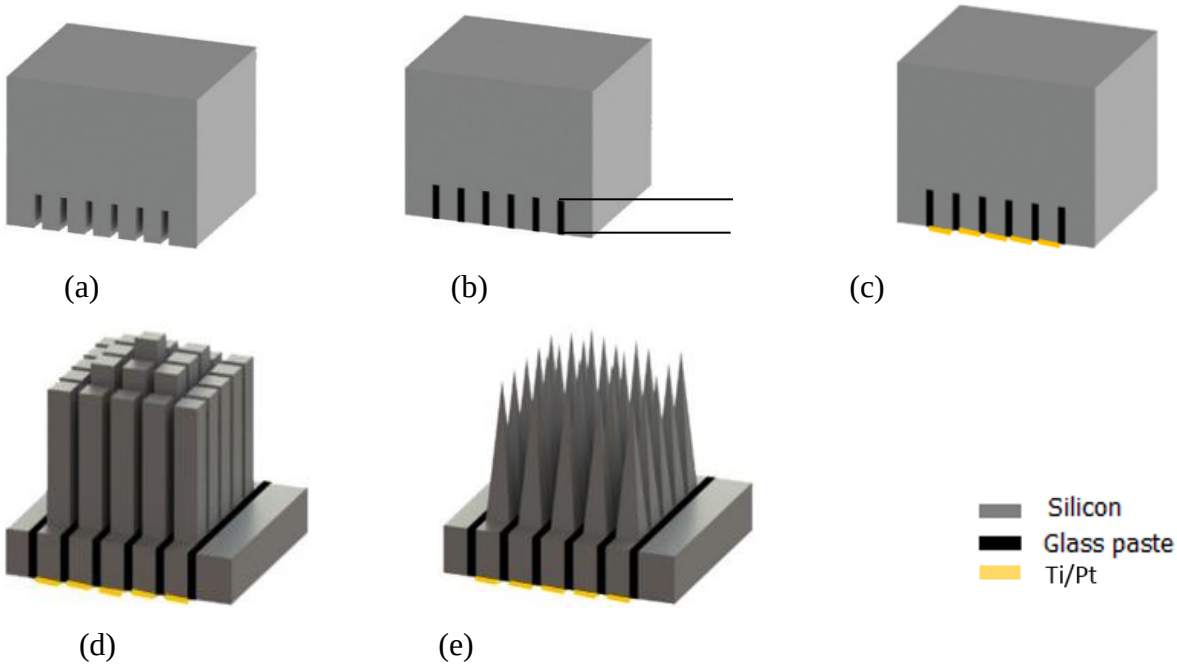

Figure 3.1. Main silicon-based MEAs micromachining steps: (a) Backside dicing, (b) Backside glassing and polishing, (c) Backside metallization, (d) Frontside dicing, (e) Frontside wet-etching.

The cutting process involved 6 cuts in two perpendicular directions with the pitch of 300 µm. Nine 5 × 5 matrices were created at the polished side of each square (Figure 3.2). A resin-bond blade (Dicing Blade Technology, B-004-4000J) was used to make the matrix. The depth of all the cuts is 500 µm (Figure 3.1(a)). After dicing the backside, the substrate was cleaned with acetone, isopropanol, and deionized (DI) water in ultrasonic bath in order to remove silicon residue.

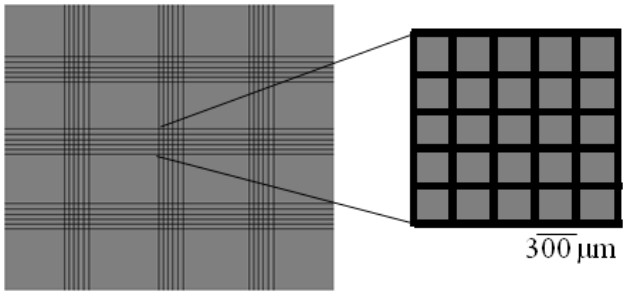

Figure 3.2. Schematic top-view of backside dicing including 9 collections of 5×5 matrix.

To insulate the electrodes one from each other, glass paste was used. First, glass powder with the mesh size of 44 µm (Corning 7070) was mixed with isopropanol and then flowed to the kerfs. The substrate was then put in a vacuum furnace at 60 °C for 15 min. This process was repeated 3 times until 3 layers were coated. The vacuum brings air bubbles of the glass paste to the surface which results uniform paste in the kerfs. The sample was then annealed in the furnace under the N_2 ambient at 1200 °C to melt the glass so that it penetrates completely to the kerfs [122]. Figure 3.1(b) shows the kerfs which have been filled with glass paste. To remove the excess glass from the surface of the silicon substrate, the dicing saw and polishing machine were used. The glass bulk was removed with a resin-bond blade (00777-8030-006-QKP). Silicon Carbide paper with grit size of 600 µm was used to remove the residue of the glass. At the end, the backside of the substrate was polished using 15, 6, and then 1 µm diamond suspensions on polishing cloth to achieve a completely smooth surface [123].

To make electrical connection to each electrode, the backside of each pin was metalized, Figure 3.1(c). To obtain the needed quality interconnects, the metal should make low ohmic contacts providing strong adhesion to the silicon substrate. Furthermore, the metalized surface should be appropriate for wire-bonding or flip-chip assembly processing. Pt was selected for ohmic contact, silicide formation, and wire-bonding. To metalize the backside, a bilayer of metals Ti/Pt was sputter-coated with thicknesses of 100 and 400 nm, respectively (Table 3.2) [124]. A lift-off process was used to create a 200 × 200 μm^2 contact pad placed between the kerfs filled with glass.

3.1.2 MEAs frontside fabrication process

Frontside dicing

To achieve electrodes with variable heights, the frontside (non-glassed side) of the substrate was cut with ADT 7100 dicing saw. To make 3D pyramid-shaped MEA, two dicing saw blades were used: resin-bond blade (Dicing Blade Technology, J-014-4000-J) and nickel alloy diamond blade (Disco, ZH05-SD2000-M-90). Three different electrode heights (1.45, 1.55, and 1.65 mm) were cut and separated with a depth of 1650 µm. This leaves a 5 × 5 matrix of rectangular columns with the above mentioned heights and 100 µm spacing (Figure 3.1(d)). The extra row of electrodes with the height of 1.35 mm was designed as a dummy row to protect electrodes in the arrays and improve the uniformity of the electrodes during etching process.

Wet-etching

Chemical etching of silicon with hydrofluoric acid (HF) and nitric acid (HNO_3) is widely used in semiconductor industry and in the production of solar cells. The etching process is employed to remove silicon from the planar wafer, removal of work damage or roughness (e.g. caused by sawing of wafers), or texturing of the surface. The mechanism of wet chemical etching of silicon in HF-HNO_3 mixtures was described by Robbins and Schwartz for planar silicon surfaces [33]. The etching of silicon in HF-HNO_3 mixtures is divided into two chemical processes:

- Oxidation of silicon to SiO_2 by HNO_3 (Eq. 3.1)
- Dissolution of the SiO_2 by HF under release of a new silicon surface (Eq. 3.2). The overall etching reaction is given in Eq. 3.3.

$$3Si + 4HNO_3 \leftrightarrow 3SiO_2 + 4NO \uparrow + 2H_2O \quad (3.1)$$

$$SiO_2 + 6HF \leftrightarrow H_2SiF_6 + 2H_2O \quad (3.2)$$

$$3Si + 4HNO_3 + 18HF \leftrightarrow 3H_2SiF_6 + 4NO \uparrow + 8H_2O \quad (3.3)$$

The critical step in these reactions is the oxidation of silicon by nitric acid. To convert columns of electrodes to the needle-shaped electrodes, two etching processes are involved; isotropic and anisotropic etching steps. For isotropic etching involving HF-HNO_3, water or acetic acid (CH_3COOH) are used as diluents. This etchant combination is known as HNA which is used to modify the reaction rate, finish of the etched surface, or cause preferential etching of specific crystallographic planes. HNA etch rates of silicon is presented as an isoetch curves for various weight percentages of the HF-HNO_3 system [33].

Figure 3.3 shows a HNA system etching characteristics. In the high HF concentration- region (I)- the contours are parallel to the constant HNO_3 axis and the etch rate is HNO_3 limited. Therefore, silicon dioxide is produced at a low rate and leaves quite rough surface. On the other hand, in HNO_3 high concentration- region (II)- etch rates are HF limited, in which the etch rates are controlled by silicon dioxide dissolution by HF. The great amount of silicon dioxide forms a layer at the silicon surface and protects it from oxidation. As a result silicon in this region has a smooth surface. In region (III), the balanced HF-HNO_3 etch rates are generally high because of

the high concentration of HF and HNO_3. High concentration of HNO_3 causes fast oxidation of silicon while high concentration of HF easily dissolves the silicon dioxide. However, in this region surface morphology is harder to control due to the aggressive etching and dissolution process. HNA etch rates of silicon plotted in isoetch contours and surface topography of etched silicon has been shown in Figure 3.3.

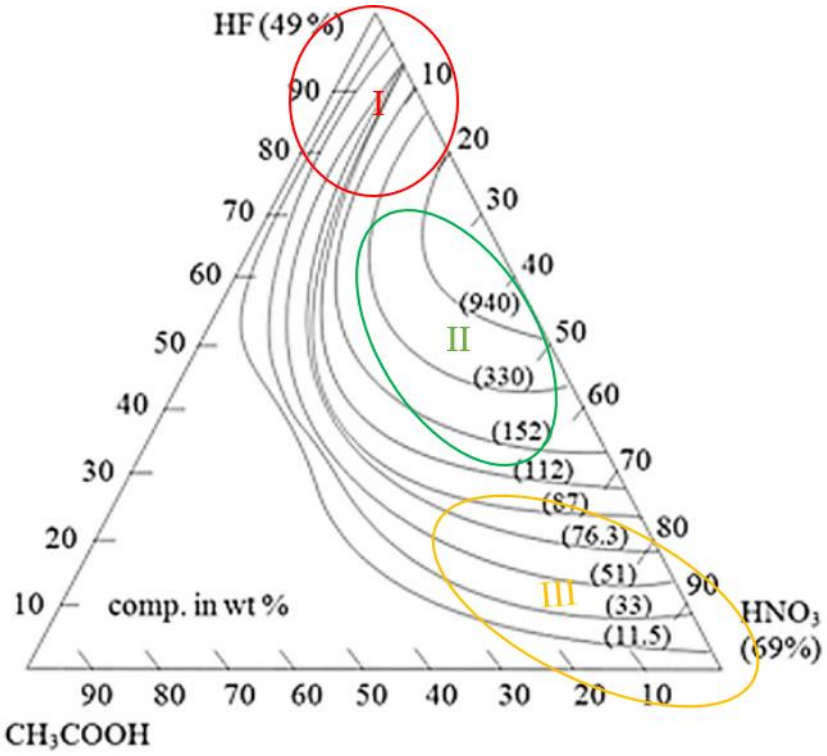

Figure 3.3. Isoetch contours and surface topography of etched silicon for the HF-HNO_3-acetic acid diluents [33]. Numbers in parentheses shows etch rates of silicon in μm/min.

To convert rectangular columns of electrodes to sharp tip needle-shapes, a wet etching process composed of 49% HF and 69% HNO_3 in a ratio of 1:19, was used. The etch rate of silicon in this mixture is a function of the stirring rate, temperature, and ratio of acids. To control the chemical etching process, it is important to identify the effect of variables involved in the planned reaction [125]. Etching microelectrodes has two steps including dynamic and static process. For the dynamic process, the sample was placed in a 2 × 2 cm custom Teflon holder, put into the acid upside down, and then the solution was rotated with a magnetic stirrer at 500 rpm for 5 min (Figure 3.4). This method is intended to increase the etching uniformity [126].

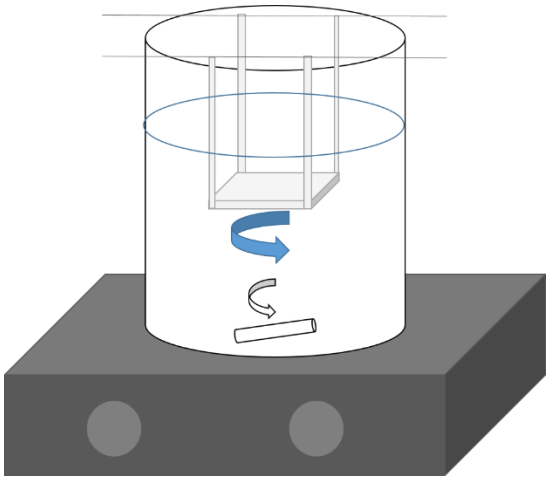

Figure 3.4. Experimental setup for dynamic etching process to round the side-walls of the square columns of the electrodes.

For the following etching step (static etch), the sample was placed facing down in an etchant solution and N_2 gas was applied to polish and sharpen the top of the columns until a complete needle shape was achieved. Etching time for this step was about 11 min (Figure 3.1(e)). Figure 3.5 presents a photograph of the static etching setup. A custom designed Teflon holder was built to take the array upside down. The gas was applied from the bottom through the 6 rods that are connected to the compressed N_2 cylinder. The static etching process etches the tops of the columns preferentially and sharpens the tips of the electrodes.

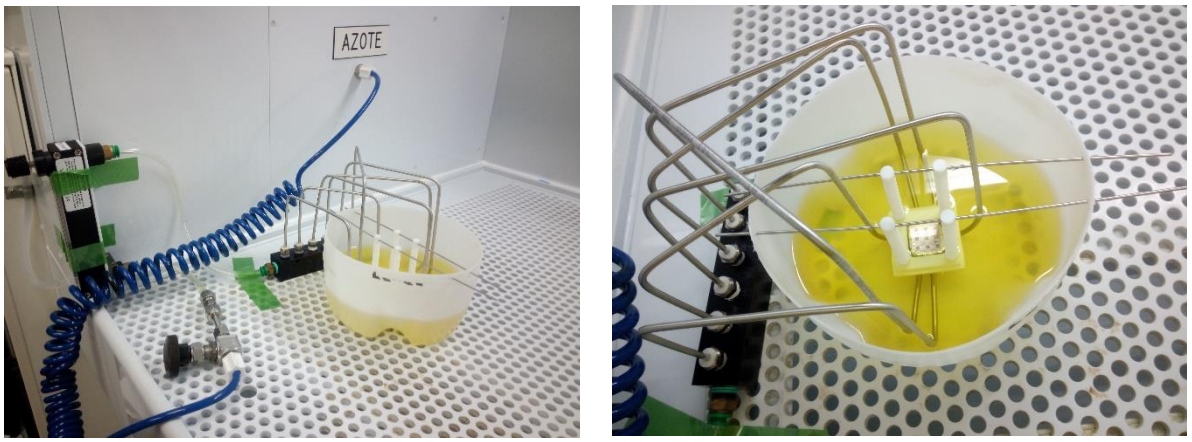

Figure 3.5. Experimental setup for static etch process: (a,b) Photographs of the static etching process. In this step of etching, the tips are sharpened by applying the N_2 gas from the bottom; (preferential etching).

3.1.3 Shank insulation

In order to insulate the body of the electrodes, parylene-C has been used due to its biocompatibility, chemical inertness, and high stability in vivo [127]. However, some studies have been reported parylene delamination and cracking along the electrode shanks over time in biological environments [128]. In addition, high-temperature steam of sterilization makes parylene more brittle and predisposed to cracking [129]. SiO_2 is a high-quality, biocompatible, stable, and chemical inert electrical insulator that can reduce biofouling in biological environment [130]. Moreover, the perfect adhesion of SiO_2 to silicon may solve the delamination issue.

A 2 µm thick parylene-C film was deposited on the frontside of the electrodes using a chemical vapor deposition (CVD) process whereas the backside of the electrodes was covered with a tape (Figure. 3.6 (a)) [131]. Parylene-C was deposited using Specialty Coating Systems (SCS) equipment. The deposition process was begun as the parylene-C dimer was vaporized under vacuum (< 10 mTorr) at 140°C. The dimerized gas was pyrolyzed at 670°C and deposited as a

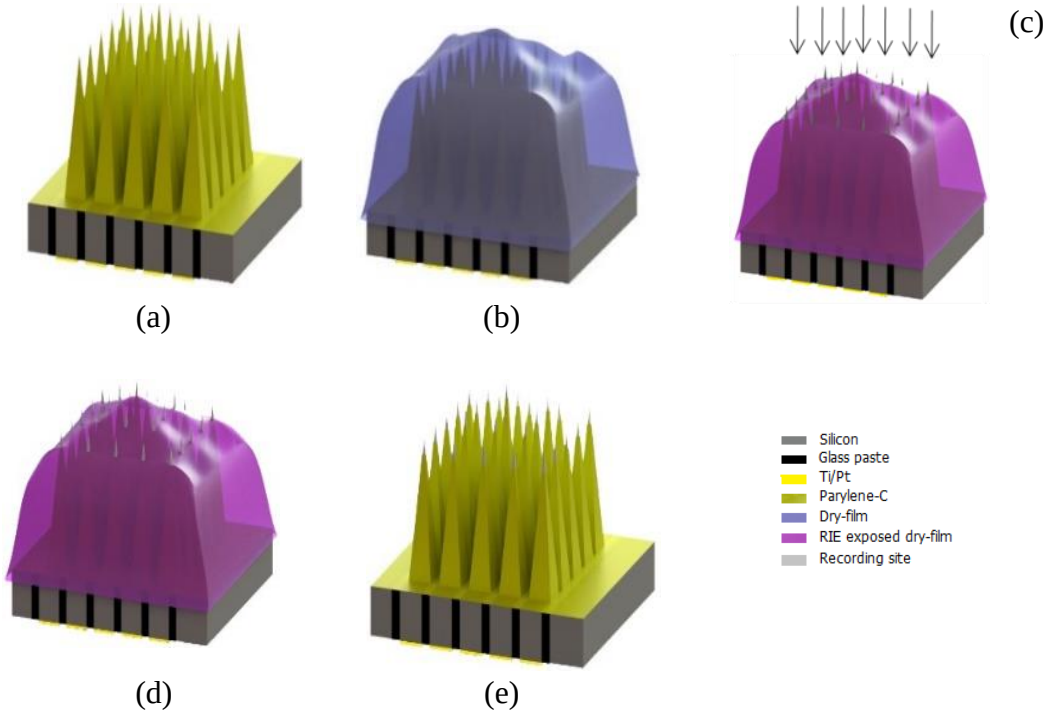

Figure 3.6. Process flow of electrodes tips-coating: (a) Parylene-C deposition, (b) Cover with dry-film photoresist, (c) Reactive Ion Etching, (d) Tip-metallization, (e) Lift-off in acetone.

conformal, pinhole-free transparent film. For the electrodes with CNT tips, native SiO_2 was considered as an insulator instead of parylene- thermal C.

3.1.4 Masking process to de-insulate active sites of the electrodes

The tips of the electrodes need to be good conductor to facilitate the charge transfer from needles to the neural tissues. Conventional masking processes to coat the electrode tips are operator-dependent, time-consuming, and may damage the electrodes during the process. To date, electrode tips are coated by of two conventional methods: poking the electrodes through an aluminum foil or using liquid photoresist as a mask. The first method—poking—is a time-consuming process that may damage electrodes during the process, and is operator-dependent. The second method— liquid photoresist mask—also has some limitations. It is a long process with many steps such as resist coating, vacuum treatment, UV exposure and development, soft and hard bake. More importantly, both methods may not be practical for 3D electrode arrays since they cannot follow 3D structure and enhance uniform tip-exposure. The novel architecture of this MEA enables recording from multiple intracortical depths of the brain.

To coat the 3D pyramid-shaped MEA, a novel masking technology was developed that only needs single masking step and reduces the conventional masking process steps from 14 to 6 (Table 3.1). The proposed masking process has several advantages including simpler fabrication process, reduced production time and cost, and more uniform tip exposure for variable-height electrodes [132]. Figure 3.6 shows the process flow of masking and tip-coating. After electrode insulation, a layer of dry-film photoresist (DuPont, FX900) with the thickness of 30 µm was used as a mask to cover the array (Figure 3.6 (b)). Arrays were placed on a thick Al foil sheet then dry-film photoresist was applied on electrodes using tweezers. The film fixes arrays on the Al foil surface. The dry-film follows the 3D structure and results a uniform tip exposure for variable-height electrodes while traditional methods; poking electrodes in Al foil or liquid photoresist are not practical for masking such a pyramid-shaped array.

Dry-film photoresist was chosen as a mask due to following reasons:

Plasticity and flexibility: dry-film photoresist follows the 3D structure of the electrodes and results in full coverage of the array. A high flexibility is desired since this helps to cover variable-height electrodes.

Adhesion: the mask must adhere sufficient well to the underlying substrate and it should not lift-off during various steps. Moreover, photoresist is sensitive to the temperature and heating. In the proper temperature and duration, the adhesion of photoresist can increase.

Plasma etching: dry-film photoresists are sensitive to plasma etch and will etch during oxygen plasma. The thickness of the resist at the sharp electrode tips is significantly thinner than the other parts so will be removed faster. This ability helps to remove photoresist from the tips.

Plasma offers two main characteristics which is practical to remove photoresist and parylene-C from the electrode tips. First, it can reach to high temperature and energy densities. Second, plasma can produce energetic particles that can begin chemical reactions which is difficult or impossible with usual chemical mechanisms.

Dry-film and parylene-C were removed from the tips using isotropic and anisotropic reactive-ion etching (RIE) process (Figure 3.6 (c)). Custom designed RIE machine was used to etch the films. In the first step, dry-film and parylene-C films were anisotropically etched by reactive-ion etching (RIE, RF source) from the top of the electrode tips at a power of 200 W and a chamber pressure of 100 mTorr for 50 minutes. In the next step, both films were etched isotropically with plasma asher (microwave source) from the side-walls of the tips at a power of 150 W and a chamber pressure of 400 mTorr for 10 min using PVA TePla system.

3.1.5 Electrodes tip-coating

Active sites of the electrodes are typically coated with platinum (Pt) or iridium oxide [133-135]. Although Pt has excellent electrochemical stability, corrosion resistance, and limited reactivity to biological environment [136, 137], it has a relatively modest charge injection limit (0.1 - 0.3 mC/cm^2) [138]. Iridium oxide is a highly conductive oxide with high-charge injection capacity. However, it has several shortcomings, including a deterioration of long term stability if used beyond their charge injection limits and a requirement for circuitry to apply an anodic bias during cathodic charge injection [139, 140].

The remarkable structural, electrical and mechanical properties of CNTs such as intrinsically large-surface areas, biocompatibility, extremely high conductance and high aspect ratios have attracted much interest as a suitable electrode material for neural tissue. These characteristics of CNT enhance both recording and electrical stimulation of neural tissues [141, 142].

Table 3.1. Comparison of conventional and proposed masking processes

Conventional method [123]	This work
First Masking process: - Photoresist coating - Vacuum degassing 30 min - Pre-baked - UV exposure - Developing - Hard-bake 7h - Tip-Metallization - Lift-off Second masking process: - Parylene-C deposition - Photoresist coating - Vacuum 30 min - Hard-bake 10h - Plasma etch - Lift-off	Single masking process: - Parylene-C deposition - Dry-film deposition - Soft-bake - Plasma etch - Tip-Metallization - Lift-off

3.1.6 Tip-metallization and lift-off

To convert electrodes to the functional devices, the tips of the electrodes should be metalized. The tips of the electrodes were sputter-coated with Pt and iridium oxide (Figure 3.6 (d)). Deposition of a layer of metal at the electrodes tip not only decreases its impedance but also facilitates charge transfer from electrode to the neural tissues. To promote the adhesion of aforementioned metals at the surface of silicon, a thin layer of titanium (Ti) was deposited prior to the Pt and iridium oxide deposition. The sputter deposition parameters for different metals are listed in Table 3.2. The mask was removed with the lift-off process by ultrasonical cleaning in acetone, isopropanol, and DI water (Figure 3.6 (e)).

Table 3. 2. Sputtered deposition parameters for the electrodes' tip-metallization

Metal	Ambient	Gas flow rate (sccm)[1]	Chamber pressure (mTorr)	Power (W)	Time (min)	Thickness (nm)
Ti	Ar	10	10	90	11	100 ± 5
Pt	Ar	10	10	90	16	400 ± 10
SIRO[2]	Ar/O_2	25/25	10/10	100	33	200 ± 10

[2]SIRO: Sputtered Iridium Oxide

[1]sccm: standard cubic centimeter per minute

In order to grow CNTs, the catalyst particles formed from the deposited Pt layer (catalyst film in general) must have a nanoscale size (typically < 200 nm). It has been previously demonstrated that a Pt film with the thickness of 8.5 nm was unsuccessful for Pt-CNT growth, perhaps because the resulting nanoparticles were too large to support CNT growth [143]. Therefore, a very thin layer of Pt (5-10nm) was evaporated at the tip of the electrodes prior to CNTs growth. A 2 nm Ti layer was evaporated prior to Pt deposition to improve Pt adhesion and to avoid the Pt diffusion in silicon during CNTs growth. Evaporation technique was used to control the more precise thickness.

3.1.7 CNTs tip-coating

Selective direct growth of CNTs on the tips of 3D MEAs using Plasma Enhanced Chemical Vapor Deposition (PECVD)

Up to now, different procedures have been proposed to coat CNTs on neural interfaces such as electrochemical deposition, electrophoresis, layer-by-layer assembly and direct growth [144]. Among these techniques, selective direct growth appears to be the most suitable and robust fabrication process. By controlling growth parameters, one can obtain vertical orientation of CNTs with high density, and high reproducibility. The most important advantage of growing CNT directly on electrodes is the stability and reliability in time compared to CNTs films coated using other methods [145]. However, direct growth is a less commonly used process since it requires additional laborious steps. A standard Chemical Vapor Deposition (CVD) process was used by

Ansaldo et al. [145] to grow CNTs on single penetrating microelectrode tip of commercially available platinum-tungsten microwires capable of enduring high temperatures and electroplated with nickel as catalyst. So far, Pt which is a very common material for bio-medical devices has rarely been used in CNTs synthesis [146-149]. A standard growth requires depositing common catalyst metals such as nikle (Ni), cobalt (Co) or iron (Fe), which are not considered as biocompatible materials. Therefore, hard purification methods must be employed post-growth to remove the catalyst particles. According to Liu et al. [150] even after post purification, CNTs preserve a significant amount of non-encapsulated or bioavailable metal residue and impurities.

We have carried out CNTs growth by using Plasma Enhanced Chemical Vapor Deposition (PECVD) which is a very relevant growth process for neural interfaces. In fact, instead of spaghetti-like structures usually obtained in CVD, plasma allows to grow well-aligned, individual and free-standing nanotubes with uniform diameters [151]. Such geometry increases the accessible surface area of CNTs leading to low impedance and it may also permit the direct excitation of a single neuron [152]. Furthermore, lower growth temperatures relative to CVD (<400°C) are possible since high-energy electrons present in the discharge plasma, supply the energy necessary for chemical reactions in the gas [153]. This allows a direct growth of CNTs on soft polymer substrates for example. Another advantage is that during the growth process, the plasma removes amorphous carbon which strongly affects the electrical properties of electrodes and may lead to an increase of impedance [148, 151].

CNTs were grown in a gas mixture of acetylene (C_2H_2) and ammonia (NH_3). The MEA is introduced into the furnace and pumped down to a base pressure of 10 mTorr using a mechanical pump. The temperature of the furnace is then ramped up to 700°C at a rate of 200°C/min in order to avoid the glass to be melted at the backside of electrodes. Before CNTs growth, we performed annealing procedures at 700°C under 20 Torr of hydrogen. This step allows the formation of catalyst islands from the Pt layer at the tips [151]. After a 10 minute annealing, the furnace is pumped down and NH_3 is introduced at 3.5 Torr with the temperature held at 700°C. A DC discharge between the cathode-sample and the anode is initiated and kept at relatively low current (1mA), while C_2H_2 is introduced using a separate mass flow controller. The flow-rate ratio was maintained at 20% (C_2H_2/NH_3, 40/200) which has been found as the optimum ratio to obtain clean CNTs [151]. The synthesis was carried out for 15 min in a stable discharge.

Single-wall carbon nanotubes (SWNTs) deposition using Coffee stains technique

Coffee stains technique has been used for the fabrication of structurally organized single-wall carbon nanotubes (SWNTs) at the tips of the electrodes. The pinning of the gas-solid-liquid contact line and its stick-slip-type motion are essential key elements in the formation of coffee stains [34]. Aqueous colloidal suspensions of sodium dodecyl sulfate (SDS) and SWNTs (Raymor) were prepared by dispersing SDS and SWNTs in DI water through harsh sonification for 30 min. Figure 3.7 demonstrates structural phases observed during self-assembly of SWNT coffee stains. SEM images of SWNT films obtained for deposition from suspensions with different concentrations of SDS surfactant and SWNTs.

There are four types of structures for various concentrations of SDS and SWNTs: (1) continuous films, (2) holey films, (3) striped films, and (4) spotty films. Continuous films are found in higher concentrations of SDS and SWNTs. SEM images of this zone also shows that films consist of an entangled network of ordered SWNTs.

The tips of the electrodes were sputter-coated with Pt prior to CNTs deposition. To coat electrodes with SWNTs, the MEA was dipped in a solution of SWNTs, DI water, and SDS for 24 h in a fix position. The concentrations of SDS and SWNTs were 0.2 wt% and 3×10^{-4} wt%, respectively. As a result, solution was drawn by capillary flow to the contact line (the electrode tip) and swept suspended particles (SWNTs) with it, which then was deposited at the tips of the electrodes. The resulting crowding particles of CNTs at the meniscus enable film formation and result in the deposition of some or all suspended particles at the edge of the droplet in the form of coffee stains.

3.2 Characterization of the neural MEAs

In order to characterize neural MEAs various techniques have been used including SEM and Energy-dispersive X-ray spectroscopy (EDX) to verify the geometry (shape and size), coatings structure, and materials of microelectrodes. The electrochemical characterization of the electrodes was done using microprobe station coupled with a Biostat VMP-300 system. A novel microstimulator designed in Polystim laboratory has been used to apply current pulsing and measure the charge injection capacity of the electrodes.

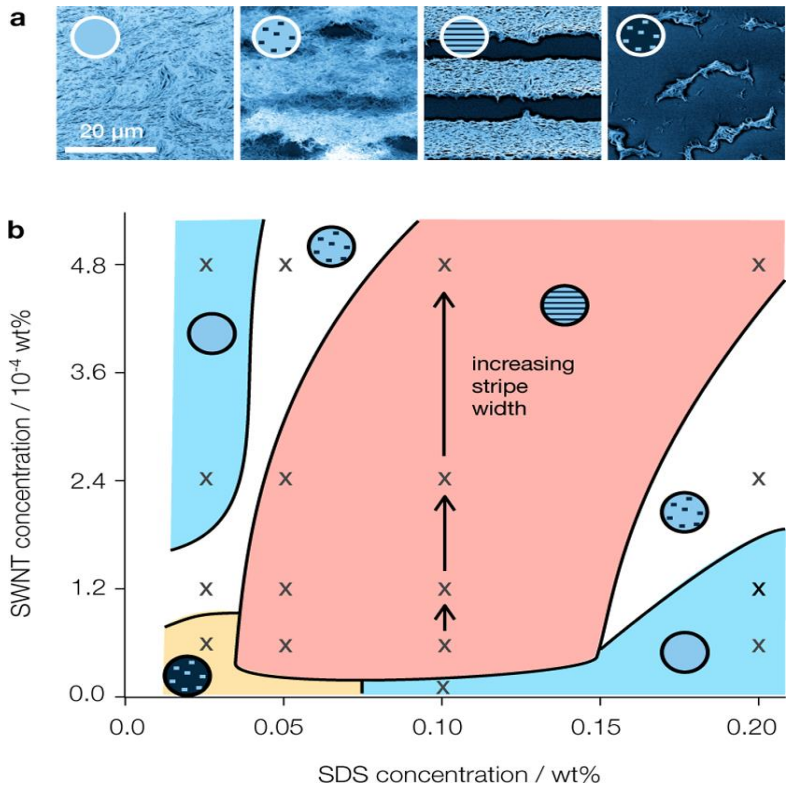

Figure 3.7. Structural phases during self-assembly of SWNT coffee stains: (a) SEM images of continuous, holey, striped, and spotty phases, (b) Schematic structural diagram as a function of SWNT and SDS concentrations. Reprinted with permission from Ref. [34].

3.2.1 Scanning electron microscopy (SEM) imaging

SEM imaging is particularly well-suited for characterization MEAs and is a powerful technique for assessing conducting and semiconducting materials. We used a Hitachi S-4700 field emission SEM in order to image microelectrodes and different coatings such as silicon, parylene-C, SiO_2, metals, and CNTs. The accelerating voltage for silicon and metals was 10 V and the working distance was set to ~8-10 mm. The accelerating voltage for CNTs was 1 V and the working distance was set to ~3-5 mm. The microscope has been operated in its high resolution mode and only the top secondary electron detector was enabled.

3.2.2 Energy-dispersive X-ray spectroscopy (EDX) analysis

In order to analyze the microelectrode elements EDX system was used. EDX is an analytical technique used for the elemental analysis of a sample relies on an interaction of some source of

X-ray excitation and a sample. We used an Inca Energy 250 EDX and the accelerating voltage for each element was 2 times of its energy-level shells.

3.2.3 Electrochemical characterization; Electrochemical impedance spectroscopy (EIS), Cyclic voltammetry (CV), and Charge injection capacity (Q_{inj})

Electrochemical impedance spectroscopy (EIS) and cyclic voltammetry (CV) were performed using Biostat VMP-300 system. For all measurements gold probes having fine 5 µm diameter tips from CascadeMicrotech were used. The instrument was operated under the computer control with EC-Lab software. A solution of 0.9% phosphate-buffered saline (PBS) was used as the electrolyte in a three-electrode cell consisting of Ag/AgCl as a reference electrode, a large area Pt wire as a counter electrode, and electrodes of the array as working electrodes (Figure 3.8). The impedance was measured applying an AC sinusoid waveform with 10 mV of amplitude as the input signal with the DC potential set to 0 V through the working electrode. The value of impedance was measured in the frequency range of 40 Hz to 10 kHz since the center of energy of action potentials is about 1 kHz.

CV was performed with the same instrument and the EC-Lab software. The setup of the electrodes (reference, working, and counting) was the same as the one used in the impedance measurement. The potential on the working electrode was swept between -0.6 and 0.8 V. The maximum cathodic (Emc) and anodic potentials on the electrode during electrical stimulation, should stay within the "water window" (-0.6 to 0.9 V versus Ag/AgCl in PBS) to prevent electrolysis of water [154, 155]. A scan rate of 50 mV/s was used. Figure 3.8 demonstrates a schematic of EIS measurement setup.

To measure charge injection capacity (Q_{inj}) of microelectrodes, we interfaced the MEAs with a novel microstimulator designed in our Laboratory [156, 157]. The MEA was immersed in 0.9% PBS solution then charge-balanced and biphasic constant current was applied to different pairs of microelectrodes. Stimulation current with the range of 10 to 110 µA were applied for pulse widths of 0.7, 0.8 and 1 ms. The stimulation frequencies were set to 500, 500 and 250 Hz respectively.

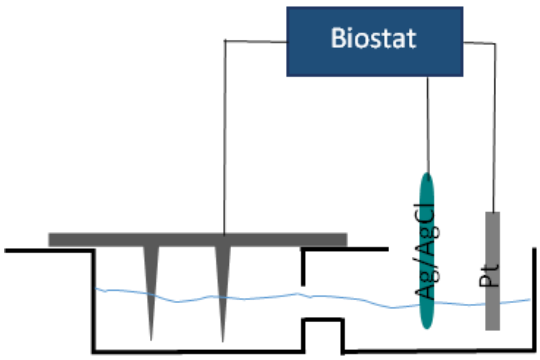

Figure 3.8. A schematic of electrochemical measurement setup. Ag/AgCl act as a reference electrode, large area Pt wire as a counter, and electrodes of the array as a working electrode.

The resulting waveforms were measured across each pair of microelectrodes using digital oscilloscope. The area under each pulse was estimated for determining the total charge injected during any anodic or cathodic pulse and divided by the electrode surface tip area.

3.3 Results and discussion

3.3.1 Fabrication of 3D MEAs

Figure 3.9 (a) and (b) show SEM images of backside dicing and glassing. The depth of the backside cut is 500 µm. A 7 × 7 matrix of rectangular columns with different heights of 1.65, 1.55, 1.45, 1.35 mm has been created at the frontside of the substrate (Figure 3.9 (c)). The outer row of electrodes is for etching process uniformity and will remove after etching step.

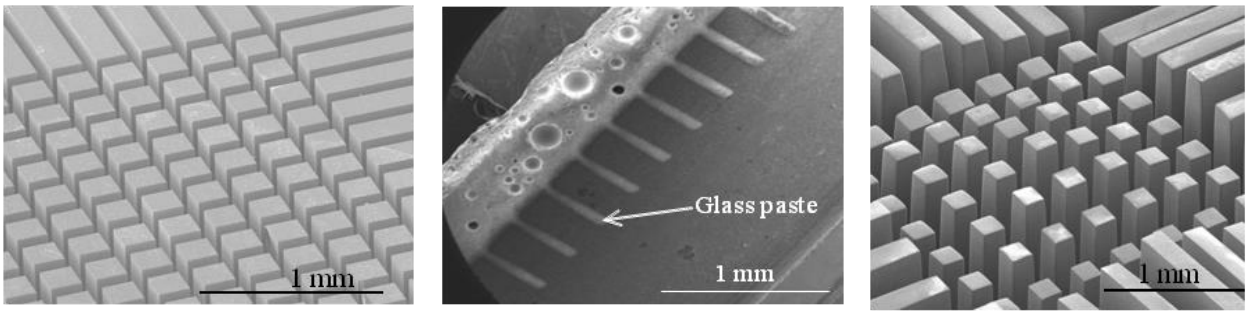

(a) (b) (c)

Figure 3.9. SEM images of electrodes backside: (a) Backside dicing, (b) Cross-section of the backside kerfs which have been filled with the glass paste, (c) 3D pyramid-shaped electrode array with three different heights. The outer row of electrodes is for etching process uniformity and will remove after etching step.

The rectangular columns of the electrodes were converted to sharp needle-shaped tips using a wet etching procedure (Figure 3.10 (a-f)). Etching duration causes significant change in the geometry of the electrodes. The thickness of the electrodes was 200 μm at the base and about 2 μm at the tip with 100 μm spacing after etching step.

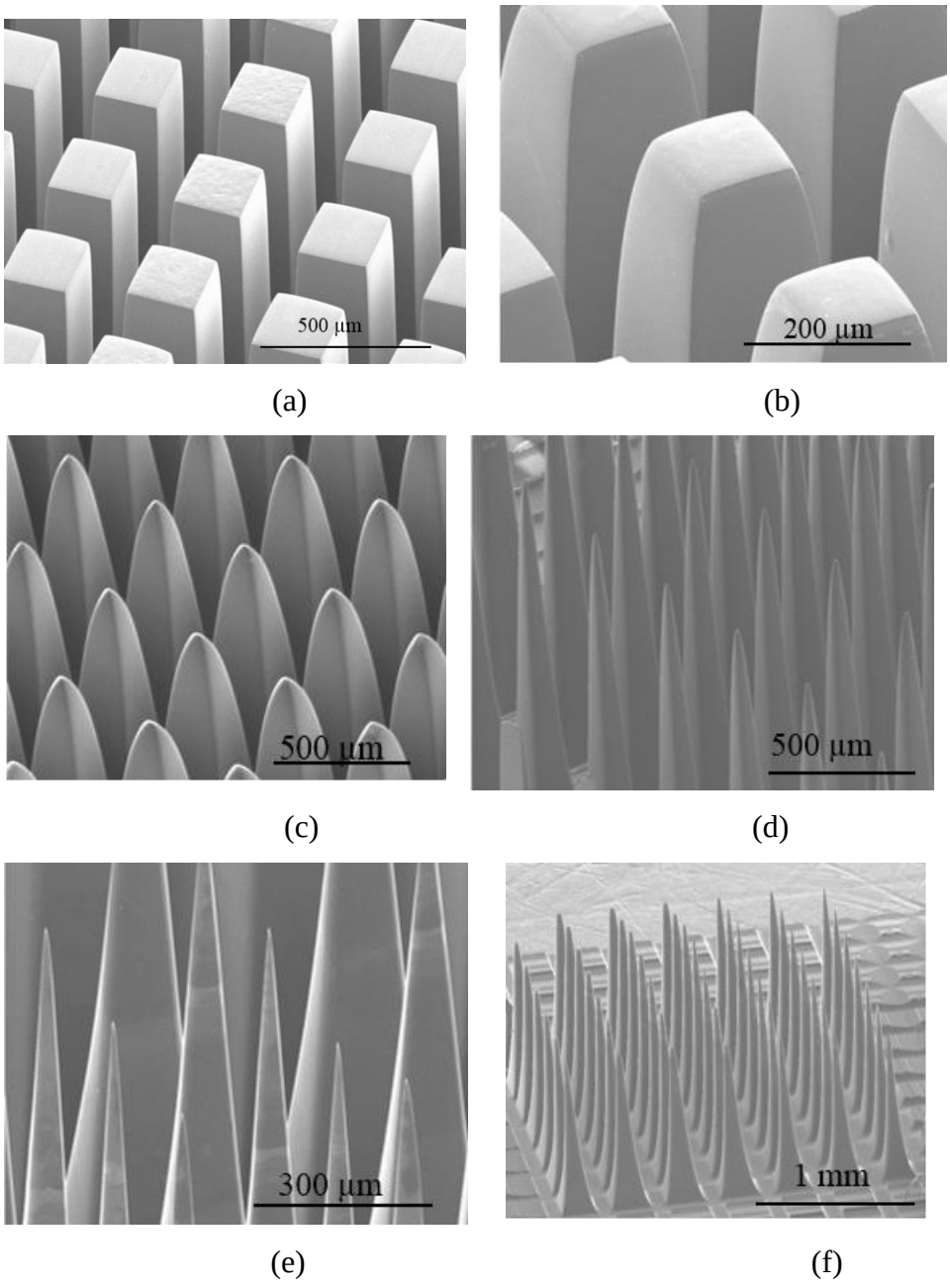

Figure 3.10. SEM images of the electrode etching process: (a) Frontside cutting, (b) Rounding corners by stirring the etching solution, (c-e) Polishing and sharpening the tips of electrodes by applying N2 gas from the bottom of the solution, (f) One 3D 7×7 MEA.

3.3.2 Masking process

In order to encapsulate the shank of the electrodes, the entire upper surface of the electrodes was covered with 2 µm parylene-C (excluding electrodes for CNTs deposition). To remove parylene-C from the tips of the electrodes, the 3D MEA was covered with dry-film photoresist. In the next step, parylene-C and dry-film were etched from the tips of the electrodes using oxygen plasma in RIE and then in plasma asher. The mask was removed ultrasonically in acetone (Figure 3.11).

As indicated above, the novel proposed method includes a single masking process and could significantly reduce the number of fabrication steps. In this method, instead of two photolithography steps which are time-consuming (total processing time: 24 h) there is only one etching step with the total processing time of 6 h. Besides, none of the conventional methods enhance the uniform tip-exposure for 3D structure of the MEA (Table 3.1).

3.3.3 Tip-metal deposition

The active sites of the electrodes were coated with Pt and sputtered iridium oxide (SIRO) to facilitate charge transfer from electrodes to the neural tissues, to reduce the impedance, and to increase charge injection capacity (Figure 3.12). The measured thickness of the sputtered metal layers on the test wafer is given in Table 3.2. A very thin layer of Ti/Pt was evaporated at the CNT-electrode tips.

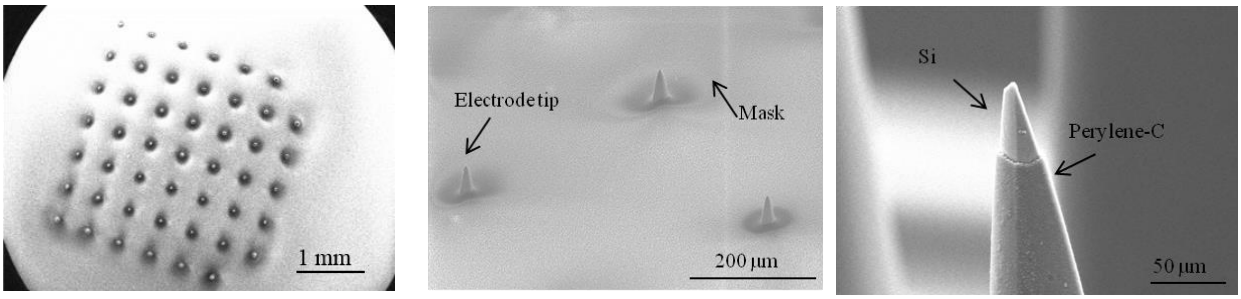

(a) (b) (c)

Figure 3.11. SEM images of masking process: (a) Electrode array covered with dry-film photoresist after RIE process. Dry-film photoresist follows the 3D structure of the electrodes, (b) Uniform tip-exposure of variable height electrodes after RIE and oxygen plasma etching process, (c) Electrode-tip after removing the mask.

The thickness of metals at the tips of the electrodes may differ from the wafer due to nonplanar shape of the electrodes.

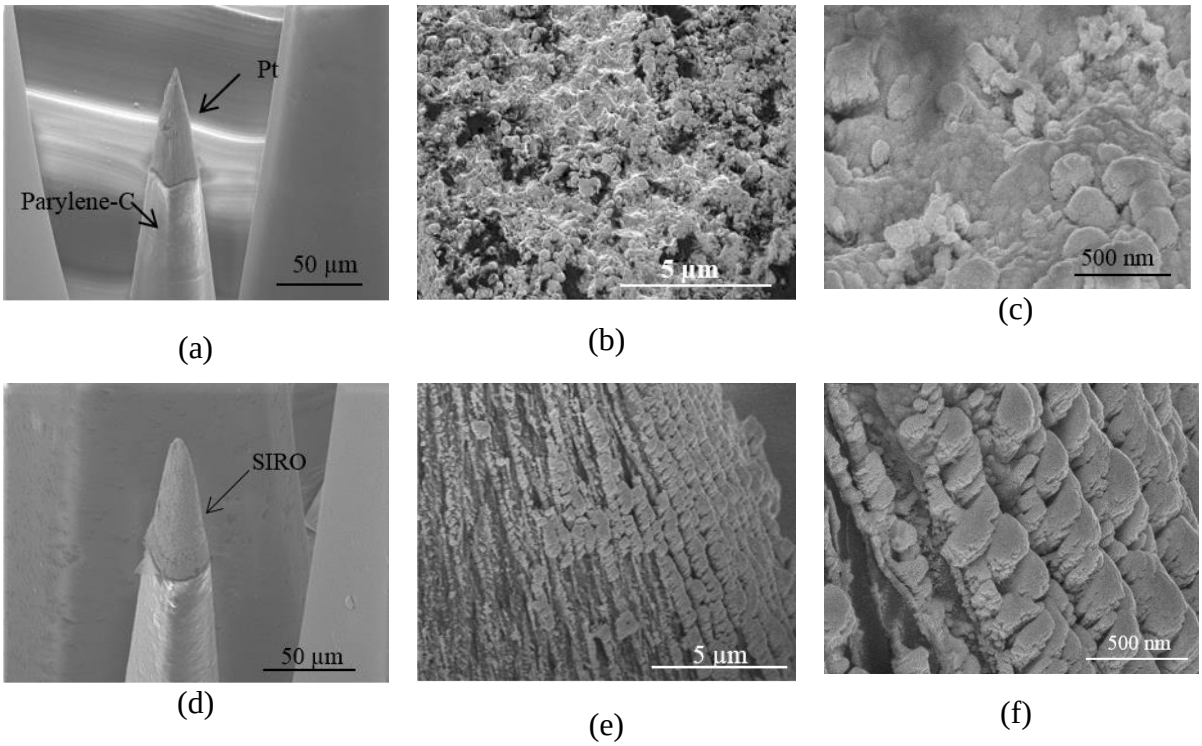

Figure 3.12. SEM images of microelectrodes after tip-metallization with Pt (a,b, c) and SIRO (d, e, f) at different magnification. The SIRO surface is rougher than Pt. SIRO has dendritic structure while Pt has granular morphology.

3.3.4 Tip-CNTs Growth

Figure 3.13 shows SEM images of MEA after CNTs growth. Zoom in on the electrode tips shows forest-like vertically aligned CNTs characterized by a typical length in the order of 600 nm and diameter between 25 and 30nm. We can distinguish the presence of Pt particles at the end of CNTs (Figure 3.13(c)). It is noteworthy that the length of CNTs can be varied by tuning the growth conditions of PECVD such as temperature, pressure, time of growth, etc [151]. However, the short length of achieved CNTs appears more appropriate for neural interface applications. In fact, a recent research result showed that the neural tissue inflammatory response to the implantation of biostable high aspect-ratio nanoparticles and the loss of nearby neurons are strongly length dependent. The study has shown that after a year implantation time in the brain,

an inflammatory response occurs when the length of ZnO nanorods is equal to or larger than the size of immune cells of the brain tissue. A significant loss of neurons was observed adjacent to the 10 µm nanorods. Furthermore, 2 µm nanorods did cause neither significant inflammatory response nor significant loss of neurons nearby [158].

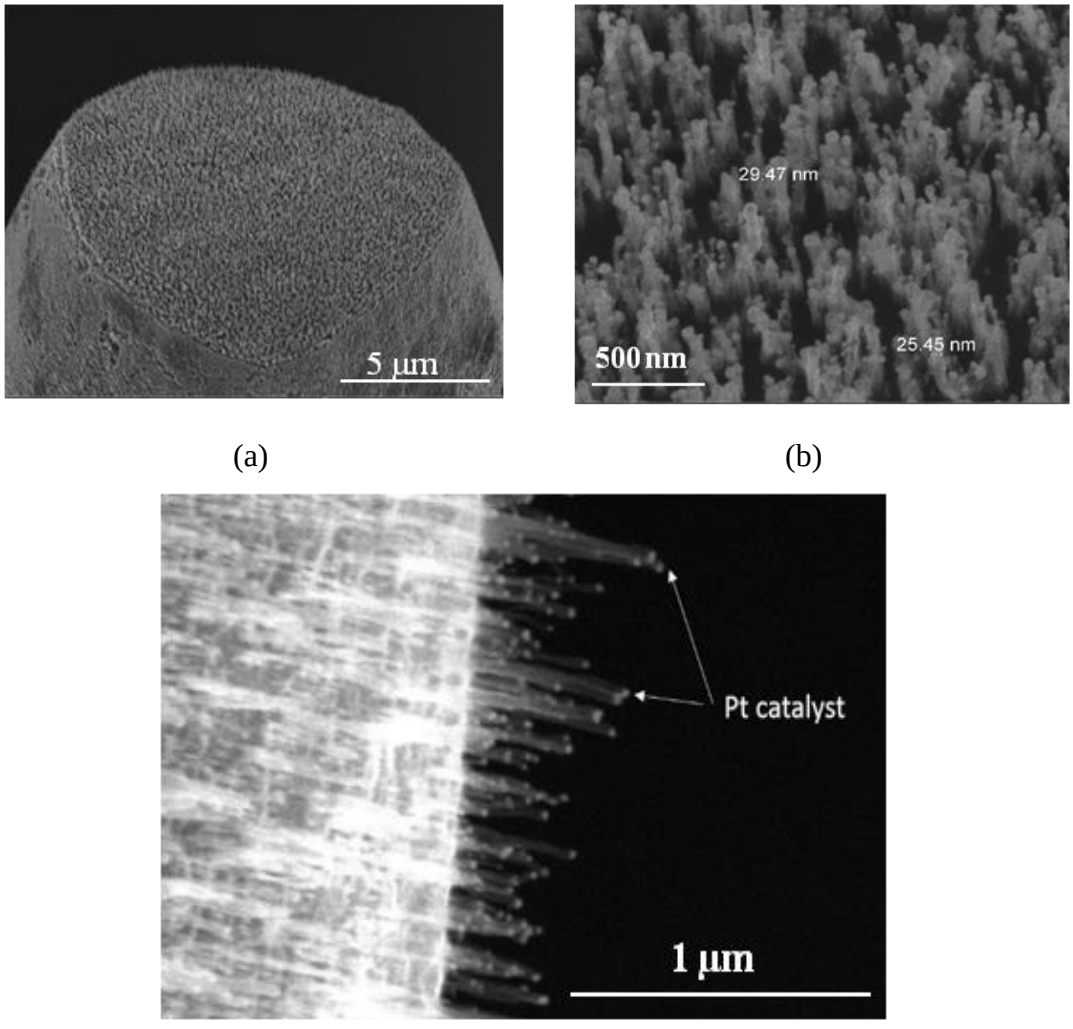

(a) (b)

(c)

Figure 3.13. SEM images of microelectrodes after tip-coating with CNTs: (a-b) At different magnification. The geometry of CNTs increased the accessible surface area, (c) Pt particles at the end of CNTs.

3.3.5 Tip-CNTs deposition (Coffee stains technique)

The formation and structure of the SWNTs at the tips of the electrodes were studied with electron microscopy. Figure 3.14 demonstrates CNTs deposition at the tips of the electrodes. The tips of the electrodes were sputter-coated with Ti/Pt prior to CNTs deposition. The thickness of Ti/Pt layers was 100/400 nm. Same condition as section 3.2.1 has been used for sputtering process (Table 3.2).

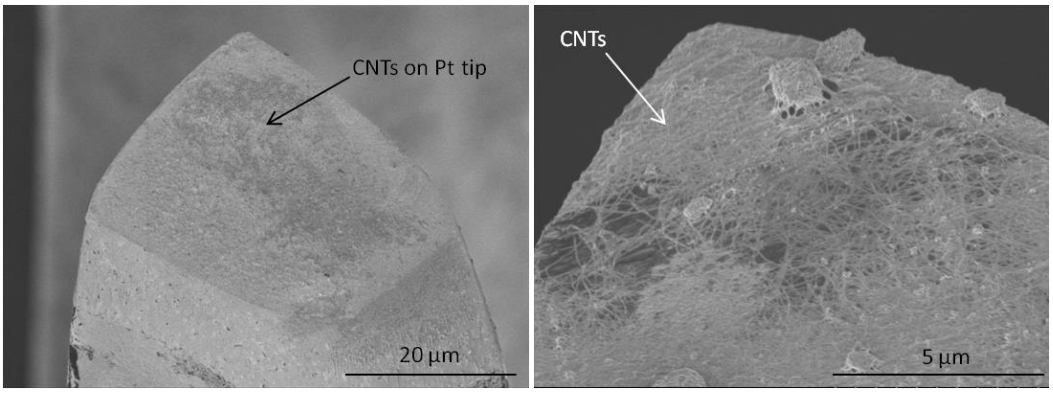

(b)

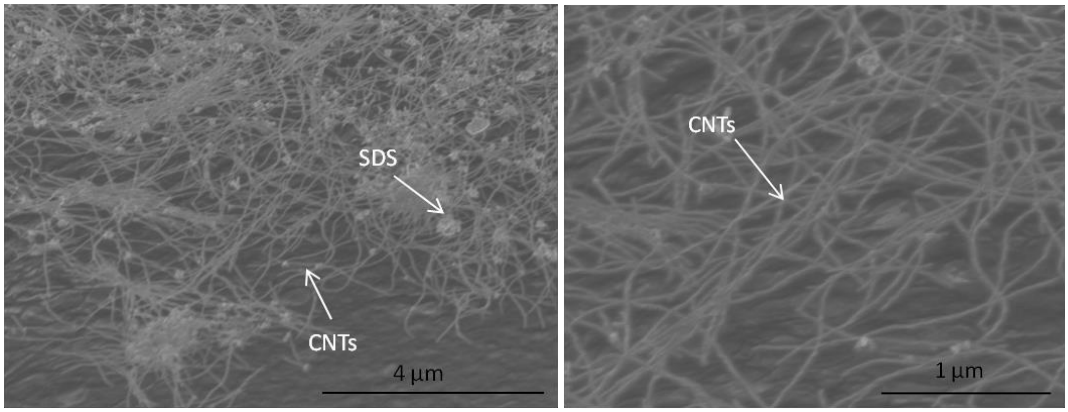

(c) (d)

Figure 3.14. SEM images of microelectrodes after tip-coating with CNTs using coffee stains technique: (a-d) At different magnification. Small white particles are SDS that were evaporated after heating the electrodes.

3.3.6 MEAs Electrical Properties

The average impedance at the biologically relevant frequency of 1 kHz of bare silicon, Pt-, CNTs-, and SIRO-coated electrodes was 850 ± 10, 70 ± 0.24, 14 ± 0.2, and 4 ± 0.2 kΩ, respectively (Figure 3.15, Table 3.3). On average CNTs coating lowered the impedance of Pt-coated electrodes by a factor of 5 at 1 kHz, and increased charge delivery capacity by a factor of 600. The CV of Pt and CNTs were illustrated in Figure 3.15 (c). The CV graph of CNTs and Pt has shown that the CNTs have a significant larger area than Pt electrodes indicating higher Q_{CDC} of CNTs MEA.

Iridium oxide-coated electrodes were not considered for charge delivery capacity (Q_{CDC}) and charge injection capacity (Q_{inj}) because of harmful pH-value changes during electrical stimulation [152].

In order to determine the Q_{CDC}, the electrodes were activated with a repetitive potential cycling at a scan rate of 50 mV/s in the potential range -0.6 to 0.8 V. The Q_{CDC} was calculated using following equation [159]:

$$Q_{CDC} = \frac{1}{\nu A}\int_{E_1}^{E_2} |i| dE \qquad (mC/cm^2) \tag{3.4}$$

where ν is the corresponding scan rate (mV/s), E is the electrode potential (V), E_1 and E_2 are the anodic and cathodic potential limits (V), A is the surface area of the electrode tip (cm^2), and i is the measured current (A).

SEM micrograph in Figure 3.13 demonstrates that CNTs increased the surface area significantly to compare with Pt and iridium oxide (Figure 3.12). Since the resistance is inversely proportional to the surface area, a larger surface area would result smaller resistance.

Surface area of the electrodes active sites is difficult to measure due to roughness and porosity of the surface. Therefore, the geometrical surface area of the electrodes tip was used to determine the charge Q_{CDC} of the electrodes.

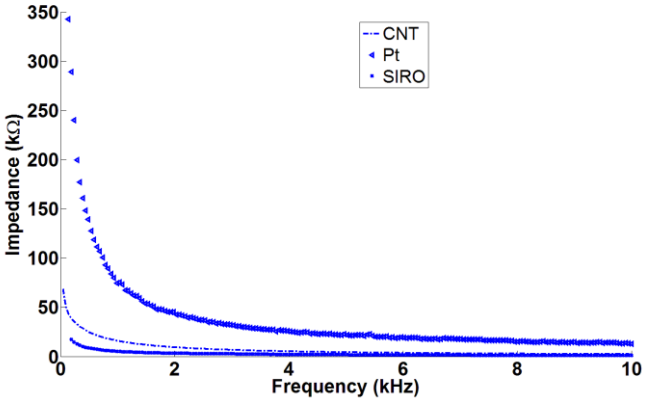

(a)

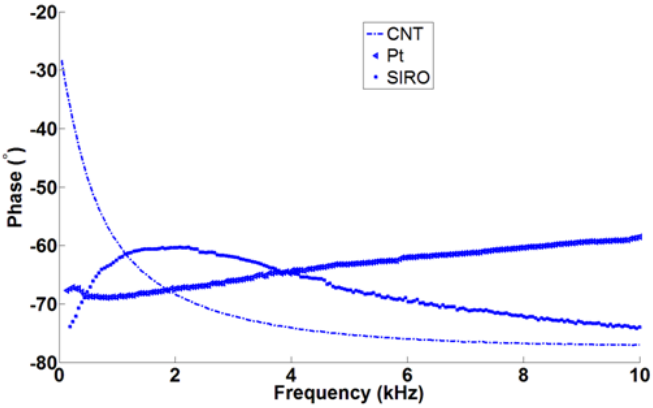

(b)

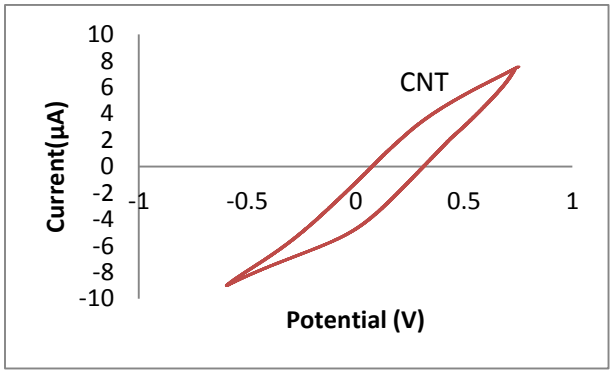

(c)

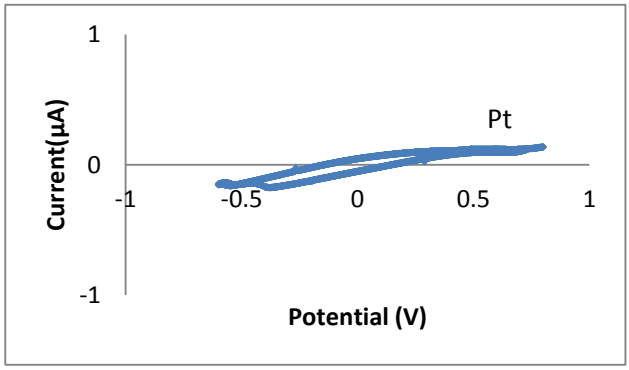

(d)

Figure 3.15. Impedance spectroscopy of Pt- and CNTs-coated electrodes: (a) Magnitude of impedance as a function of frequency, (b) Phase of the impedance as a function of frequency, (c) & (d) CV curves for CNTs- and Pt-coated electrodes of the MEA under similar condition, respectively.

Table 3.3. Average impedance of different electrode-tip coatings

Tip Coating	Bare Si	Pt	CNTs	SIRO[1]
Z (kΩ) at 1 kHz	850 ± 10	70 ± 0.24	14 ± 0.2	4 ± 0.2

[1]SIRO: Sputtered Iridium Oxide

The lateral surface area (LSA) of the active site with the tip-exposure of 50 µm was calculated by the following equation:

$$LSA = \pi r \sqrt{h^2 + r^2} \tag{3.5}$$

where r and h are the radius and height of the cone, respectively (Figure 3.16). These values were measured with SEM. The LSA of the electrode tips was calculated about 1.6×10^{-5} cm^2 for the tip exposure (h) of 50 µm.

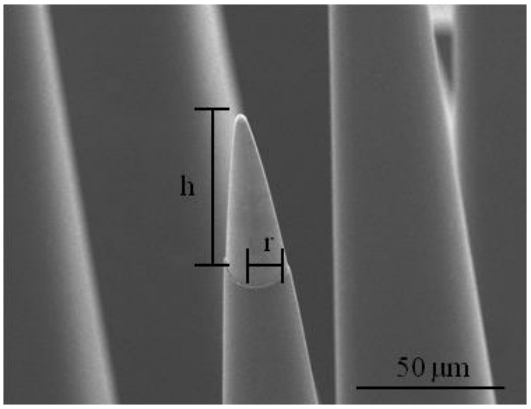

Figure 3.16. Electrode tip dimensions; the height (h) and radius (r) of the tip.

The average cathodic charge delivery capacity of Pt- and CNTs-coated MEAs were 21.7 ± 10.2 and 13020.11 ± 6510.23 mC/cm^2, respectively. Therefore, there is a significant improvement in Q_{CDC} when the electrode tips were coated with CNTs.

The calculated average of Q_{inj} for the Pt- and CNT-coated microelectrodes is 0.3 and 10 mC/cm^2, respectively, for a stimulation current of 92 uA and pulse-width of 0.8 ms.

3.3.7 Equivalent circuit model

The equivalent circuit model includes a constant phase element impedance (Z_{CPE}) that represents the electrode capacitive impedance shunted by a charge transfer resistance R_{CT}, both in series with the solution resistance R_s. C_s is all the shunt capacitance to the ground comprises the capacitance from the metal of the electrode to the solution through the insulation (Figure 3.17) [31, 160]. When the current is applied to the electrode-electrolyte interface, a double-layer of charges simulates a charged capacitor. The double layer capacitance occurs from the movement of charges and ions at the interface. Layers of charges are formed by two mechanisms; Faradic and non-Faradic transfer. Non-Faradic charge transfer is a reversible process and is characterized by the motion of charges at the interface to form a charge separation region. The charging of the capacitor is referred to non-Faradic process. The later can be modeled as a parallel-plate capacitor whose capacitance given by:

$$C = \varepsilon\varepsilon_0 S/d \qquad (3.6)$$

Where ε is the dielectric constant of the medium and ε_0 is the dielectric permittivity of vacuum, S is the surface area, and d is the distance between charge layers. Non-faradic capacitance is empirically represented by a constant phase element (CPE). The CPE impedance is given by:

$$Z_{CPE} = \frac{1}{A(i\omega)^{\alpha}}, \qquad 0 \leq \alpha \leq 1 \qquad (3.7)$$

Where ω is the angular frequency ($\omega = 2\pi f$) and A is the measure of the magnitude of Z_{CPE}. CPE describes an ideal capacitor for $\alpha = 1$ and ideal resistor for $\alpha = 0$. The impedance is purely imaginary for a capacitor and real for a resistor. For a combination of a capacitor and a resistor, a large phase angle value indicates that the impedance is mainly capacitive and for the small phase angle values is a resistive [161].

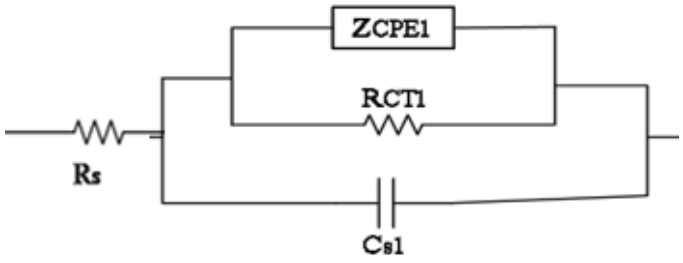

Figure 3.17. Electrochemical measurement setup: Equivalent circuit of the electrode-electrolyte interface.

Increasing the roughness and surface area of the electrodes decreases α due to the increase of atomic scale heterogeneity on a rougher surface. Faradic process involves transfer of electrons across the electrode-electrolyte interface and was modeled as an electrical resistor (R_{CT}). The resistance is inversely proportional to the surface area ($R = \rho l/S$), therefore larger S would result in smaller resistance. Micrographs in Figures 3.12 and 3.13 confirmed differences in surface roughness and clearly indicated that CNTs have a significantly larger surface area to compare with Pt and SIRO. Fitting parameters are given in Table 3.4 while simulated plots using these parameters were shown in Figure 3.18.

Table 3. 4. Fitting results from the EIS model

Coating	α	A (F)	R_{CT} (kΩ)	C_s (F)
Pt	0.85	2.30×10^{-8}	1900	9×10^{-11}
SIRO	0.80	2.10×10^{-7}	400	2.70×10^{-8}
CNTs	0.77	7.20×10^{-6}	24	8.60×10^{-9}

An equivalent circuit model has been used to describe the electrode-electrolyte interface impedance using electrochemical impedance spectroscopy. The electrolyte resistance for all the coatings was 2.2 kΩ. As it has been shown in table 3.3, Pt-coated MEAs are smoother (α) than CNTs-coated while the capacitance (A) is lower. The resistance (R_{CT}) of CNTs is significantly smaller than Pt electrodes. The resistance and capacitance of these coatings could be related to the effective surface area. The double layer capacitance around the interface is proportional with the

active site surface area (equation 3.3). The large surface area would result in a higher capacitance as in the case of CNTs. The resistance is inversely proportional to the surface area so a larger surface area would result in a smaller resistance. A good match between the measurement results and the curves generated using the equivalent circuit model indicates that the appropriate model has been chosen.

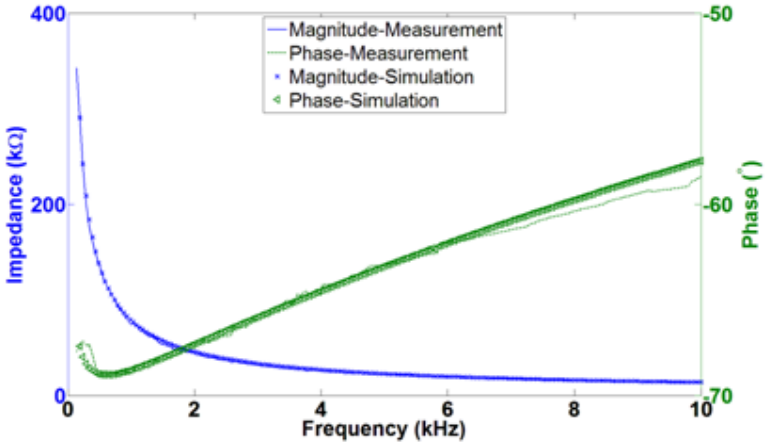

(a)

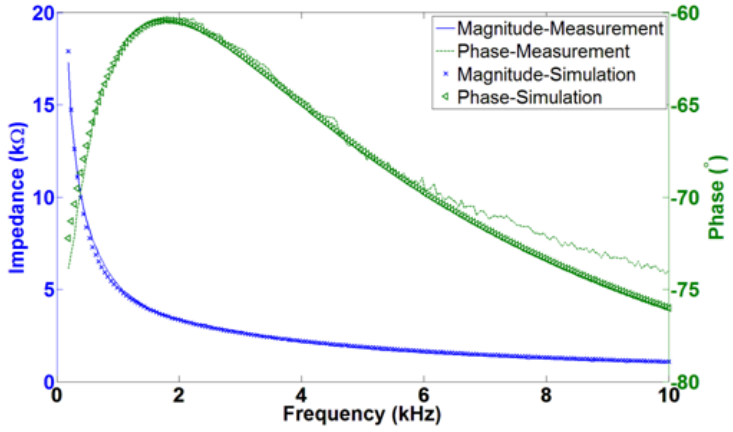

(b)

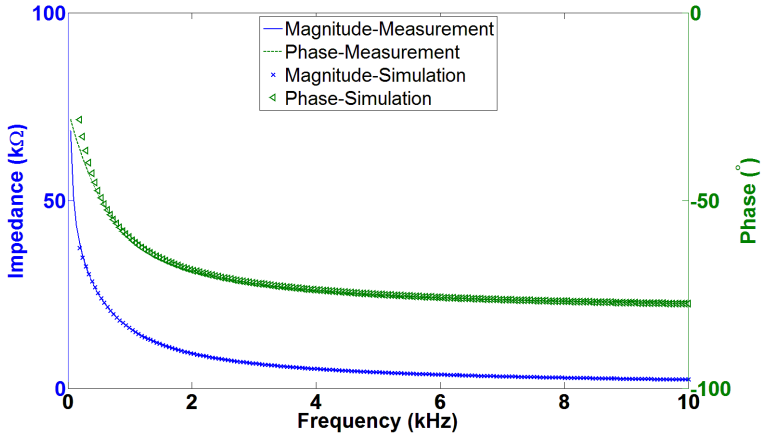

(c)

Figure 3.18. Simulation and experimental results of equivalent electrode-electrolyte interface: (a) Pt-tips, (b) SIRO tip, (c) CNT-tips.

A comparison of electrochemical properties of currently available microelectrodes and this work has been listed in Table 3.5.

Table 3. 5. Comparison of neural Microelectrode arrays

MEAs	Characteristics					
	Geometry	Tip-coating	Z (kΩ) at 1 kHz	Q_{inj} (mC/cm^2)	Q_{CDC} (mC/cm^2)	Density (Electrodes /1.96 mm^2)
(Negi 2010) (Parker 2012)	2D Quasi-3D	Pt, SIROF[1], CNTs (Electrochemical deposition, not stable)	Pt: 125 SIROF: 6 CNTs: 49.71	Pt: 0.3 SIROF: 2 CNTs[2]	Pt: 4.4 ± 3.1 SIRO: 34.3 ± 21.7 CNTs: 1217.359 nC	16
(Ansaldo 2011)	NA	Pt/tungsten microwire (Wire diameter: 20 µm)	CVD-CNT: 15 PPy-CNT[3]: 7 Au-CNT: 50	CVD-CNT: 4 PPy-CNT[3]: 7 Au-CNT: 0.8	CVD-CNT: 1743.4 ±161.7 PPy-CNT: 2920.3 ± 191.4	Single probe
This work	3D	Pt, CNTs (Direct growth, stable & reliable)	Pt: 70 CVD-CNTs:14	Pt: 0.3 CNTs: 10	Pt: 21.7 ± 10.2 CNTs: 13020.1±6510.2	25

[1]SIROF: Sputtered Iridium Oxide Film
[2]CNTs: Charge injection capacity is not reported. Cathodal charge storage capacity (Q_{CCSC}) is 1217.359 nC.
[3]Ppy-CNT: Polypyrrole-CNT
[4]Au-CNT: Gold-CNT

3.4 Discussions

Comparing this microelectrode with currently available intracortical penetrating MEAs, presented MEA has provided 3D high electrode-density (25 electrodes/ 1.96 mm^2), with lower impedance and higher charge injection capacity which are desired for neural stimulation. The importance of such pyramid-shaped MEA has not been quantified but may have significance during injection electrodes inside the tissue. A new fabrication technology has several advantages including different possible geometries (3D structure with variable-height electrodes) and ease of fabrication. The wet etching time were optimized by cutting the wafer to square pieces and applying the gas from the bottom in order to produce narrow and uniform pins. [126]. The usage of this masking method not only resulted in uniform tip-exposure for variable-height electrodes but also reduced the lead time and cost of fabrication significantly. It would take 6 h compared to 24 h by the conventional masking method [123, 162].

The direct growth of CNTs on electrodes led to stable, reliable, and high-density coverage compared to CNT films coated using electrochemical deposition. The impedance of CNT electrodes was significantly lower than Pt but still not as low as iridium oxide [5]. Iridium oxide-coated electrodes were not considered because of deterioration of long term stability if used beyond their charge injection limits [152].

EIS measurements have been done in vitro to characterize the quality of the microelectrodes coated with Pt and CNTs. Pt electrodes have lower impedance compared with currently available microelectrodes. The measured impedance of Pt-coated microelectrodes was 70 kΩ at 1 kHz. CNT-electrodes exhibited better electrochemical properties compared to Pt. The impedance of CNT-electrodes at 1 kHz was 5 times smaller than Pt, while CNT was 600 times higher than that of Pt. More importantly, CNT Q_{inj} is thirty three times higher than that of Pt. Iridium oxide-electrodes were not considered because of harmful pH-value changes during electrical stimulation[5, 25].

Ansaldo et al have studied electrical properties of three different coatings on sharp Pt/tungsten wire microelectrodes including CVD growth of CNT, polypyrrole-CNT (PPy-CNT) and gold-CNT (Au-CNT) composites by electrochemical co-deposition method (Ansaldo, Castagnola et al. 2011). The authors have shown that the PPy-CNT improved the Q_{CDC} and lowered impedance

compared with CVD-CNT electrodes; however, PPy-CNT's electrical properties degrade with time (Table 3.4).

Abidian et al deposited PEDOT nanotubes on planar neural electrodes and have measured the charge capacity density (Q_{CCD}) and impedance which were about 110 mC/cm^2 and 10 kΩ at 1 kHz, respectively (Abidian and Martin 2009). The authors have later shown that the combination of PEDOT nanotubes with PEDOT and hydrogel improved the Q_{CCD} to 220 mC/cm^2 and lowered impedance to about 2.5 kΩ at 1 kHz. The impedance of PEDOT + PEDOT nanotubes + hydrogel is less than CVD-CNT; however, the coating process of PEDOT with different combinations is more complicated compared with CVD-CNT.

Direct growth of CNTs at the tips of presented microelectrodes could increase the Q_{CDC} 5 times more than PPY-CNT electrodes. The Q_{CDC} of this MEA is even higher than electrodes coated with polymers and hydrogels which involve the hydrophilicity.

Another parameter which is important to compare the MEAs materials for neural devices is Q_{inj}. The Q_{CDC} of materials can be increased by increasing the surface area but it may not increase the charge injection capacity [163, 164]. As mentioned above the Q_{CSC} of CVD-CNT electrode was 56.9 ± 0.8 mC/cm^2 while the Q_{inj} is only 4 mC/cm^2. As shown by Abidian et al the Q_{CSC} of large surface area PEDOT was 220 m/cm^2 while Nyberg et al demonstrated 3.6 mC/cm^2 for PEDOT-poly styrenesulfonate electrodes [164]. As mentioned above the Q_{CDC} of direct growth of CNT-electrodes is 13020.1±6510.2 mC/cm^2 while the Q_{inj} is only 10 mC/cm^2. The Q_{inj} of presented MEA is higher than PPY-CNT electrodes.

In order to minimize the immune response of the neural tissue to implanted MEAs, the surface of the electrodes could be coated with polymers and bioactive molecules such as polyethylene glycol (PEG) and peptides. These materials not only improve the biological compatibility of the electrodes but also can be absorbed to the CNTs surface through noncovalent interactions. CNT has inherently large surface area but most of its large surface area is inaccessible in electrolyte aqueous solution and cannot contribute to charge injection. Various surface modification techniques exist to enhance the hydrophilicity of the CNTs electrodes. One of the techniques to modify CNTs is coating electrodes with peptides. The peptide binds strongly to the nanotube side wall via van der Waals and hydrophobic interactions, while the PEG chain extend into water. As a result, the CNT-coated microelectrodes turned more hydrophilic (Wang, Fishman et al. 2006). Another hydrophobic to hydrophilic transition happens during incubating electrodes

with cell culture medium. Wang et al has showed that functionalized hydrophilic CNT microelectrodes could increase effective surface area about 300 times and enhance high charge injection during stimulation [138].

3.5 Conclusion

A novel, high-density, penetrating, pyramid-shaped microelectrode array for recording and stimulation neurons was designed and implemented. Due to its geometry, the proposed 3D MEA provides higher contact density than available electrode arrays and allows recording from different depths of the cortex. The fabrication technology, described in this work, is simpler and faster than currently available techniques. Besides, the novel masking technology provides a uniform tip exposure for 3D structures. In addition, selective direct growth of CNTs on the tips of 3D MEAs using Pt as a catalyst material has been done. On average CNT coating lowered the impedance of Pt-coated electrodes by a factor of 5 at 1 kHz and increased charge transfer by a factor of 600. The next step will be coating MEAs with biocompatible polymers and biomolecules to improve biocompatibility of these electrodes, create a biologically active electrode-tissue interface, and improve the charge injection capacity of the electrodes by hydrophilizing CNT-electrodes. *In vitro* cell culture tests will be performed to evaluate the growth of cells in presence of the electrodes.

CHAPTER 4 BIOCOMPATIBILITY OF MEAs

4.1 Bioactive molecule deposition

As we mentioned before one of the strategies that can be used to minimize immune response to implanted electrodes is by coating them with bioactive molecules such as cell adhesion peptides or proteins. These peptides not only improve cell adhesion but also increase the cell proliferation [51]. Among the biomolecules, Tyr-Ile-Gly-Ser-Ar (YIGSR), Ile-Lys-Val-Ala-Val (IKVAV) polypeptide fragments [105, 106], and poly-D-lysine (PDL) [110] are promising candidates that are likely to modify neural cell behavior, facilitate neural adhesion onto the electrode devices, minimize astrogliosis, and suppress chronic microglial activation. PDL is a widely used synthetic peptide can improve neural-cell adhesion, spreading and growth, especially on metallic surfaces. Due to its positive charge, it attracts (negatively charged) neurons primarily due to electrostatic interactions [110, 165, 166].

The peptide-polymer conjugation method [112] has a number of advantages over other methods including electrochemical polymerization, covalent bonding, self-assembling monolayers, and electron spinning when used to cover silicon micromachined electrodes that have been coated with polymers and metals. For example, this method can be used on electrically conductive and insulating surfaces in order to cover both electrode sites and nonfunctional areas of the device. Furthermore, the peptide-polymer conjugation method is simpler to employ when compared with other peptide deposition methods. Furthermore, the peptide-polymer conjugation method is simpler to employ when compared with other peptide deposition methods.

In this part of the project, microelectrode arrays (MEAs) with various tip-coatings of platinum (Pt), gold (Au), molybdenum (Mo), sputtered iridium oxide (SIRO), and carbon nanotubes (CNTs) have been used when their shank was covered with parylene-C and polyethylene glycol (PEG) (excluding CNT-MEAs that covered with SiO_2 and PEG), in order to reduce responses to foreign bodies and decrease the mechanical mismatch between metals and tissue [167]. Hydrogels are excellent scaffolding materials for repairing and regenerating a variety of tissues due to their highly swollen 3D structure similar to soft tissues [168]. PEG hydrogel and parylene-C are biocompatible polymers that are widely used for coating MEAs in both *in vitro*

and *in vivo* studies [131, 169-171]. Mo and molybdenum oxide thin films are highly conductive, resistance to corrosion, and biocompatible [172, 173].

The goal of this study is to evaluate the role of PDL for promoting and stabilizing cell attachment on the surface of unique microelectrode arrays. The impedance of the electrodes was measured before and after PDL deposition. *In vitro* cell culture tests were performed to evaluate the growth of neuroblast cells on the PDL-coated electrodes [174]. A significant advantage of *in vitro* study is that the cells response and health can be observed over time. Optical microscopy and scanning electron microscopy (SEM) were used to evaluate the biological compatibility of the electrodes.

4.1.1 MEAs preparation

In order to insulate the shank and improve the biocompatibility of the electrodes, the entire upper surface of some of the electrodes (i.e. excluding the CNT-MEAs) was covered with parylene-C using a chemical vapor deposition (CVD) process. Parylene-C films were deposited using a SCS Labcoter (PDS 2010). Parylene-C dimer was vaporized under vacuum (< 10 mTorr) at 140°C. The dimerized gas was pyrolyzed at 670°C and deposited as a conformal, pinhole-free transparent film. For the electrodes with CNT tips, native SiO_2 was considered as an insulator instead of parylene-C.

A novel masking technology was developed to coat the active sites of the 3D MEAs. Following insulation of the electrodes, a layer of dry-film photoresist (DuPont, FX900) was used as a mask on the array. The dry-film follows the 3D structure and enhances the uniform tip exposure.

Dry-film and parylene-C were removed from the tips using reactive ion etching techniques. Custom designed reactive-ion-etching (RIE) and plasma-asher machines were used to etch the films. In the first step, dry-film and parylene-C films were anisotropically etched by reactive-ion etching (RIE, RF source) from the top of the electrode tips at a power of 200 W and a chamber pressure of 100 mTorr for 50 minutes. In the next step, both films were etched isotropically with plasma asher (microwave source) from the side-walls of the tips at a power of 150 W and a chamber pressure of 400 mTorr for 10 min using PVA TePla system.

The tips of each MEA were separately sputter-coated with Pt, SIRO, Au, and Mo. All the metals were deposited in a custom designed multi-cathode sputtering system. Ti was used as an adhesion layer for Pt, Au, and iridium oxide. The Ti layer was sputtered in Ar ambient at the

chamber pressure of 10 mTorr and gas flow rate of 10 sccm (standard cubic centimeter per minute) at the power of 90 W, for 11 min. The thickness of Ti was 100 nm. Pt and Au were sputter-deposited at the tips of 12 MEAs. Pt and Au puttering were done in a chamber pressure of 10 mTorr with Ar flow rate of 10 sccm at the power of 90 W, for 16 and 13 min, respectively. Sputtered iridium oxide (SIRO) was deposited at the tips of 6 MEAs in Ar and O_2 plasma with both gases flow rate at 25 sccm. The power was 100 W with the deposition pressure of 5 mTorr, for 33 min. Mo was sputter-deposited on the tips of 6 MEAs at the pressure of 10 mTorr with Ar flow rate of 10 sccm. The power was 200 W, for 16 min. The thickness of Pt, Au, and Mo was 400 nm and the thickness of SIRO was 200 nm (Table 4.1). The mask was removed with the lift-off process and ultrasonically cleaned in acetone, isopropanol, and DI water.

For 6 MEAs, electrode sites were coated with carbon nanotubes (CNTs) using direct growth and the coffee stain methods. We have carried out CNTs growth by using Plasma Enhanced Chemical Vapor Deposition (PECVD) (section 4.4.2). In coffee stain method, MEAs were dipped in a solution of single-walled CNTs, deionized water, and sodium dodecyl sulfate (SDS) as a surfactant for 24 h in a fix position.

Forty-five pyramid-shaped MEAs were fabricated to verify the biocompatibility of the electrodes and *in vitro* test.

Table 4. 1. Sputtered deposition parameters for the electrodes' tip-metallization

Metal	Ambient	Gas flow rate (sccm)[1]	Chamber pressure (mTorr)	Power (W)	Time (min)	Thickness (nm)
Ti	Ar[2]	10	10	90	11	100 ± 5
Pt	Ar	10	10	90	16	400 ± 10
SIRO	Ar/O_2	25/25	5	100	33	200 ± 10
Au	Ar	10	10	90	13	400 ± 10
Mo	Ar	10	10	200	16	400 ± 10

[2]Ar: Argon

[1]Sccm: standard cubic centimeter per minute

4.1.2 Coating of the MEAs with polyethylene glycol (PEG)

The PEG coating was added to the MEA by incubating them for 24 h (4 °C) in a solution of 10 mg/mL PEG in Phosphate-buffered saline (PBS) at pH=7.2 [131, 175]. Twenty-four arrays were coated with parylene-C whereas 3 MEAs were covered with the PEG hydrogel. Six uncoated samples were used as controls. Figure 4.1 shows a schematic image of the 3D MEAs.

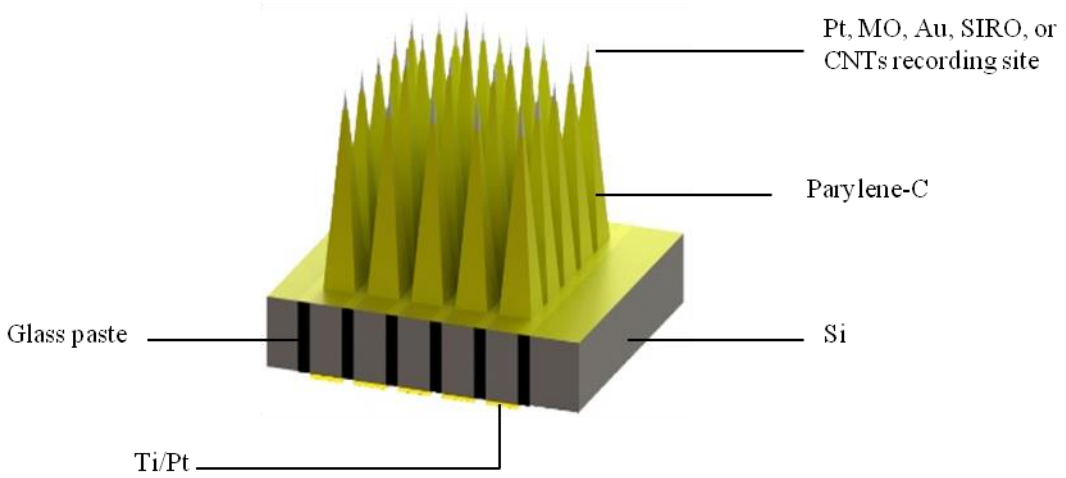

Figure 4.1. Schematic view of a silicon micromachined neural MEA with variable heights of 1.45, 1.55, and 1.65 mm. The shank was covered with parylene-C (or PEG) and the recording sites of each array were coated with Pt, Mo, Au, SIRO, or CNTs. The thickness of the electrodes was 200 μm at the base and less than 2 μm at the tip with 100 μm spacing.

4.1.3 Conjugation of peptide (poly-D-lysine) to the MEAs

The conjugation of peptides to the MEAs was carried out according to the protocol described by Smith et al. [112]. Electrodes with different coatings were rinsed with acetone, isopropanol alcohol and deionized (DI) water then soaked in DI water for 24 h. After the cleaning process, three arrays of each tip-coating and three parylene-C-coated MEAs with no metal in the tips were immersed in 0.1 M phosphate buffered saline (PBS) at pH 7.4. All reactions were performed at 4°C using a solution of 0.1 mg/mL PDL. The solutions, including electrodes, were magnetically stirred at 100 rpm for 24 h.

4.1.4 Fourier transform infrared spectroscopy (FTIR) analysis

Fourier transform infrared spectroscopy (FTIR) was performed in order to characterize the chemical composition of the parylene-C/PDL coatings [171, 176]. A Thermo Scientific model Nicolet 6700 spectrometer, with a SMART iTR attenuated total reflectance probe, was used to record spectra in the 500-4000 cm^{-1} range, using a 4 cm^{-1} resolution. Sixteen scans were combined in order to improve the signal-to-noise. Spectra were smoothed using Qtiplot software.

4.2 Cell cultures and *in vitro* cell test

4.2.1 Culture neuroblast cell line (CCL-131)

After deposition of the PDL, electrodes were placed in culture dishes and sterilized by ultraviolet light in a laminar flow hood. A neuroblast cell line (CCL-131), isolated from mouse muscles and obtained from American Type Culture Collection (ATCC), was used. Cells were cultured in Eagle's minimal essential medium (EMEM), supplemented with 10% fetal bovine serum (FBS) and 1% penicillin/streptomycin. They were maintained at 37°C in a humidified incubator with 5% CO_2 until they were seeded into 24-well plates.

4.2.2 Cell-counting

Knowing the number of input and output cells per each well is important for measuring the impact of the experiments. To calculate cell proliferation, the number of the cells for each well was determined with 2 different methods; capturing several images for each sample and manual counting of cells using hemocytometer (Figure 4.2). In the first method the total cells and the cells within each circle with radius of 150 µm around each electrode tip were counted. The number of cells per each well has been counted before placing MEAs in their own wells and after 24 h. In the second method to assure that no cells were washed away after imaging, the cell cultures were incubated directly in trypsin. When all cells were detached, cell culture medium was added and the cells were counted.

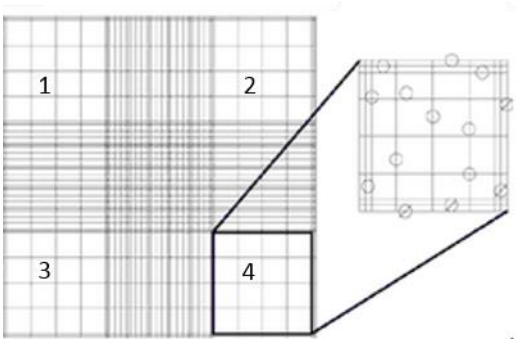

Figure 4.2. A schematic view of hemocytometer as seen from the microscope. The cells marked as a circle in sections 1, 2, 3, and 4 was counted.

4.2.3 Cell incubation with the electrodes before and after PDL coating

Peptide-coated and uncoated MEA were placed in their own specified wells for cell attachment and proliferation monitoring over 4 days. A Zeiss microscope (Primo Vert) was used to image cells on the electrode arrays after 6, 12, 24, 48 h, and 4 days. All experiments were carried out three times, using triplicate measurements.

4.2.4 Statistical analysis

Data has been reported as the mean ± standard deviation of the mean. Cell attachment, before and after PDL deposition, was compared for statistical significance using a t-Test at a significance level of $p = 0.05$. Standard deviation calculations have been used. For the cell proliferation studies at least 20 images per sample were captured. All experiments were repeated 3 times with triplicate samples.

4.3 Results

4.3.1 Conjugation of PDL and PEG to the MEAs

The PDL and PEG coatings could be observed by SEM (Figure 4.3). Furthermore FTIR spectroscopy was used to analyze the chemical composition of the electrodes.

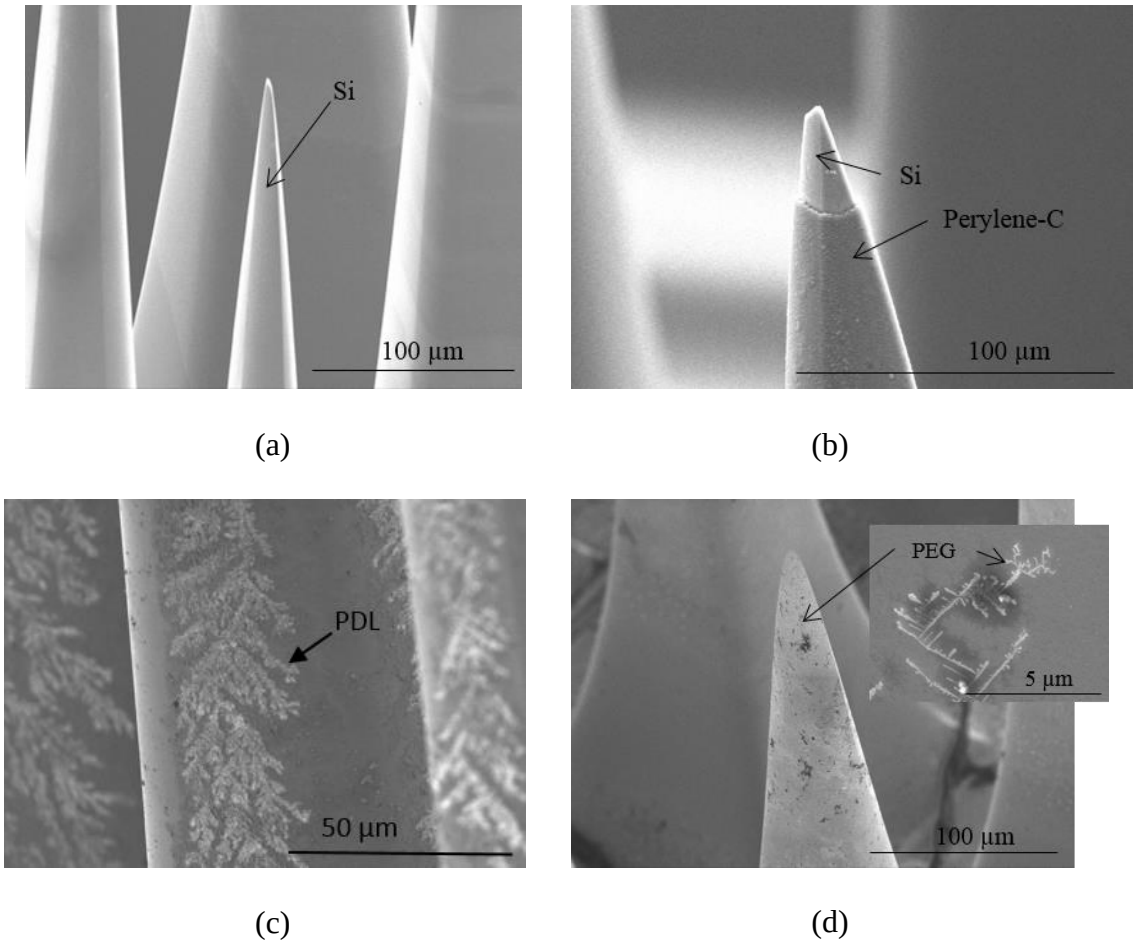

Figure 4.3. SEM images of microelectrodes: (a) Silicon-based microelectrode before coating with parylene-C and PEG, (b) Microelectrode coated with parylene-C, (c) Microelectrode covered with PDL, (d) Microelectrode covered with PEG.

4.3.2 Conjugation of peptides to MEAs

SEM images of electrode tips were acquired before and after PDL deposition followed by rinsing of the surfaces. The micrographs suggested that there was an excellent adhesion of the peptides onto the electrode surface. The morphology of the surface bound peptide appeared to be very different than the parylene-C coating. A nodular fractal structure of PDL, forming finger-like patterns on the surface of the electrode was observed (Figure 4.4).

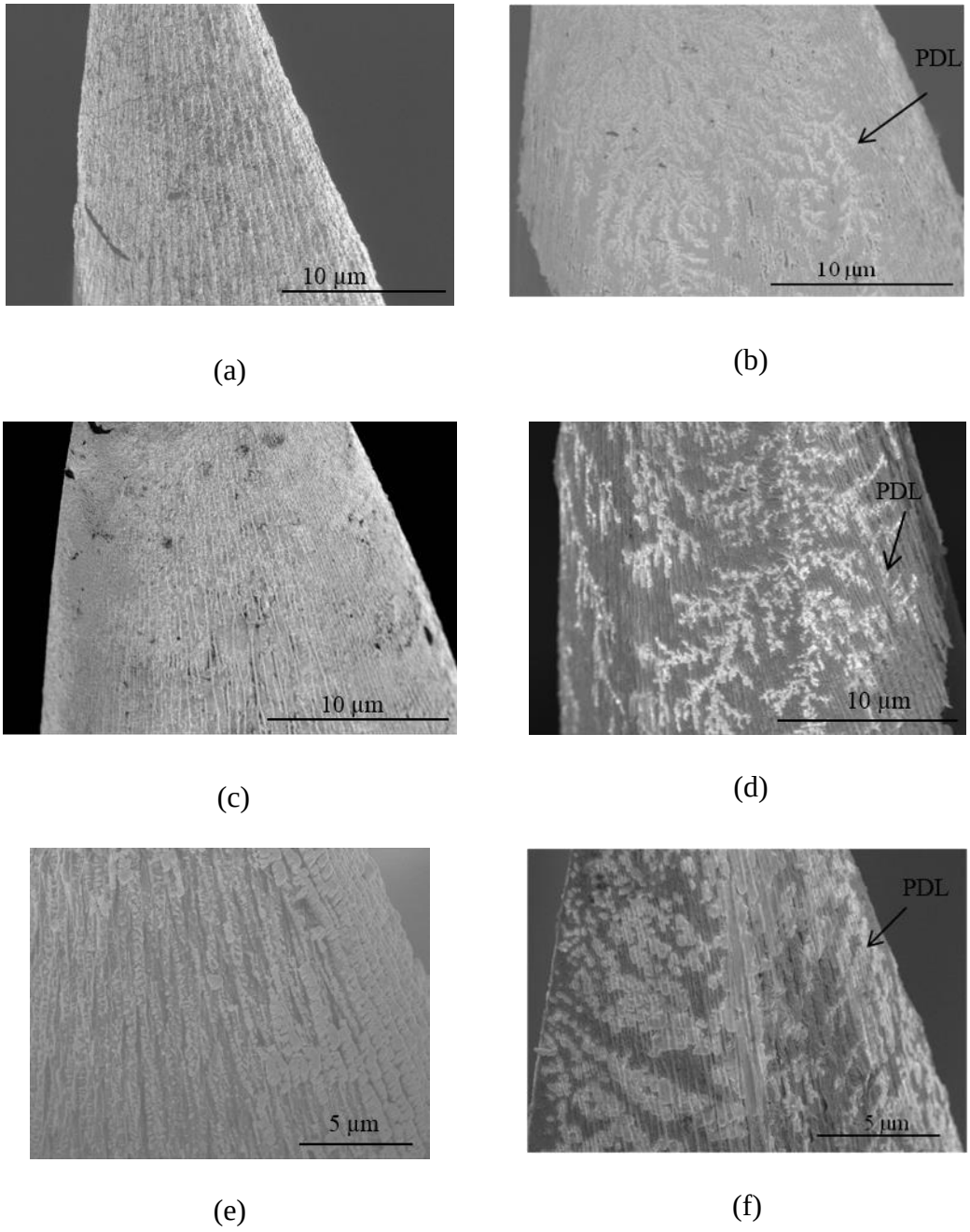

Figure 4.4. SEM images of the MEA surfaces coated with: (a) and (b) Pt, (c) and (d) Au, (e) and (f) SIRO before and after coating with the PDL, respectively.

4.3.3 FTIR analysis

The attachment of PDL to the silicon MEA, insulated with parylene-C and different tip-coatings was observed by FTIR. The spectra, in the range of 600 cm^{-1} to 4000 cm^{-1}, are shown for the Mo and Pt tip-coatings before and after PDL coating (Figure 4.5). CH_2 groups of lysyl residue side

chains of PDL and those of parylene-C, in the range of 3200 to 2850 cm^{-1}, were masked by a broad band corresponding to the hydrogen bonding of the hydration water. The vibrational stretches of C-H at approximately 3032 cm^{-1} (again superimposed with the broad band due to hydrogen bonding), aromatic C-C stretches at 1500 cm^{-1}, aromatic C=C at 1450 cm^{-1} as well as the vibrational stretches of C-Cl at 1055 cm^{-1} could also be unambiguously attributed to the parylene-C coating of the microelectrode [171]. When PDL was added to the surfaces, N-H stretching of amide groups in the range of 3100-3400 cm^{-1} and carbonyl groups in the range of 1650-1690 cm^{-1}, were also observed [176]. The conjugation of the PDL to the MEA with the Au, SIRO, and CNTs tips was also confirmed by FTIR spectroscopy (Figure 4.6).

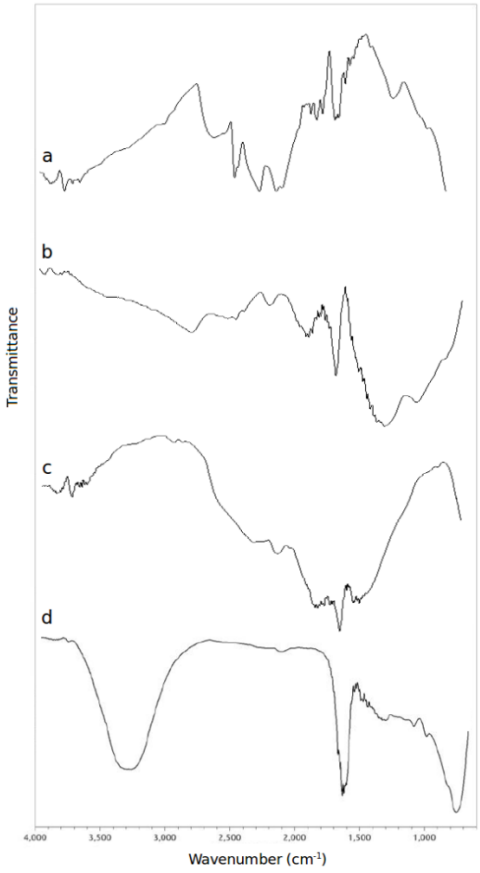

Figure 4.5. FTIR spectrum of silicon MEA insulated with parylene-C and tip coated with PDL: (a) and (b) Mo tip-coating before and after coating with the PDL, respectively. (c) and (d) Pt tip-coating before and after coating with the PDL, respectively.

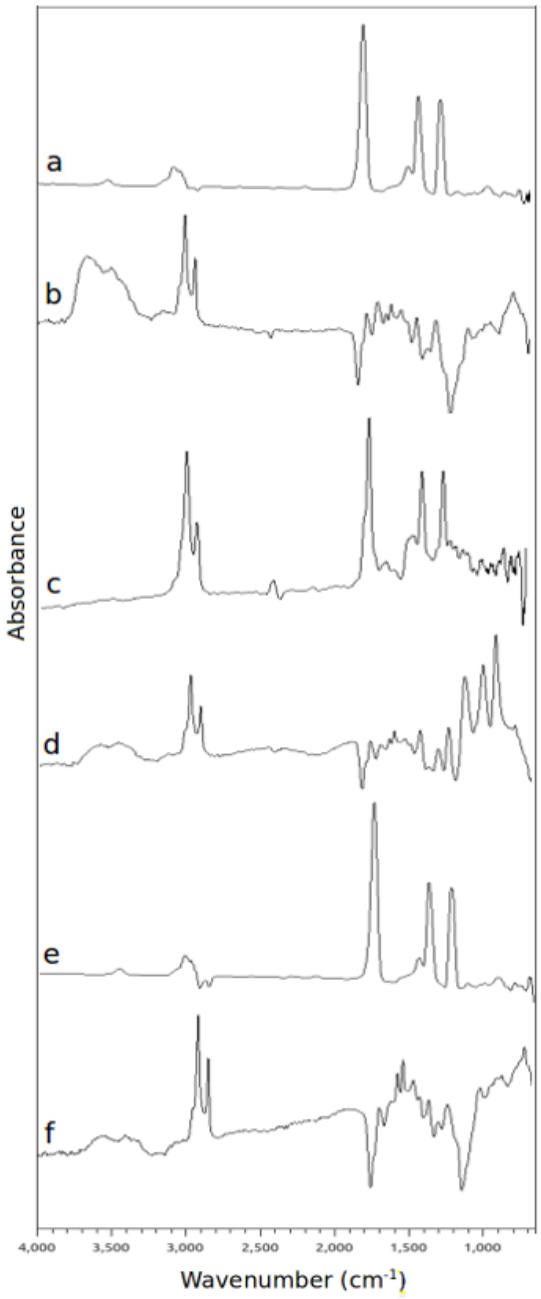

Figure 4.6. FTIR spectrum of silicon MEA insulated with parylene-C and tip coated with PDL: (a) and (b) Au tip-coating before and after coating with the PDL, respectively. (c) and (d) SIRO tip-coating before and after coating with the PDL, respectively. (e) and (f) CNTs tip-coating before and after coating with the PDL, respectively. These measurements have been done using Perkin Elmer spectrum with a 65 FTIR spectrometer.

4.3.4 Effect of polymer coating on the cell size, morphology, and proliferation

Cells continued to grow and proliferate when incubated with the electrodes coated with parylene-C and PEG. The results confirmed that the electrodes and coatings were not harmful to the cells *in vitro*. When compared to the control electrodes (without coating), the size and morphology of the cells and the cell numbers were not significantly affected by the addition of the two polymers (Figures 4.7 and 4.8).

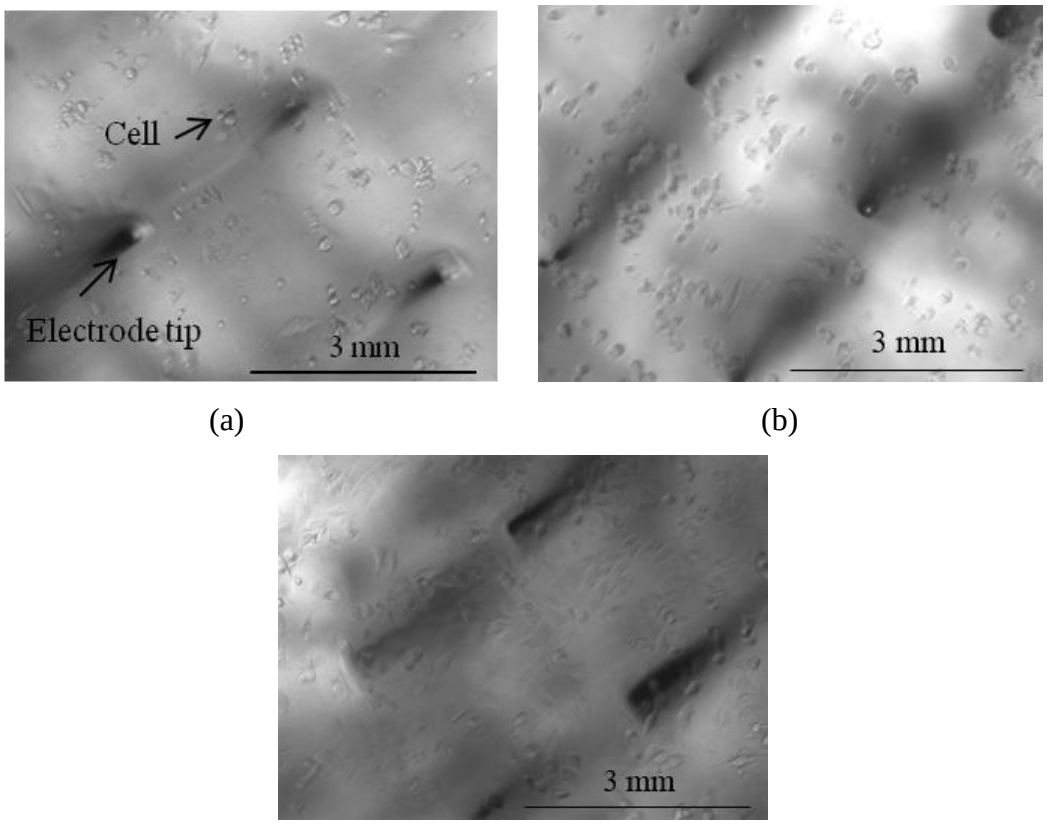

(a) (b)

(c)

Figure 4.7. Optical microscopy of the electrode tips incubated with neuroblast cells: (a) Before coating with polymers, (b) Following coating with parylene-C, (c) Following coating with PEG hydrogel.

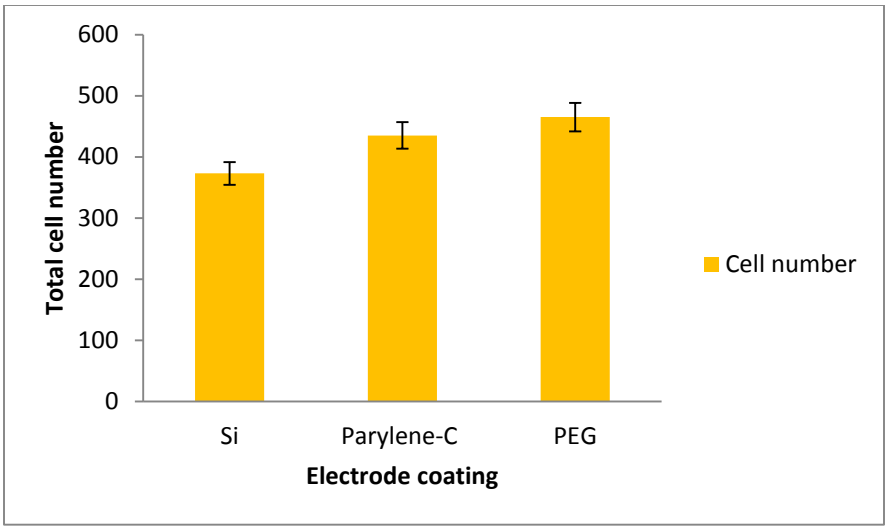

Figure 4.8. Total cell number before and after parylene-C and PEG deposition, (N=6).

4.3.5 Cell proliferation on the peptide-conjugated MEAs

Peptide-coated and uncoated MEA were cultured with mouse neuroblast cells for 4 days and monitored after 6, 12, 24, 48 h, and 4 days. In the optical images (Figure 4.9), the black spots correspond to the electrode tips surrounded by the cells. An increased cell proliferation due to the PDL-conjugation of the samples was clearly observed by optical microscopy. Cells grew and proliferated normally in the presence of polymer, metal, and CNT coated electrodes. Indeed, the number of the cells that were quantified on the PDL-coated electrodes (five different active sites) was significantly (One-tailed t-Test, p = 0.0016) greater than the cell numbers on the uncoated electrodes (Table 4.2, Figure 4.10). The PDL coating increased cell adhesion by more than 50%. Figure 4.11 shows growth curve for neuroblast cells via manual count using hemocytometer after 6, 12, 24, and 48 h. It is noteworthy that the electrodes with CNT active sites had greater cell numbers than the electrodes with metallic tips, both before and after PDL deposition. These results show that the CNTs increased biocompatibility and enhanced cellular responsiveness by attracting more neural cells, in agreement with previous work [177].

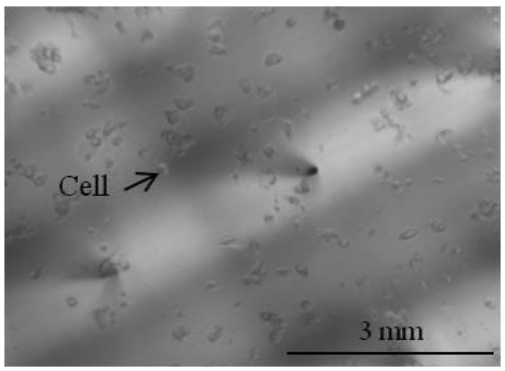

(a)

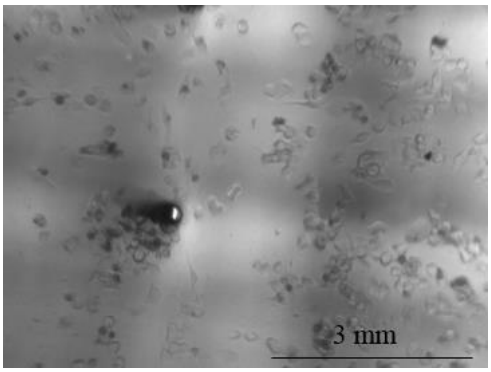

(b)

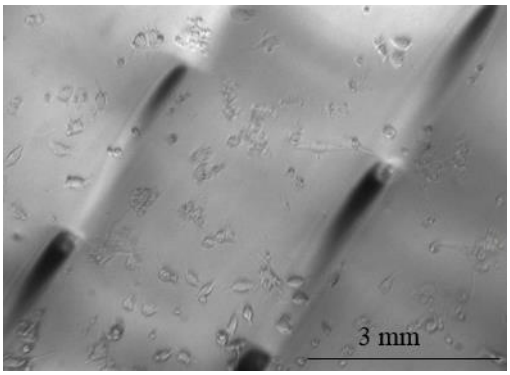

(c)

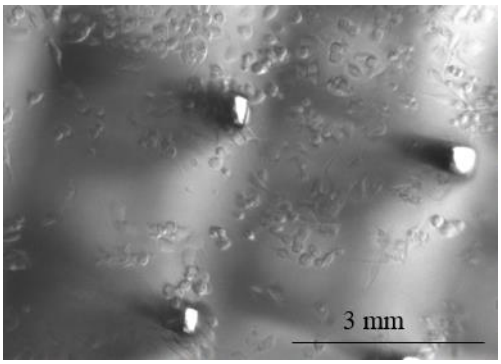

(d)

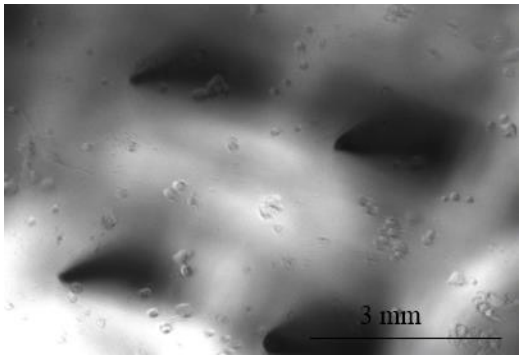

(e)

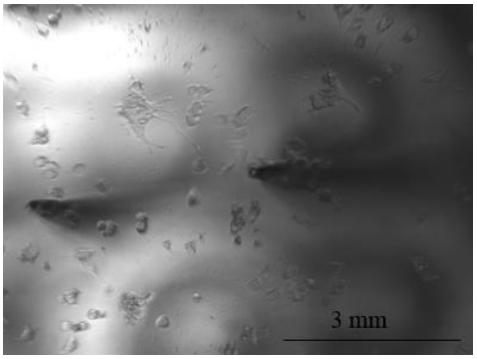

(f)

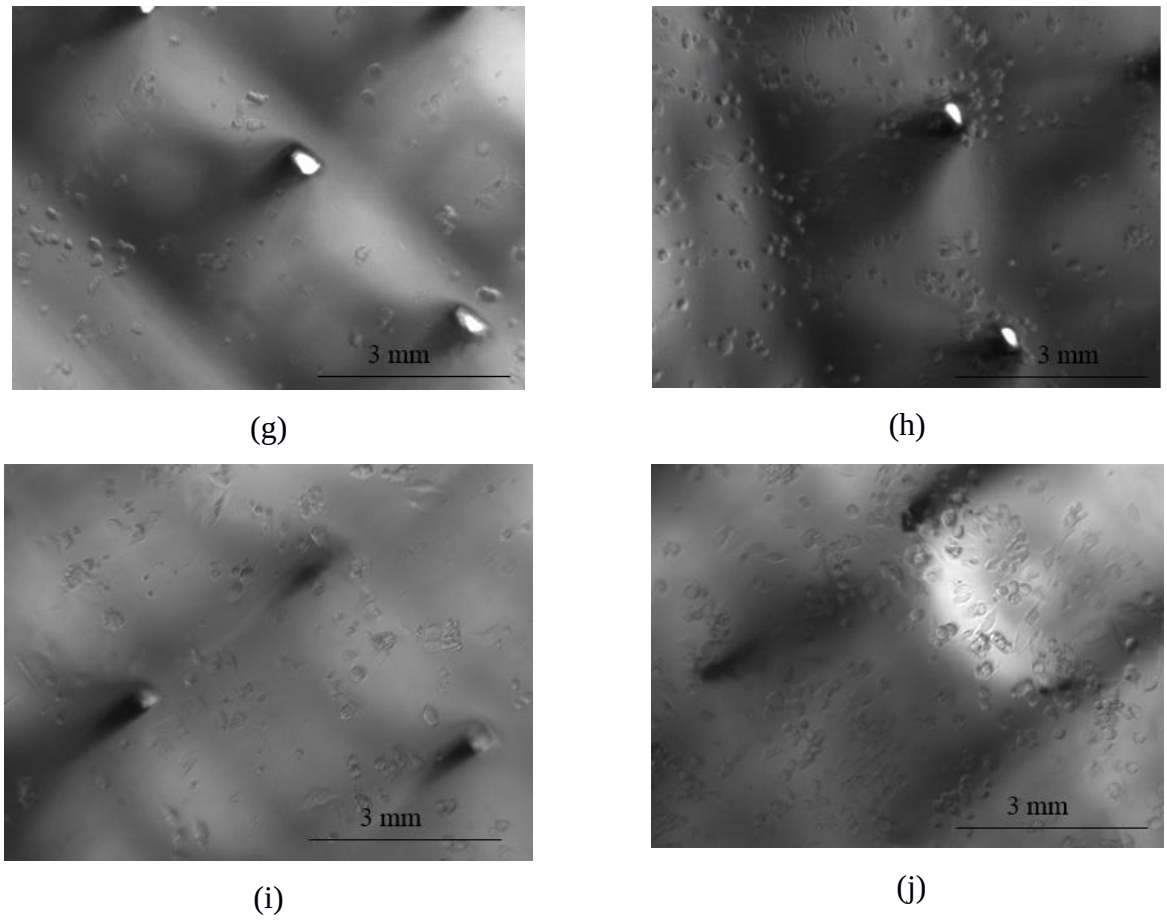

(g) (h)

(i) (j)

Figure 4.9. Optical microscopy of the MEAs incubated with neuroblast cells: (a) and (b) Pt, (c) and (d) Au, (e) and (f) SIRO, (g) and (h) Mo, (i) and (j) CNTs tips before and after PDL coating, respectively. Significantly more cells were attached to the PDL-coated electrodes than the uncoated ones (Table 4.2).

Table 4. 2. The number of cells per electrode site for each tip coating before and after PDL coating.

Electrode tip-coating	Cell number per electrode before PDL-coating	Cell number per electrode after PDL-coating
Pt	20.4 ± 1.13	81.33 ± 2.34
Au	25.1 ± 1.69	83.55 ± 2.69
SIRO	17.22 ± 1.71	69.33 ± 2.64
Mo	15.11 ± 1.36	57 ± 1.32
CNTs	24.55 ± 2.12	115.66 ± 2.23

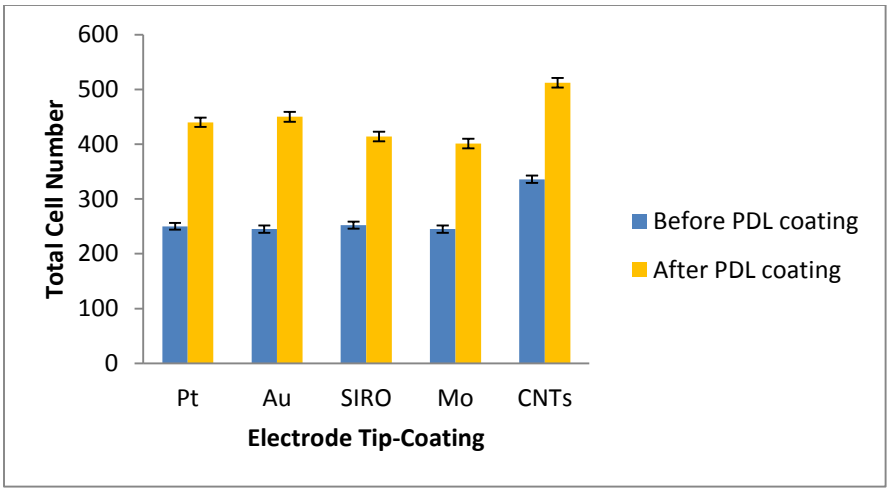

(a)

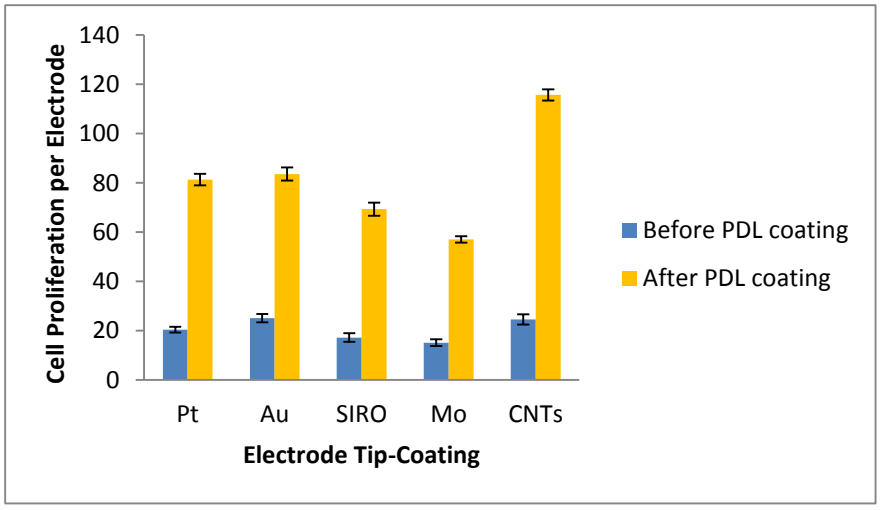

(b)

Figure 4.10. Cell proliferation before and after PDL coating: (a) Total cell number of each tip-coating before and after peptide deposition. (b) Cell proliferation per electrode site for each tip-coating before and after peptide deposition (N = 9). The cell proliferation has increased in the presence of the electrodes conjugated with PDL.

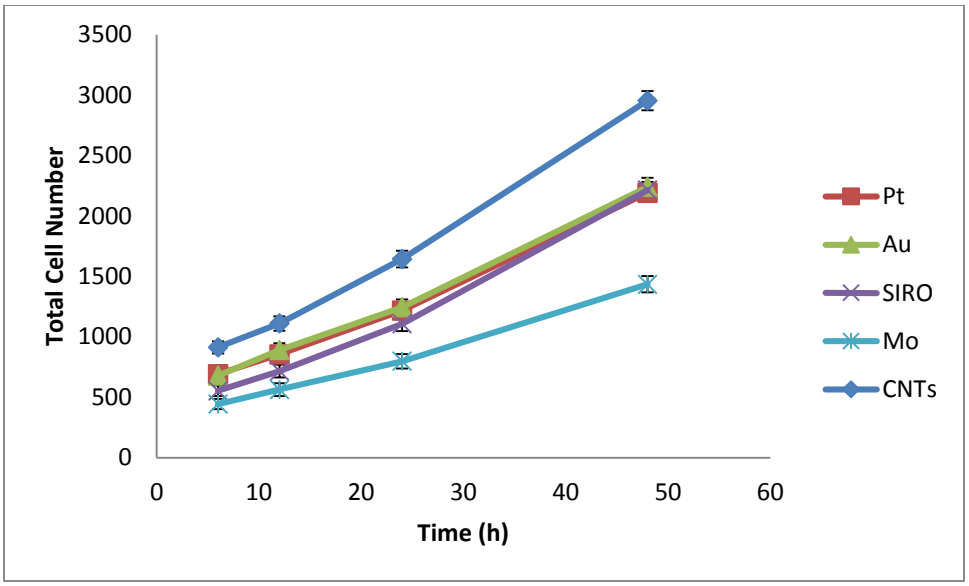

Figure 4.11. Growth curve for neuroblast cells via manual count using hemocytometer after 6, 12, 24, and 48 h. The lines present a mean value of four points obtained in three separate experiments. Standard deviations have been indicated.

4.4 Discussion

The peptide-polymer conjugation method not only enhanced biomolecule deposition at the surface of the microelectrodes but also controlled the distribution of the cells with a high spatial resolution. More importantly, cells were attracted to coated electrode sites, which may improve the communication between the cells and stimulation/recording systems. Given that the experiments were performed in parallel, these results can be directly related to differences in the tip chemical compositions or the differences in the amount of PDL attached to the tips. To improve biocompatibility of the MEAs, the surface of the electrodes were covered with PEG hydrogel and parylene-C, which are biocompatible polymers. Parylene-C plays a significant role as a biocompatible polymer in implantable biomedical devices due to its unique mechanical properties and inertness. In addition, parylene-C has demonstrated high stability in *in vitro* and *in vivo* studies [127, 171]. PEG-based hydrogels are promising materials for working with the central nervous system because they are nonionic and relatively resistant to protein adsorption. More importantly, in culture, neuro cells that are encapsulated in PEG-based hydrogels can survive indicating that the PEG hydrogels are not cytotoxic [178]. Cells grew and proliferated in the presence of the electrodes coated with both PEG and parylene-C.

In this study, the effect of PDL on the proliferation of neuroblast cells was determined. Therefore, we just verified their size, morphology and proliferation. The results have shown that cells grew and proliferated normally in the presence of the electrodes and peptides. Teppola et al optimized cell growth on MEA plates coating them with PDL, poly-L-lysine, and polyethyleneimine (PEI). Neuroblastoma cells were cultured on MEA plates before and after coating. The results showed that the MEA coating agents had a strong impact on cell morphology, growth, and viability [179].

The cytotoxicity effects include the effects of external biomaterials on the cells, whereas the biocompatibility study is not only on their cytotoxicity, but also on the effects of cells on these materials. A potential mechanism of cytotoxicity includes the formation of reactive oxygen species (ROS) such as hydrogen peroxide (H_2O_2), hydroxyl radical (OH^-), hydroperoxyl radical ($HO_2^{\cdot}$), and superoxide onion (O_2^-) [180]. Cell-based cytotoxicity tests of implantable MEAs ensure that the material used in the devices is biocompatible [181]. The dynamic replacement of proteins with the bigger ones on the bio-hardware interface (including neural MEAs) results in undesired layer instabilities that are difficult to control (Vroman effect) [182, 183].Therefore, surface modification of the MEAs including polymerization and bioactive molecule-coating significantly improves the biocompatibility of neural implants in the vicinity of tissues and cells. More investigation is needed to quantify the ROS produced in neuroblast cells cultured with MEAs and corona proteins on the surface of these implants.

4.5 Conclusion

A novel, high-density, penetrating, pyramid-shaped MEA for recording and stimulation from/ of neurons was designed and implemented. Due to its geometry, a high-density 3D electrode array provides more contacts between the electrodes and targeted neural tissue, which may cause more recording from different depths of the brain. The deposition of PDL on the electrodes was performed and created biologically active electrode-tissue interface. More important, PDL improved cell-adhesion and proliferation. Cells are significantly attracted to the electrode sites coated with peptides *in vitro*. After *in vitro* test, the electrodes can be implanted into the living system to act as an interface between electronics and neural tissue. Further investigation is

needed to determine the biocompatibility of the MEAs on neuroblast cells. The next step will be chronic implantation of MEAs to validate long-lasting functional devices.

CHAPTER 5 CONCLUSION, GENERAL DISCUSSION, AND PERSPECTIVES

5.1 Summary of the results and contributions

We have made in the present thesis significant contributions towards the advancement of the process technology and fabrication of the neural microelectrode arrays (MEAs). The geometrical and electrical characteristics of the MEAs has made it unique among the currently available micromachined electrode arrays, as it has provided low-impedance pathway for higher charge injection with higher density contacts between the electrodes and targeted neural tissue facilitating stimulation and/or recording from different depths of the brain. Our findings point toward the necessity to consider a fabrication technology that is simple, flexible, and robust in order to produce variable-height electrodes with uniform exposed tip sizes of the same order of neurons magnitude.

The primary objective of this thesis was design and implementation of a high performance biocompatible 3D MEA with high selectivity and sensitivity and high electrode-density. A novel masking technology resulted in uniform tip-exposure for variable-height electrodes and improved process time and cost significantly. We have reported for the first time a selective direct growth of carbon nanotubes (CNTs) on the tips of 3D MEAs using the coated Pt as a catalyst material that could enhance both the impedance and charge transfer significantly. Biocompatibility of the electrodes was improved by coating them with hydrogels and bioactive molecules. The detailed conclusions can be summarized as follows:

Implement a novel pyramid-shaped, high-density, penetrating MEA

We have developed a micromachining technique for the fabrication of penetrating 3D MEAs with a high electrode-density when the tips are no longer in the same plane. The issue with current available array is that it is 2D and provides recording data from a plane of the brain. Even the slanted one is quasi-3D instead of 3D. Furthermore, such 3D high electrode-density array (25 electrodes/1.96 mm^2) can record or stimulate from/of different depths of the brain and provide more contacts between the electrodes and targeted neural tissue (greater access to neurons). A unique combination of variable depth dicing and isotropic wet-etching was employed to fabricate novel geometry of pyramid-shaped MEAs. The wet-etching process were optimized by cutting the wafer to square pieces and applying the gas from the bottom in order to produce narrow and

uniform pins. The etching method offers some advantages including reduction in the processing time and higher throughput. The importance of such pyramid-shaped MEA has not been quantified but may have significance during injection electrodes inside the tissue. Variable-height electrodes may help to investigate about neurons causal interactions ("effective connectivity").

Novel masking technique for tip-coating of variable-height microelectrodes

A novel masking technology for tip-coating of variable-height electrodes was developed that uses dry-film photoresist instead of liquid ones. In this technique the dry-film follows the 3D structure and there is no need to control the tip exposure by varying the speed spin of the liquid photoresist, degassing, soft and hard backing, and UV exposure. The usage of this masking method not only resulted in uniform tip-exposure for variable-height electrodes but also leads to reduction in processing time and cost significantly. This technique needs single masking step and reduced the conventional masking process steps from 14 to 6. A comparison between the new method and conventional masking process shows that the new procedure has several advantages including simpler and easier fabrication process, reduced production time and cost, and more uniform tip-exposure. More importantly, the conventional masking methods may not be practical for 3D MEAs since they cannot follow 3D structures.

This technique results in production of highly controlled tip exposure and allows better control in the electrical properties (impedance) of the MEAs. The uniform electrode impedance would reduce variability in stimulation and recording characteristics.

Selective direct growth of CNTs on the tips of 3D MEAs

To optimize the electrical properties of MEAs, for the first time the tips of the electrodes were coated with CNTs by selective direct growth using Plasma Enhanced Chemical Vapor Deposition (PECVD) which is a very relevant growth process for neural interfaces. Forest-like vertically aligned CNTs with uniform diameters between 25 and 30nm and a typical length in the order of 600 nm have been grown. It is noteworthy that the length of CNTs can be varied by tuning the growth conditions of PECVD such as temperature, pressure, time of growth and plasma. However, the short length of achieved CNTs appears more appropriate for neural interface applications and may cause less inflammatory response. Such geometry increased the accessible

surface area of active sites leading to low impedance and high charge transfer. The average impedance of CNT-coated electrodes at 1 kHz was 14 kΩ. The CNT coating led to a 5-fold decrease in impedance and a 600-fold increase in charge transfer compared with Pt electrode. Low impedance, high charge transfer, and stability have made CNT a promising stimulation and/or recording material for neural prosthetic devices.

Improve biocompatibility of the MEAs

In order to minimize the immune response of the neural tissue to implanted MEAs, the surface of the electrodes were coated with polyethylene glycol (PEG) and poly-D-lysine (PDL). These materials not only improved the biological compatibility of the electrodes but also increased cell adhesion and proliferation. An *in vitro* study was performed to test the capacity of PDL to improve neural-cell adhesion and proliferation. A significant advantage of *in vitro* study is that the cells response and health can be observed over time. Increased proliferation of the neuroblast cells on the microelectrodes was observed in the presence of the PDL. The presence of the peptide on the electrode surface was confirmed using Fourier transform infrared spectroscopy (FTIR) and scanning electron microscopy (SEM). Peptide-coated and uncoated MEA were cultured with mouse neuroblast cells for 4 days and monitored after 6, 12, 24, 48 h, and 4 days. An increased cell proliferation due to the PDL-conjugation of the samples was clearly observed by optical microscopy. Cells grew and proliferated normally in the presence of polymer, metal, and CNT coated electrodes. Indeed, the number of the cells that were quantified on the PDL-coated electrodes (five different active sites) was significantly (t-Test, $p = 0.0016$) greater than the cell numbers on the uncoated electrodes. The PDL coating increased cell adhesion by more than 50%. More importantly, cells were attracted to coated electrode sites, which may improve the communication between the cells and stimulation/ recording systems. It is noteworthy that the electrodes with CNT active sites had greater cell numbers than the electrodes with metallic tips, both before and after PDL deposition. These results show that the CNTs increased biocompatibility and enhanced cellular responsiveness by attracting more neural cells, in agreement with previous work.

5.2 Perspectives for future work

Micromachining techniques turn out to be a privilege viable approach for fabrication of microelectrode arrays. The scientific understanding of the electrical stimulation of neural tissue, recording of neural electrical activity, and functional/ structural neuron's behavior is critical for the future design of neural MEAs. Design an appropriate MEA which is compatible with both brain function and structure and electrical circuitry is crucial to the quality optimization and the cost reduction in the future MEAs manufacturing. In particular the architecture, materials, electrochemical and biological behavior of the electrodes should be taken into account as primary concerns in device design. This thesis work opens a number of interesting possibilities that I believe can have considerable impact for different reasons. In the following, we discuss several avenues and possibilities for research in this field based on the studies that we have conducted during these years.

Improve electrical properties of CNTs-MEAs

The immediate contribution of this thesis, as mentioned in chapter 4, is investigation of conductive polymer deposition on CNTs. Many studies have shown that CNTs can be used as electrochemical supercapacitors. However, due to its high aspect ratio, nanotubes are not stable and stick together to form microbundles when they are exposed to liquids. Therefore, large surface area of CNTs is inaccessible in electrolyte aqueous solution and cannot contribute to charge injection. A uniform free standing of nanotubes are desired as an electrical-neural interface. This can be achieved by depositing a conformal layer of conductive polymers such as polypyrrole (Ppy) around the CNTs [152].

Another strategy to increase the accessible area of CNTs is incubation CNTs-MEAs with the polyethylene glycol-lipid conjugates (PEG-PL). PEG-LP binds strongly to the nanotube side wall via van der Waals and hydrophobic interactions, while the PEG chain extends into water [138]. As a result, the CNTs-coated microelectrodes turned more hydrophilic and conduct to higher charge injection. A similar hydrophobic-to-hydrophilic process for CNTs is incubation of CNTs-MEAs with cell culture medium. In this method, the proteins in cell medium will absorb to the nanotube surface.

Although high-temperature PECVD method allows growing well-aligned, individual and free-standing nanotubes with uniform diameters, using soft polymer substrates in electrodes structure continue to be challenging. Lower growth temperatures relative to CVD (<400°C) are possible since high-energy electrons present in the discharge plasma, supply the energy necessary for chemical reactions in the gas [153]. Another advantage is that during the growth process, the plasma removes amorphous carbon which strongly affects the electrical properties of electrodes and may lead to an increase of impedance.

Select an appropriate insulator

One of the major failure modes of implant MEAs is material failures including broken electrode tips, insulation leakage, or insulator cracks and delamination. To choose an appropriate insulator we should consider two main aspects:

- The material properties of the insulator such as hydration, fraction strength, tensile strength, and biocompatibility
- Adhesion to the substrate which is critical to prevent delamination

In order to insulate electrodes with CNTs tip-coating, we need materials with conformal coverage and thermal stability. Some of the experiments that need to be undertaken in order to improve the insulation layer are:

- Deposit high quality SiO_2 using Low Pressure Chemical Vapor Deposition (LPECVD) technique for Hot Filament Chemical Vapor Deposition (HFCVD) CNTs growth
- Wet silanization process prior to parylene-C deposition in order to promote the adhesion of parylene to the silicon for low temperature PECVD CNTs growth

MEAs in vivo test

MEAs have been tested *in vitro* successfully. Cells grew and proliferated normally in the presence of polymer, metal, and CNT coated electrodes. After *in vitro* test, the electrode arrays should be implanted into the living system *(in vivo)* and evaluated both in terms of electrical performance (impedance as a preliminary marker) and mechanical stability. Electrode recording sites of chronically implanted arrays can be influenced by physical changes in the electrodes (corrosion, damage insulation, and change in tip surface area) or by immune response of the

brain (inflammatory response, astrogliosis, disruption of blood-brain barrier, and glial encapsulation).

BIBLIOGRAPHY

[1] K. C. Cheung, "Implantable microscale neural interfaces," *Biomedical Microdevices,* vol. 9, pp. 923-38, Dec 2007.

[2] K. D. Wise, J. B. Angell, and A. Starr, "An integrated-circuit approach to extracellular microelectrodes," *Biomedical Engineering, IEEE Transactions on,* pp. 238-247, 1970.

[3] P. K. Campbell, K. E. Jones, R. J. Huber, K. W. Horch, and R. A. Normann, "A silicon-based, three-dimensional neural interface: manufacturing processes for an intracortical electrode array," *IEEE transactions on bio-medical engineering,* vol. 38, pp. 758-68, Aug 1991.

[4] T. Stieglitz, H. Beutel, M. Schuettler, and J. U. Meyer, "Micromachined, polyimide-based devices for flexible neural interfaces," *Biomedical microdevices,* vol. 2, pp. 283-294, 2000.

[5] S. Negi, R. Bhandari, L. Rieth, and F. Solzbacher, "In vitro comparison of sputtered iridium oxide and platinum-coated neural implantable microelectrode arrays," *Biomedical materials,* vol. 5, p. 15007, Feb 2010.

[6] M. R. Abidian and D. C. Martin, "Experimental and theoretical characterization of implantable neural microelectrodes modified with conducting polymer nanotubes," *Biomaterials,* vol. 29, pp. 1273-1283, Mar 2008.

[7] M. A. L. Nicolelis, "Brain–machine interfaces to restore motor function and probe neural circuits," *Nature Reviews Neuroscience,* vol. 4, pp. 417-422, 2003.

[8] D. R. Kipke, "Implantable neural probe systems for cortical neuroprostheses," *Conference proceedings : ... Annual International Conference of the IEEE Engineering in Medicine and Biology Society. IEEE Engineering in Medicine and Biology Society. Conference,* vol. 7, pp. 5344-7, 2004.

[9] A. Branner, R. B. Stein, E. Fernandez, Y. Aoyagi, and R. A. Normann, "Long-term stimulation and recording with a penetrating microelectrode array in cat sciatic nerve," *IEEE transactions on bio-medical engineering,* vol. 51, pp. 146-57, Jan 2004.

[10] K. C. Cheung, P. Renaud, H. Tanila, and K. Djupsund, "Flexible polyimide microelectrode array for in vivo recordings and current source density analysis," *Biosensors & Bioelectronics,* vol. 22, pp. 1783-90, Mar 15 2007.

[11] C. Nick, S. Yadav, R. Joshi, J. J. Schneider, and C. Thielemann, "A three-dimensional microelectrode array composed of vertically aligned ultra-dense carbon nanotube networks," *Appl. Phys. Lett.,* vol. 107(1), 2015.

[12] C. Nick, S. Quednau, R. Sarwar, H. F. Schlaak, and C. Thielemann, "High aspect ratio gold nanopillars on microelectrodes for neural interfaces," *Microsystem Technologies-Micro-and Nanosystems-Information Storage and Processing Systems,* vol. 20, pp. 1849-1857, Oct 2014.

[13] T. Kawano, H. Miura, R. Nagamine, K. Urabe, S. Matsuda, T. Mawatari, *et al.*, "Factors affecting patellar tracking after total knee arthroplasty," *Journal of Arthroplasty,* vol. 17, pp. 942-947, Oct 2002.

[14] H. A. Swadlow, Y. Bereshpolova, T. Bezdudnaya, M. Cano, and C. R. Stoelzel, "A multi-channel, implantable microdrive system for use with sharp, ultra-fine "Reitboeck" microelectrodes," *Journal of Neurophysiology,* vol. 93, pp. 2959-2965, May 2005.

[15] M. J. Lopez-Martinez and E. M. Campo, "Micro-Nano Technologies for Cell Manipulation and Subcellular Monitoring," in *Biomedical Engineering - From Theory to Applications*, ed: INTECH, 2011.

[16] S. Musallam, M. J. Bak, P. R. Troyk, and R. A. Andersen, "A floating metal microelectrode array for chronic implantation," *Journal of Neuroscience Methods,* vol. 160, pp. 122-127, Feb 15 2007.

[17] E. W. Keefer, B. R. Botterman, M. I. Romero, A. F. Rossi, and G. W. Gross, "Carbon nanotube coating improves neuronal recordings," *Nature Nanotechnology,* vol. 3, pp. 434-9, Jul 2008.

[18] K. D. Wise, A. M. Sodagar, Y. Yao, M. N. Gulari, G. E. Perlin, and K. Najafi, "Microelectrodes, microelectronics, and implantable neural microsystems," *Proceedings of the Ieee,* vol. 96, pp. 1184-1202, Jul 2008.

[19] R. J. Vetter, J. C. Williams, J. F. Hetke, E. A. Nunamaker, and D. R. Kipke, "Chronic neural recording using silicon-substrate microelectrode arrays implanted in cerebral cortex," *IEEE transactions on bio-medical engineering,* vol. 51, pp. 896-904, Jun 2004.

[20] S. Takeuchi, T. Suzuki, K. Mabuchi, and H. Fujita, "3D flexible multichannel neural probe array," *Journal of Micromechanics and Microengineering,* vol. 14, pp. 104-107, Jan 2004.

[21] Y. C. Chen, H. L. Hsu, Y. T. Lee, H. C. Su, S. J. Yen, C. H. Chen, *et al.*, "An active, flexible carbon nanotube microelectrode array for recording electrocorticograms," *Journal of Neural Engineering,* vol. 8, p. 034001, Jun 2011.

[22] P. Norlin, M. Kindlundh, A. Mouroux, K. Yoshida, and U. G. Hofmann, "A 32-site neural recording probe fabricated by DRIE of SOI substrates," *Journal of Micromechanics and Microengineering,* vol. 12, pp. 414-419, Jul 2002.

[23] R. A. Normann, "Technology insight: future neuroprosthetic therapies for disorders of the nervous system," *Nature clinical practice. Neurology,* vol. 3, pp. 444-52, Aug 2007.

[24] A. E. Ayoub, B. Gosselin, and M. Sawan, "A microsystem integration platform dedicated to build multi-chip-neural interfaces," *Conference proceedings : ... Annual International Conference of the IEEE Engineering in Medicine and Biology Society. IEEE Engineering in Medicine and Biology Society. Annual Conference,* vol. 2007, pp. 6605-8, 2007.

[25] T. A. Fofonoff, S. M. Martel, N. G. Hatsopoulos, J. P. Donoghue, and I. W. Hunter, "Microelectrode array fabrication by electrical discharge machining and chemical etching," *IEEE transactions on bio-medical engineering,* vol. 51, pp. 890-5, Jun 2004.

[26] Patch-clamp method. Available: motifolio.com, 2015.

[27] T. Kawano, Y. Kato, M. Futagawa, H. Takao, K. Sawada, and M. Ishida, "Fabrication and properties of ultrasmall Si wire arrays with circuits by vapor-liquid-solid growth," *Sensors and Actuators a-Physical,* vol. 97-8, pp. 709-715, Apr 1 2002.

[28] P. Fromherz, "Electrical interfacing of nerve cells and semiconductor chips," *Chemphyschem,* vol. 3, pp. 276-284, Mar 12 2002.

[29] D. H. Szarowski, M. D. Andersen, S. Retterer, A. J. Spence, M. Isaacson, H. G. Craighead, *et al.*, "Brain responses to micro-machined silicon devices," *Brain Research,* vol. 983, pp. 23-35, Sep 5 2003.

[30] J. H. Chang, J. Park, Y. K. Pak, and J. J. Pak, "Fitting improvement using a new electrical circuit model for the electrode-electrolyte interface," *2007 3rd International IEEE/EMBS Conference on Neural Engineering, Vols 1 and 2,* pp. 572-574, 2007.

[31] D. A. Robinson, "The electrical properties of metal microelectrodes," *Proceedings of the IEEE* vol. 56, pp. 1065-1071, June 1968.
[32] E. Barsoukov and J. R. Macdonald, *Impedance Spectroscopy Theory, Experiment, and Applications*: A John Wiley & Sons, Inc., Publication, 2005.
[33] B. Schwartz and H. Robbins, "Chemical etching of silicon IV. Etching technology," *J. Electrochem. Soc.* , vol. 123(12), pp. 1903-09, 1976.
[34] H. Li, T. C. Hain, A. Muzha, F. Schoppler, and T. Hertel, "Dynamical Contact Line Pinning and Zipping during Carbon Nanotube Coffee Stain Formation," *Acs Nano,* vol. 8, pp. 6417-6424, Jun 2014.
[35] E. E. Fetz, "Operant conditioning of cortical unit activity," *Science,* vol. 163, pp. 955-8, Feb 28 1969.
[36] D. R. Humphrey, E. M. Schmidt, and W. D. Thompson, "Predicting measures of motor performance from multiple cortical spike trains," *Science,* vol. 170, pp. 758-62, Nov 13 1970.
[37] R. A. Normann, E. M. Maynard, P. J. Rousche, and D. J. Warren, "A neural interface for a cortical vision prosthesis," *Vision Research,* vol. 39, pp. 2577-87, Jul 1999.
[38] P. Konrad and T. Shanks, "Implantable brain computer interface: challenges to neurotechnology translation," *Neurobiol Dis,* vol. 38, pp. 369-75, Jun 2010.
[39] G. S. Brindley and W. S. Lewin, "The sensations produced by electrical stimulation of the visual cortex," *The Journal of physiology,* vol. 196, pp. 479-93, May 1968.
[40] G. Brindley and D. Rushton, "Implanted stimulators of the visual cortex as visual prosthetic devices," *Trans. Am. Acad. Ophthalmol. Otoaryngol.* , vol. 78, pp. 741-745, 1974.
[41] W. H. Dobelle, "Artificial vision for the blind by connecting a television camera to the visual cortex," *ASAIO journal,* vol. 46, pp. 3-9, Jan-Feb 2000.
[42] E. M. Schmidt, M. J. Bak, F. T. Hambrecht, C. V. Kufta, D. K. O'Rourke, and P. Vallabhanath, "Feasibility of a visual prosthesis for the blind based on intracortical microstimulation of the visual cortex," *Brain : a journal of neurology,* vol. 119 (Pt 2), pp. 507-22, Apr 1996.
[43] P. T. McCarthy, M. P. Rao, and K. J. Otto, "Simultaneous recording of rat auditory cortex and thalamus via a titanium-based, microfabricated, microelectrode device," *Journal of Neural Engineering,* vol. 8, p. 046007, Aug 2011.
[44] W. L. C. Rutten, "Selective electrical interfaces with the nervous system," *Annual Review of Biomedical Engineering,* vol. 4, pp. 407-452, 2002.
[45] W. L. C. Rutten, H. J. Vanwier, and J. H. M. Put, "Sensitivity and Selectivity of Intraneural Stimulation Using a Silicon Electrode Array," *Ieee Transactions on Biomedical Engineering,* vol. 38, pp. 192-198, Feb 1991.
[46] W. L. C. Rutten, H. J. Vanwier, J. H. M. Put, R. Rutgers, and R. A. I. Devos, "Sensitivity, Selectivity and Bioacceptance of an Intraneural Multielectrode Stimulation Device in Silicon Technology," *Electrophysiological Kinesiology /,* vol. 804, pp. 135-139, 1988.
[47] Z. Yu, T. E. McKnight, M. N. Ericson, A. V. Melechko, M. L. Simpson, and B. Morrison, 3rd, "Vertically aligned carbon nanofiber arrays record electrophysiological signals from hippocampal slices," *Nano Letters,* vol. 7, pp. 2188-95, Aug 2007.
[48] T. Gabay, M. Ben-David, I. Kalifa, R. Sorkin, Z. R. Abrams, E. Ben-Jacob, *et al.*, "Electro-chemical and biological properties of carbon nanotube based multi-electrode arrays," *Nanotechnology,* vol. 18, p. 035201, Jan 24 2007.

[49] J. C. Barrese, N. Rao, K. Paroo, C. Triebwasser, C. Vargas-Irwin, L. Franquemont, *et al.*, "Failure mode analysis of silicon-based intracortical microelectrode arrays in non-human primates," *J Neural Eng,* vol. 10, p. 066014, Dec 2013.

[50] J. N. Turner, W. Shain, D. H. Szarowski, M. Andersen, S. Martins, M. Isaacson, *et al.*, "Cerebral astrocyte response to micromachined silicon implants," *Exp Neurol,* vol. 156, pp. 33-49, Mar 1999.

[51] V. S. Polikov, P. A. Tresco, and W. M. Reichert, "Response of brain tissue to chronically implanted neural electrodes," *J Neurosci Methods,* vol. 148, pp. 1-18, Oct 15 2005.

[52] N. Agarwal, A. Tolia, D. R. Hansberry, E. J. Duffis, J. C. Barrese, C. D. Gandhi, *et al.*, "Current differential diagnoses and treatment options of vascular occlusions presenting as bilateral thalamic infarcts: a review of the literature," *J Neurointerv Surg,* vol. 5, pp. 419-25, Sep 1 2013.

[53] J. W. Judy, "Microelectrode technologies for neuroengineered systems," *Proceedings of the 25th Annual International Conference of the Ieee Engineering in Medicine and Biology Society, Vols 1-4,* vol. 25, pp. 3806-3809, 2003.

[54] F. Strumwasser, "Long-term recording' from single neurons in brain of unrestrained mammals," *Science,* vol. 127, pp. 469-70, Feb 28 1958.

[55] K. L. Drake, K. D. Wise, J. Farraye, D. J. Anderson, and S. L. BeMent, "Performance of planar multisite microprobes in recording extracellular single-unit intracortical activity," *IEEE transactions on bio-medical engineering,* vol. 35, pp. 719-32, Sep 1988.

[56] J. Subbaroyan, D. C. Martin, and D. R. Kipke, "A finite-element model of the mechanical effects of implantable microelectrodes in the cerebral cortex," *Journal of Neural Engineering,* vol. 2, pp. 103-13, Dec 2005.

[57] M. P. Ward, P. Rajdev, C. Ellison, and P. P. Irazoqui, "Toward a comparison of microelectrodes for acute and chronic recordings," *Brain Research,* vol. 1282, pp. 183-200, Jul 28 2009.

[58] K. D. Wise, J. B. Angell, and A. Starr, "An integrated-circuit approach to extracellular microelectrodes," *IEEE transactions on bio-medical engineering,* vol. 17, pp. 238-47, Jul 1970.

[59] S. Kuri, M. M. Billah, S. M. Rana, Z. Naim, M. M. Islam, M. Hasanuzzaman, *et al.*, "Phytochemical and in vitro biological investigations of methanolic extracts of Enhydra fluctuans Lour," *Asian Pac J Trop Biomed,* vol. 4, pp. 299-305, Apr 2014.

[60] M. Hasanuzzaman, K. Nahar, M. M. Alam, R. Roychowdhury, and M. Fujita, "Physiological, biochemical, and molecular mechanisms of heat stress tolerance in plants," *Int J Mol Sci,* vol. 14, pp. 9643-84, 2013.

[61] C. Cha, Y. J. Hong, E. Y. Chang, H. K. Chang, J. T. Oh, and S. J. Han, "Minimally invasive surgery in infants with congenital diaphragmatic hernia: outcome and selection criteria," *J Korean Surg Soc,* vol. 85, pp. 84-8, Aug 2013.

[62] J. Coulombe, M. Sawan, and J. F. Gervais, "A highly flexible system for microstimulation of the visual cortex: design and implementation," *Ieee Transactions on Biomedical Circuits and Systems,* vol. 1, pp. 258-69, Dec 2007.

[63] S. Zhang, B. Wen, B. Zhou, L. Yang, C. Cha, S. Xu, *et al.*, "Quantitative analysis of the human AKR family members in cancer cell lines using the mTRAQ/MRM approach," *J Proteome Res,* vol. 12, pp. 2022-33, May 3 2013.

[64] C. Cha and J. Oh, "An optofluidic mechanical system for elasticity measurement of thin biological tissues," *Biotechnol Lett,* vol. 35, pp. 825-30, May 2013.

[65] T. F. Tzeng, J. H. Chen, P. J. Hsiao, M. C. Hsieh, and S. J. Shin, "Insulin action and insulin secretion in newly diagnosed type 2 diabetic patients," *The Kaohsiung journal of medical sciences,* vol. 17, pp. 468-74, Sep 2001.

[66] B. S. Sheu, J. J. Wu, C. Y. Lo, H. W. Wu, J. H. Chen, Y. S. Lin, *et al.*, "Impact of supplement with Lactobacillus- and Bifidobacterium-containing yogurt on triple therapy for Helicobacter pylori eradication," *Aliment Pharmacol Ther,* vol. 16, pp. 1669-75, Sep 2002.

[67] J. H. Chen, X. B. Chang, A. A. Aleksandrov, and J. R. Riordan, "CFTR is a monomer: biochemical and functional evidence," *The Journal of membrane biology,* vol. 188, pp. 55-71, Jul 1 2002.

[68] J. H. Chen, D. H. Ma, and R. J. Tsai, "Amniotic membrane transplantation for pseudomonal keratitis with impending perforation," *Chang Gung medical journal,* vol. 25, pp. 144-52, Mar 2002.

[69] C. J. Liao, C. F. Chen, J. H. Chen, S. F. Chiang, Y. J. Lin, and K. Y. Chang, "Fabrication of porous biodegradable polymer scaffolds using a solvent merging/particulate leaching method," *Journal of biomedical materials research,* vol. 59, pp. 676-81, Mar 15 2002.

[70] L. E. Moore and E. Neher, "Fluctuation and relaxation analysis of monazomycin-induced conductance in black lipid membranes," *The Journal of membrane biology,* vol. 27, pp. 347-62, Jun 30 1976.

[71] E. Neher and B. Sakmann, "Single-channel currents recorded from membrane of denervated frog muscle fibres," *Nature,* vol. 260, pp. 799-802, Apr 29 1976.

[72] H. Doi, T. Nakayama, K. Satoh, K. Sumitomo, T. Kawano, and A. Tatsumi, "[A case of multicentric Castleman's disease with multiple pulmonary nodules]," *Nihon Kokyuki Gakkai zasshi = the journal of the Japanese Respiratory Society,* vol. 40, pp. 771-6, Sep 2002.

[73] T. Kawano, T. Shinomaru, and I. Ueda, "Highly active Pd(II) catalysts with trans-bidentate pyridine ligands for the Heck reaction," *Organic letters,* vol. 4, pp. 2545-7, Jul 25 2002.

[74] S. Löffler, Y. Xie, P. Klimach, A. Richter, P. Detemple, T. Stieglitz, *et al.*, "Long term in vivo stability and frequency response of polyimide based flexible array probes," *Biomed Tech,* vol. 57, p. 1, 2012.

[75] C. Hassler, T. Boretius, and T. Stieglitz, "Polymers for neural implants," *Journal of Polymer Science Part B: Polymer Physics,* vol. 49, pp. 18-33, 2011.

[76] Y. Iwashita, T. Kawano, T. Maeda, S. Nagasaki, and S. Kitano, "Pancreatic arteriovenous malformation treated by transcatheter embolization," *Hepatogastroenterology,* vol. 49, pp. 1722-1723, Nov-Dec 2002.

[77] T. Kawano, "Soft balloon method in esophageal endoscopic ultrasound with a 20-MHz ultrasound thin probe," *Gastrointest Endosc,* vol. 56, pp. S107-S107, Oct 2002.

[78] T. Kawano, J. Kuwana, C. X. Du, and I. Ueda, "Copper(I) ion mediated self-organization of molecular rectangular boxes from 1,2-bis(2-pyridylethynyl)benzene ligands with bulky substituents," *Inorg Chem,* vol. 41, pp. 4078-4080, Aug 12 2002.

[79] T. Kawano, M. Morioka, S. Yano, J. Hamada, Y. Ushio, E. Miyamoto, *et al.*, "Decreased Akt activity is associated with activation of forkhead transcription factor after transient forebrain ischemia in gerbil hippocampus," *Journal of Cerebral Blood Flow and Metabolism,* vol. 22, pp. 926-934, Aug 2002.

[80] Y. Kumagai, H. Inoue, K. Nagai, T. Kawano, and T. Iwai, "Magnifying endoscopy, stereoscopic microscopy, and the microvascular architecture of superficial esophageal carcinoma," *Endoscopy,* vol. 34, pp. 369-375, May 2002.

[81] T. Komatsu, T. Kimura, Y. Kuriyama, Y. Isshiki, T. Kawano, T. Hirao, *et al.*, "Anaerobic digestion of organic waste in Japan: the first demonstration plant at Kyoto City," *Water Science and Technology,* vol. 45, pp. 113-118, 2002.

[82] R. A. B. Fernandes, B. Diniz, R. Ribeiro, and M. Humayun, "Artificial vision through neuronal stimulation," *Neuroscience letters,* vol. 519, pp. 122-128, Jun 25 2012.

[83] E. C. Lanes, S. Y. Motoike, K. N. Kuki, C. Nick, and R. D. Freitas, "Molecular characterization and population structure of the macaw palm, Acrocomia aculeata (Arecaceae), ex situ germplasm collection using microsatellites markers," *The Journal of heredity,* vol. 106, pp. 102-12, Jan-Feb 2015.

[84] T. K. Chowdhury, "Fabrication of extremely fine glass micropipette electrodes," *Journal of scientific instruments,* vol. 2, pp. 1087-90, Dec 1969.

[85] M. Verzeano and K. Negishi, "Neuronal activity in cortical and thalamic networks," *The Journal of general physiology,* vol. 43(6)Suppl, pp. 177-95, Jul 1960.

[86] J. K. Chapin, "Using multi-neuron population recordings for neural prosthetics," *Nature Neuroscience,* vol. 7, pp. 452-5, May 2004.

[87] D. H. Hubel, "Tungsten Microelectrode for Recording from Single Units," *Science,* vol. 125, pp. 549-50, Mar 22 1957.

[88] R. F. Thompson and M. M. Patterson, *Bioelectric recording techniques*: Academic Press, Waltham, 1674.

[89] G. E. Loeb, R. A. Peck, and J. Martyniuk, "Toward the ultimate metal microelectrode," *Journal of Neuroscience Methods,* vol. 63, pp. 175-83, Dec 1995.

[90] V. Ortmann and B. Baziyan, "Intracortical neural interface for prosthetic applications," *Conference proceedings : ... Annual International Conference of the IEEE Engineering in Medicine and Biology Society. IEEE Engineering in Medicine and Biology Society. Annual Conference,* vol. 2007, pp. 6372-5, 2007.

[91] R. Rathnasingham, D. R. Kipke, S. C. Bledsoe, Jr., and J. D. McLaren, "Characterization of implantable microfabricated fluid delivery devices," *IEEE transactions on bio-medical engineering,* vol. 51, pp. 138-45, Jan 2004.

[92] K. D. Wise, D. J. Anderson, J. F. Hetke, D. R. Kipke, and K. Najafi, "Wireless implantable microsystems: High-density electronic interfaces to the nervous system," *Proceedings of the Ieee,* vol. 92, pp. 76-97, Jan 2004.

[93] S. J. Tanghe, K. Najafi, and K. D. Wise, "A Planar Iro Multichannel Stimulating Electrode for Use in Neural Prostheses," *Sensors and Actuators B-Chemical,* vol. 1, pp. 464-467, Jan 1990.

[94] K. Najafi, "Solid-State Microsensors for Cortical Nerve Recordings," *Ieee Engineering in Medicine and Biology Magazine,* vol. 13, pp. 375-387, Jun-Jul 1994.

[95] T. Gabay, M. Ben-David, I. Kalifa, R. Sorkin, Z. R. Abrams, E. Ben-Jacob, *et al.*, "Electro-chemical and biological properties of carbon nanotube based multi-electrode arrays," *Nanotechnology,* vol. 18, Jan 24 2007.

[96] K. D. Wise, "Silicon microsystems for neuroscience and neural prostheses," *IEEE Eng Med Biol Mag,* vol. 24, pp. 22-9, Sep-Oct 2005.

[97] P. J. Rousche, D. S. Pellinen, D. P. Pivin, J. C. Williams, R. J. Vetter, and D. R. Kipke, "Flexible polyimide-based intracortical electrode arrays with bioactive capability," *Ieee Transactions on Biomedical Engineering,* vol. 48, pp. 361-371, Mar 2001.

[98] J. P. Seymour, N. B. Langhals, D. J. Anderson, and D. R. Kipke, "Novel multi-sided, microelectrode arrays for implantable neural applications," *Biomedical Microdevices,* vol. 13, pp. 441-51, Jun 2011.

[99] D. T. Kewley, M. D. Hills, D. A. Borkholder, I. E. Opris, N. I. Maluf, C. W. Storment, *et al.*, "Plasma-etched neural probes," *Sensors and Actuators a-Physical,* vol. 58, pp. 27-35, Jan 1997.

[100] R. A. Normann, "Technology insight: future neuroprosthetic therapies for disorders of the nervous system," *Nat Clin Pract Neurol,* vol. 3, pp. 444-52, Aug 2007.

[101] B. Ghane-Motlagh and M. Sawan, "Design and Implementation Challenges of Microelectrode Arrays: A Review," *Materials Sciences and Applications,* vol. 4, pp. 483-495, 2013.

[102] J. Pine, "Recording action potentials from cultured neurons with extracellular microcircuit electrodes," *Journal of Neuroscience Methods,* vol. 2, pp. 19-31, Feb 1980.

[103] M. A. L. Nicolelis, D. Dimitrov, J. M. Carmena, R. Crist, G. Lehew, J. D. Kralik, *et al.*, "Chronic, multisite, multielectrode recordings in macaque monkeys," *Proceedings of the National Academy of Sciences of the United States of America,* vol. 100, pp. 11041-11046, Sep 16 2003.

[104] X. Cui, V. A. Lee, Y. Raphael, J. A. Wiler, J. F. Hetke, D. J. Anderson, *et al.*, "Surface modification of neural recording electrodes with conducting polymer/biomolecule blends," *J Biomed Mater Res,* vol. 56, pp. 261-72, Aug 2001.

[105] X. Cui, J. Wiler, M. Dzaman, R. A. Altschuler, and D. C. Martin, "In vivo studies of polypyrrole/peptide coated neural probes," *Biomaterials,* vol. 24, pp. 777-87, Feb 2003.

[106] L. Kam, W. Shain, J. N. Turner, and R. Bizios, "Selective adhesion of astrocytes to surfaces modified with immobilized peptides," *Biomaterials,* vol. 23, pp. 511-5, Jan 2002.

[107] M. Borkenhagen, J. F. Clemence, H. Sigrist, and P. Aebischer, "Three-dimensional extracellular matrix engineering in the nervous system," *J Biomed Mater Res,* vol. 40, pp. 392-400, Jun 5 1998.

[108] M. Nomizu, B. S. Weeks, C. A. Weston, W. H. Kim, H. K. Kleinman, and Y. Yamada, "Structure-activity study of a laminin alpha 1 chain active peptide segment Ile-Lys-Val-Ala-Val (IKVAV)," *FEBS Lett,* vol. 365, pp. 227-31, May 29 1995.

[109] D. S. Grant, K. Tashiro, B. Segui-Real, Y. Yamada, G. R. Martin, and H. K. Kleinman, "Two different laminin domains mediate the differentiation of human endothelial cells into capillary-like structures in vitro," *Cell,* vol. 58, pp. 933-43, Sep 8 1989.

[110] M. J. Ignatius, N. Sawhney, A. Gupta, B. M. Thibadeau, O. R. Monteiro, and I. G. Brown, "Bioactive surface coatings for nanoscale instruments: effects on CNS neurons," *J Biomed Mater Res,* vol. 40, pp. 264-74, May 1998.

[111] N. K. Guimard, N. Gomez, and C. E. Schmidt, "Conducting polymers in biomedical engineering," *Progress in Polymer Science,* vol. 32, pp. 876-921, Aug-Sep 2007.

[112] E. Smith, J. Bai, C. Oxenford, J. Yang, R. Somayaji, and H. Uludag, "Conjugation of arginine-glycine-aspartic acid peptides to thermoreversible N-isopropylacrylamide polymers," *Journal of Polymer Science Part a-Polymer Chemistry,* vol. 41, pp. 3989-4000, Dec 15 2003.

[113] T. Pakalns, K. L. Haverstick, G. B. Fields, J. B. McCarthy, D. L. Mooradian, and M. Tirrell, "Cellular recognition of synthetic peptide amphiphiles in self-assembled monolayer films," *Biomaterials,* vol. 20, pp. 2265-79, Dec 1999.

[114] M. Huber, P. Heiduschka, S. Kienle, C. Pavlidis, J. Mack, T. Walk, *et al.*, "Modification of glassy carbon surfaces with synthetic laminin-derived peptides for nerve cell attachment and neurite growth," *J Biomed Mater Res,* vol. 41, pp. 278-88, Aug 1998.

[115] M. S. Boeckl, T. Baas, A. Fujita, K. O. Hwang, A. L. Bramblett, B. D. Ratner, *et al.*, "Template-assisted nano-patterning of solid surfaces," *Biopolymers,* vol. 47, pp. 185-193, 1998.

[116] S. P. Massia, S. S. Rao, and J. A. Hubbell, "Covalently immobilized laminin peptide Tyr-Ile-Gly-Ser-Arg (YIGSR) supports cell spreading and co-localization of the 67-kilodalton laminin receptor with alpha-actinin and vinculin," *J Biol Chem,* vol. 268, pp. 8053-9, Apr 15 1993.

[117] S. Sam, A. C. Gouget-Laemmel, J. N. Chazalviel, F. Ozanam, and N. Gabouze, "GlyHisGlyHis immobilization on silicon surface for copper detection," *Applied Surface Science,* vol. 269, pp. 166-170, Mar 15 2013.

[118] Y. Chi, W. Li, H. Wen, X. Cui, H. Cai, and X. Bi, "[Studies on separation, purification and chemical structure of polysaccharide from Atractylodes macrocephala]," *Zhong Yao Cai,* vol. 24, pp. 647-8, Sep 2001.

[119] L. A. Geddes, "Historical evolution of circuit models for the electrode-electrolyte interface," *Annals of Biomedical Engineering,* vol. 25, pp. 1-14, Jan-Feb 1997.

[120] B. Onaral and H. P. Schwan, "Linear and nonlinear properties of platinum electrode polarisation. Part 1: frequency dependence at very low frequencies," *Medical & biological engineering & computing,* vol. 20, pp. 299-306, May 1982.

[121] W. Franks, I. Schenker, P. Schmutz, and A. Hierlemann, "Impedance characterization and modeling of electrodes for biomedical applications," *IEEE transactions on bio-medical engineering,* vol. 52, pp. 1295-302, Jul 2005.

[122] K. E. Jones, P. K. Campbell, and R. A. Normann, "A glass/silicon composite intracortical electrode array," *Ann Biomed Eng,* vol. 20, pp. 423-37, 1992.

[123] R. Bhandari, S. Negi, and F. Solzbacher, "Wafer-scale fabrication of penetrating neural microelectrode arrays," *Biomedical Microdevices,* vol. 12, pp. 797-807, Oct 2010.

[124] S. Kim, R. Bhandari, M. Klein, S. Negi, L. Rieth, P. Tathireddy, *et al.*, "Integrated wireless neural interface based on the Utah electrode array," *Biomedical Microdevices,* vol. 11, pp. 453-466, Apr 2009.

[125] D. L. Klein and D. J. D'Stefan, "Controlled Etching of Silicon in the HF-HN03 System," *J. Electrochem. Soc.,* vol. 109, pp. 37-42, 1962.

[126] R. Bhandari, S. Negi, L. Rieth, and F. Solzbacher, "A Wafer-Scale Etching Technique for High Aspect Ratio Implantable MEMS Structures," *Sens Actuators A Phys,* vol. 162, pp. 130-136, Jul 1 2010.

[127] T. Y. Chang, V. G. Yadav, S. De Leo, A. Mohedas, B. Rajalingam, C. L. Chen, *et al.*, "Cell and protein compatibility of parylene-C surfaces," *Langmuir,* vol. 23, pp. 11718-25, Nov 6 2007.

[128] E. M. Schmidt, J. S. McIntosh, and M. J. Bak, "Long-term implants of Parylene-C coated microelectrodes," *Medical & biological engineering & computing,* vol. 26, pp. 96-101, Jan 1988.

[129] C. Hassler, R. P. von Metzen, P. Ruther, and T. Stieglitz, "Characterization of parylene C as an encapsulation material for implanted neural prostheses," *Journal of biomedical materials research. Part B, Applied biomaterials,* vol. 93, pp. 266-74, Apr 2010.

[130] G. Voskerician, M. S. Shive, R. S. Shawgo, H. von Recum, J. M. Anderson, M. J. Cima, *et al.*, "Biocompatibility and biofouling of MEMS drug delivery devices," *Biomaterials,* vol. 24, pp. 1959-67, May 2003.

[131] J. M. Hsu, L. Rieth, R. A. Normann, P. Tathireddy, and F. Solzbacher, "Encapsulation of an integrated neural interface device with Parylene C," *IEEE Trans Biomed Eng,* vol. 56, pp. 23-9, Jan 2009.

[132] B. Ghane-Motlagh and M. Sawan, "High-Density 3D Pyramid-Shaped Microelectrode Arrays for Brain-Machine Interface Applications " in *Biomedical Circuits and Systems Conference (BioCAS), IEEE,* Lausanne 2014, pp. 364 - 367

[133] L. A. Geddes and R. Roeder, "Criteria for the selection of materials for implanted electrodes," *Ann Biomed Eng,* vol. 31, pp. 879-90, Jul-Aug 2003.

[134] S. B. Brummer, L. S. Robblee, and F. T. Hambrecht, "Criteria for selecting electrodes for electrical stimulation: theoretical and practical considerations," *Ann N Y Acad Sci,* vol. 405, pp. 159-71, 1983.

[135] S. F. Cogan, "Neural stimulation and recording electrodes," *Annu Rev Biomed Eng,* vol. 10, pp. 275-309, 2008.

[136] R. L. White and M. S. Fox, "On the molecular basis of high negative interference," *Proc Natl Acad Sci U S A,* vol. 71, pp. 1544-8, Apr 1974.

[137] D. R. Merrill, M. Bikson, and J. G. Jefferys, "Electrical stimulation of excitable tissue: design of efficacious and safe protocols," *J Neurosci Methods,* vol. 141, pp. 171-98, Feb 15 2005.

[138] K. Wang, H. A. Fishman, H. Dai, and J. S. Harris, "Neural stimulation with a carbon nanotube microelectrode array," *Nano Letters,* vol. 6, pp. 2043-8, Sep 2006.

[139] T. S. Phely-Bobin, T. Tiano, B. Farrell, R. Fooksa, L. Robblee, D. J. Edell, *et al.*, "Carbon Nanotube Based Electrodes for Neuroprosthetic Applications," *Mater. Res. Soc. Symp. Proc.*, vol. 926, 2006.

[140] T. S. Phely-Bobin, T. Tiano, B. Farrell, R. Fooksa, L. Robblee, J. David, *et al.*, "Carbon nanotube based electrodes for neuroprosthetic applications," *Mater. Res. Soc. Symp. Proc.*, vol. 926, 2006.

[141] R. A. Green, C. M. Williams, N. H. Lovell, and L. A. Poole-Warren, "Novel neural interface for implant electrodes: improving electroactivity of polypyrrole through MWNT incorporation," *J Mater Sci Mater Med,* vol. 19, pp. 1625-9, Apr 2008.

[142] M. David-Pur, L. Bareket-Keren, G. Beit-Yaakov, D. Raz-Prag, and Y. Hanein, "All-carbon-nanotube flexible multi-electrode array for neuronal recording and stimulation," *Biomed Microdevices,* vol. 16, pp. 43-53, Feb 2014.

[143] B. Brown, C. B. Parker, B. R. Stoner, and J. T. Glass, "Growth of vertically aligned bamboo-like carbon nanotubes from ammonia/methane precursors using a platinum catalyst," *Carbon,* vol. 49, pp. 266-274, Jan 2011.

[144] S. Minnikanti, N. Peixoto, and J. M. M. (Ed.), "Implantable Electrodes with Carbon Nanotube Coatings, Carbon Nanotubes Applications on Electron," *ISBN: 978-953-307-496-2, InTech,* August 1 2011.

[145] A. Ansaldo, E. Castagnola, E. Maggiolini, L. Fadiga, and D. Ricci, "Superior electrochemical performance of carbon nanotubes directly grown on sharp microelectrodes," *Acs Nano,* vol. 5, pp. 2206-14, Mar 22 2011.

[146] J. H. Han, S. H. Choi, T. Y. Lee, J. B. Yoo, C. Y. Park, T. Jung, *et al.*, "Growth characteristics of carbon nanotubes using platinum catalyst by plasma enhanced chemical vapor deposition," *Diamond and Related Materials,* vol. 12, pp. 878-883, Mar-Jul 2003.

[147] D. Takagi, Y. Homma, H. Hibino, S. Suzuki, and Y. Kobayashi, "Single-walled carbon nanotube growth from highly activated metal nanoparticles," *Nano Letters,* vol. 6, pp. 2642-5, Dec 2006.

[148] I. Martin-Fernandez, G. Gabriel, G. Rius, R. Villa, F. Perez-Murano, E. Lora-Tamayo, *et al.*, "Vertically aligned multi-walled carbon nanotube growth on platinum electrodes for bio-impedance applications," *Microelectronic Engineering,* vol. 86, pp. 806-808, Apr-Jun 2009.

[149] H. Kondo, N. Fukuoka, and T. Maruyama, "low temperature growth of single-walled carbon nanotubes from Pt catalysts under low ethanol pressure by alcohol gas source method," *Journal of Nanotechnology,* 2012.

[150] X. Liu, L. Guo, D. Morris, A. B. Kane, and R. H. Hurt, "Targeted removal of bioavailable metal as a detoxification strategy for carbon nanotubes," *Carbon,* vol. 46, pp. 489-500, Mar 2008.

[151] M. Chhowalla, K. B. K. Teo, C. Ducati, N. L. Rupesinghe, G. A. J. Amaratunga, A. C. Ferrari, *et al.*, "Growth process conditions of vertically aligned carbon nanotubes using plasma enhanced chemical vapor deposition," *Journal of Applied Physics,* vol. 90, pp. 5308-5317, Nov 15 2001.

[152] T. D. Nguyen-Vu, H. Chen, A. M. Cassell, R. Andrews, M. Meyyappan, and J. Li, "Vertically aligned carbon nanofiber arrays: an advance toward electrical-neural interfaces," *Small,* vol. 2, pp. 89-94, Jan 2006.

[153] M. Meyyappan, "A review of plasma enhanced chemical vapour deposition of carbon nanotubes," *Journal of Physics D-Applied Physics,* vol. 42, Nov 7 2009.

[154] T. L. Rose and L. S. Robblee, "Electrical stimulation with Pt electrodes. VIII. Electrochemically safe charge injection limits with 0.2 ms pulses," *IEEE transactions on bio-medical engineering,* vol. 37, pp. 1118-20, Nov 1990.

[155] E. M. Hudak, J. T. Mortimer, and H. B. Martin, "Platinum for neural stimulation: voltammetry considerations," *Journal of Neural Engineering,* vol. 7, p. 26005, Apr 2010.

[156] M. Hasanuzzaman, R. Raut, and M. Sawan, "Energy-Efficient High-Voltage Compliant Implantable Brain-Machine Interfaces," *2013 Ieee Biomedical Circuits and Systems Conference (Biocas),* pp. 81-84, 2013.

[157] M. Hasanuzzaman, R. Raut, and M. Sawan, "High-voltage compliant microelectrode array drivers for intracortical microstimulation," *Int. J. Crit. Theor. Appl.,* To appear in 2015.

[158] L. Gallentoft, L. M. Pettersson, N. Danielsen, J. Schouenborg, C. N. Prinz, and C. E. Linsmeier, "Size-dependent long-term tissue response to biostable nanowires in the brain," *Biomaterials,* vol. 42, pp. 172-83, Feb 2015.

[159] E. Slavcheva, R. Vitushinsky, W. Mokwa, and U. Schnakenberg, "Sputtered iridium oxide films as charge injection material for functional electrostimulation," *Journal of the Electrochemical Society,* vol. 151, pp. E226-E237, 2004.

[160] M. Sawan, Y. Laaziri, F. Mounaim, E. Elzayat, J. Corcos, and M. M. Elhilali, "Electrode-tissues interface: modeling and experimental validation," *Biomedical materials,* vol. 2, pp. S7-S15, Mar 2007.

[161] E. Barsoukov and J. R. Macdonald, *Impedance Spectroscopy: Theory, Experiment, and Applications*: John WILEY, 2005.

[162] R. Bhandari, S. Negi, L. Rieth, R. A. Normann, and F. Solzbacher, "A novel method of fabricating convoluted shaped electrode arrays for neural and retinal prostheses," *Sensors and Actuators a-Physical,* vol. 145, pp. 123-130, Jul-Aug 2008.

[163] J. D. Weiland, D. J. Anderson, and M. S. Humayun, "In vitro electrical properties for iridium oxide versus titanium nitride stimulating electrodes," *IEEE transactions on bio-medical engineering,* vol. 49, pp. 1574-9, Dec 2002.

[164] T. Nyberg, A. Shimada, and K. Torimitsu, "Ion conducting polymer microelectrodes for interfacing with neural networks," *Journal of Neuroscience Methods,* vol. 160, pp. 16-25, Feb 15 2007.

[165] E. M. Harnett, J. Alderman, and T. Wood, "The surface energy of various biomaterials coated with adhesion molecules used in cell culture," *Colloids Surf B Biointerfaces,* vol. 55, pp. 90-7, Mar 15 2007.

[166] C. D. James, R. Davis, M. Meyer, A. Turner, S. Turner, G. Withers, *et al.*, "Aligned microcontact printing of micrometer-scale poly-L-lysine structures for controlled growth of cultured neurons on planar microelectrode arrays," *IEEE Trans Biomed Eng,* vol. 47, pp. 17-21, Jan 2000.

[167] R. A. Green, R. T. Hassarati, J. A. Goding, S. Baek, N. H. Lovell, P. J. Martens, *et al.*, "Conductive hydrogels: mechanically robust hybrids for use as biomaterials," *Macromol Biosci,* vol. 12, pp. 494-501, Apr 2012.

[168] J. H. Chen and Y. H. Ai, "[Application of the fiber bronchus lens in difficult endotracheal intubation]," *Hunan yi ke da xue xue bao = Hunan yike daxue xuebao = Bulletin of Hunan Medical University,* vol. 26, p. 580, Dec 28 2001.

[169] X. W. Tan, L. Hartman, K. P. Tan, R. Poh, D. Myung, L. L. Zheng, *et al.*, "In vivo biocompatibility of two PEG/PAA interpenetrating polymer networks as corneal inlays following deep stromal pocket implantation," *J Mater Sci Mater Med,* vol. 24, pp. 967-77, Apr 2013.

[170] S. Uppal, M. D. Graaf, and K. D. Moeller, "Microelectrode Arrays and the Use of PEG-Functionalized Diblock Copolymer Coatings," *Biosensors,* vol. 4, pp. 318-328, 2014.

[171] Y. Li, L. Su, C. Shou, C. Yu, J. Deng, and Y. Fang, "Surface-enhanced molecular spectroscopy (SEMS) based on perfect-absorber metamaterials in the mid-infrared," *Sci Rep,* vol. 3, p. 2865, 2013.

[172] M. S. Oh, B. S. Yang, J. H. Lee, S. H. Oh, U. S. Lee, Y. J. Kim, *et al.*, "Improvement of electrical and optical properties of molybdenum oxide thin films by ultralow pressure sputtering method," *Journal of Vacuum Science & Technology A,* vol. 30, May 2012.

[173] C. Hinuber, C. Kleemann, R. J. Friederichs, L. Haubold, H. J. Scheibe, T. Schuelke, *et al.*, "Biocompatibility and mechanical properties of diamond-like coatings on cobalt-chromium-molybdenum steel and titanium-aluminum-vanadium biomedical alloys," *J Biomed Mater Res A,* vol. 95, pp. 388-400, Nov 2010.

[174] E. Flampouri and S. Kintzios, "Nafion and Polylysine treated PEDOT mammalian cell biosensor," *Eurosensors Xxv,* vol. 25, 2011.

[175] S. Zalipsky and J. M. Harris, "Introduction to chemistry and biological applications of poly(ethylene glycol)," *Poly(Ethylene Glycol),* vol. 680, pp. 1-13, 1997.
[176] L. Vidal, V. Thuault, A. Mangas, R. Covenas, A. Thienpont, and M. Geffard, "Lauryl-poly-L-lysine: A New Antimicrobial Agent?," *J Amino Acids,* vol. 2014, p. 672367, 2014.
[177] C. Cha, S. R. Shin, N. Annabi, M. R. Dokmeci, and A. Khademhosseini, "Carbon-based nanomaterials: multifunctional materials for biomedical engineering," *ACS Nano,* vol. 7, pp. 2891-7, Apr 23 2013.
[178] K. B. Bjugstad, K. Lampe, D. S. Kern, and M. Mahoney, "Biocompatibility of poly(ethylene glycol)-based hydrogels in the brain: an analysis of the glial response across space and time," *J Biomed Mater Res A,* vol. 95, pp. 79-91, Oct 2010.
[179] H. Teppola, J. Selinummi, J. R. Sarkanen, A. Pettinen, T. O. Jalonen, O. Yli-Harja, *et al.*, "Automated image analysis of neuroblastoma cell networks cultured on microelectrode array plates," presented at the Front. Neuroinform. Conference Stockholm, Sweden, 2008.
[180] S. Klein, A. Sommer, L. V. R. Distel, W. Neuhuber, and C. Kryschi, "Superparamagnetic iron oxide nanoparticles as radiosensitizer via enhanced reactive oxygen species formation," *Biochemical and Biophysical Research Communications,* vol. 425, pp. 393-397, Aug 24 2012.
[181] R. A. Green, J. S. Ordonez, M. Schuettler, L. A. Poole-Warren, N. H. Lovell, and G. J. Suaning, "Cytotoxicity of implantable microelectrode arrays produced by laser micromachining," *Biomaterials,* vol. 31, pp. 886-93, Feb 2010.
[182] A. Blau, "Cell adhesion promotion strategies for signal transduction enhancement in microelectrode array in vitro electrophysiology: An introductory overview and critical discussion," *Current Opinion in Colloid & Interface Science,* vol. 18, pp. 481-492, Oct 2013.
[183] S. L. Hirsh, D. R. McKenzie, N. J. Nosworthy, J. A. Denman, O. U. Sezerman, and M. M. Bilek, "The Vroman effect: competitive protein exchange with dynamic multilayer protein aggregates," *Colloids Surf B Biointerfaces,* vol. 103, pp. 395-404, Mar 1 2013.